Planetary Boundary Layer Height Variations Over the Tibetan Plateau in Relation to Local Climate Variables and Large-Scale Circulation

Nils Slättberg

Degree of Master of Science (120 credits)
with a major in Earth Sciences
60 hec

Department of Earth Sciences
University of Gothenburg
2020 B1114

Faculty of Science

UNIVERSITY OF GOTHENBURG

UNIVERSITY OF GOTHENBURG
Department of Earth Sciences
Geovetarcentrum/Earth Science Centre

Planetary Boundary Layer Height Variations Over the Tibetan Plateau in Relation to Local Climate Variables and Large-Scale Circulation

Nils Slättberg

ISSN 1400-3821

B1114
Master of Science (120 credits) thesis
Göteborg 2020

Mailing address
Geovetarcentrum
S 405 30 Göteborg

Address
Geovetarcentrum
Guldhedsgatan 5A

Telephone
031-786 19 56

Geovetarcentrum
Göteborg University
S-405 30 Göteborg
SWEDEN

Abstract

The lowest layer of the Earth's atmosphere, the planetary boundary layer (PBL), may reach extremely high above the Tibetan Plateau (TP). Moreover, the TP is a hotspot region for climate interactions, exerting far-reaching influences on atmospheric conditions. However, very little is known about the temporal and spatial variations in planetary boundary layer height (PBLH) across the vast plateau and how the PBLH may be related to other climate variables. Therefore, this study utilises the recently available reanalysis dataset ERA5 to investigate firstly how the PBLH has varied during the last four decades to establish a PBLH climatology for the TP, and secondly how it may be related to local climate variables and large-scale circulation. It is shown that the variations in TP PBLH are large. Over the interior of the plateau the PBLH sometimes exceeds 6000 m in the afternoon, while it only grows to about half of this height in the southeastern TP. PBLH trends range from -65 m per decade in the monsoon season in central TP to +70 m per decade in southeastern TP in the dry season, resulting in a very weak overall trend. The spatial patterns in the PBLH trends are strikingly similar to the trends of surface sensible heat flux, which is strongly correlated with PBLH over most of the plateau in both the dry season and the monsoon season, suggesting that surface sensible heat flux is the dominating factor behind the PBLH trends. In addition, it is found that even in the absence of a stratospheric intrusion the low extra-tropical tropopause may reach very close to the high PBL tops which could potentially lead to enhanced stratosphere-troposphere exchanges. Further, PBLH is analysed in relation to large-scale climate indices such as the El Niño Southern Oscillation (ENSO) index and the Indian Summer Monsoon (ISM) index. Although the relations are generally weak, some associations can be discerned, such as statistically significant anticorrelation between PBLH and ENSO for the dry season as well as detrended PBLH and detrended ISM for the summer mean.

Sammanfattning

Den understa delen av jordens atmosfär, det atmosfäriska gränsskiktet, kan nå extremt högt över Tibetplatån (TP). TP är dessutom en viktig region för klimatinteraktioner och utövar långtgående påverkan på atmosfären. Det saknas dock kunskap om variationer i gränsskiktets höjd över den vidsträckta platån och om hur höjden varierar i relation till andra klimatvariabler. Därför används återanalysdata från ERA5 i den här studien till att analysera gränsskiktshöjdens variationer under de senaste fyra decennierna för att upprätta en gränsskiktshöjds-klimatologi för TP, samt undersöka hur höjden relaterar till lokala klimatvariabler och storskalig cirkulation. Studien visar att det finns stora skillnader inom TP. I de centrala delarna av platån kan gränsskiktets höjd ibland överstiga 6000 m under eftermiddagen, medan det bara når ungefär hälften så högt i sydöstra TP. Trenderna varierar från -65 m per decennium i centrala TP under monsunsäsongen till +70 m per decennium i de sydöstra delarna av platån under torrsäsongen. Likheten i rumslig fördelning är slående mellan gränsskiktets trender och trender i det sensibla värmeflödet från markytan, vilket dessutom är starkt korrelerat med gränsskiktets höjd över nästan hela platån under både monsun- och torrsäsongen. Förändringar i det sensibla värmeflödet tycks därför vara den dominerande faktorn bakom trenderna i gränsskiktets höjd. Studien visar också att den utomtropiska tropopausen kan nå mycket nära gränsskiktets höga toppar även när ingen stratosfärisk intrusion äger rum, vilket potentiellt sett skulle kunna innebära ett ökat utbyte mellan troposfären och stratosfären. Gränsskiktets höjd analyseras också i relation till storskaliga klimatindex såsom El Niño Southern Oscillation (ENSO) index och Indian Summer Monsoon (ISM) index. Även om relationerna mestadels är svaga så kan vissa associationer urskiljas, till exempel statistiskt signifikanta antikorrelationer mellan gränsskiktets

höjd och ENSO under torrsäsongen samt avtrendad gränsskiktshöjd och avtrendad ISM under sommaren.

List of Abbreviations

ASM	Asian Summer Monsoon
CBL	Convective Boundary Layer
CPT	Cold Point Tropopause
CPTL	Cold Point Tropopause Level
ΔT	The difference between ground temperature and air temperature
CTP	Central Tibetan Plateau (areal extent defined in Section 2.3)
EASM	East Asian Summer Monsoon
ECMWF	European Centre for Medium-Range Weather Forecasts
ISM	Indian Summer Monsoon (also known as South Asian summer monsoon)
IP	Iranian Plateau
LRT	Lapse Rate Tropopause
LRTH	Lapse Rate Tropopause Height
LRTL	Lapse Rate Tropopause Level
PBL	Planetary Boundary Layer (also known as Atmospheric Boundary Layer)
PBLH	Planetary Boundary Layer Height
PV	Potential Vorticity
Prc	Total Precipitation
SETP	South-Eastern Tibetan Plateau (areal extent defined in Section 2.3)
SH	Surface Sensible Heat flux
TP	Tibetan Plateau
TP-SHAP	Tibetan Plateau Sensible Heat driving Air Pump
T2m	2 meter air Temperature

Contents

List of Tables

List of Figures

1 Introduction

In the Central Asian high elevation area known as the Tibetan Plateau (TP), the climate is changing rapidly. Over the past 50 years the region has warmed twice as fast as the global average and together with precipitation changes, the warming has led to drastic and accelerating glacial retreat in many parts of the region. Changes have been detected in the atmosphere as well as the water cycle, cryosphere, land surface and ecosystems in the region. Suggested contributors to the enhanced TP warming includes snow-albedo feedbacks and cloud-radiation interactions as well as changes in land use, atmospheric circulation and surface water vapour content (Yao et al., 2019; Rangwala, Miller, & Xu, 2009; Bibi et al., 2018). However, the uncertainties regarding the effects and future evolution of climate change at the TP are enormous. Interactions and feedbacks between the different components of the climate system are strong at the TP and the spatial and temporal differences in the characteristics and effects of climate change are substantial (Bibi et al., 2018; Immerzeel, Van Beek, & Bierkens, 2010). Lack of data strongly adds to the difficulties in assessing changes in this region (R. Zhang, Koike, Xu, Ma, & Yang, 2012).

In addition to being highly sensitive to climate change and its impacts, the TP in turn exerts a strong influence on other regions. The mechanical and thermal forcing of the vast plateau, acting on the atmosphere as an elevated heat source, affects atmospheric circulation including the regional monsoon systems (Ye & Wu, 1998; Ge et al., 2017; Flohn, 1957). Features of the TP atmosphere, such as low-level vortices originating over the TP, influence heavy rains and droughts in China (Tao & Ding, 1981). Moreover, major rivers supplying freshwater to 1.4 billion people originates at the plateau (Immerzeel et al., 2010). Changes at the TP therefore enhances the vulnerability of nearby regions which are dependent on monsoon rainfall as well as these rivers for water and food security. In addition, risks from geohazards like landslides and glacial lake outbursts increase as glaciers and permafrost melt (Yao et al., 2019).

Among the outstanding features of the TP climate is the unusual heights that its Planetary Boundary Layer (PBL) sometimes reaches. The PBL is the lowermost part of the atmosphere's bottom layer, the troposphere, and it is characterised by the turbulence and rapid variations caused by its interaction with the underlying surface. Over the TP, the Planetary Boundary Layer Height (PBLH) can reach unusually high altitudes and may even interact with the tropopause, which marks the transition between the troposphere and the overlying stratosphere (X. Chen et al., 2016, 2013; K. Yang et al., 2004). In the following sections of the introduction, the TP and the climate characteristics of the region as well as the influences of the plateau on the atmosphere are described. Next, the PBL and its potential interactions with larger-scale circulation are discussed. Thereafter, the tropopause and its interactions with the top of the high PBL over TP are explored. Finally, the aim and research questions of this study are presented.

1.1 The Tibetan Plateau

The Tibetan Plateau, bounded to the east by the Hengduan Mountains, to the south and west by the Himalayas and to the north by the Kunlun Mountains, is the highest plateau on Earth. Indeed, its average elevation of 4000-5000 m above sea level (R. Zhang et al., 2012) has given it the nickname *The Roof of the World*. It spans 2.5 million km^2 and its complex terrain is characterised by numerous glaciers, lakes, valleys, hills, mountains and land-forms sculptured by ice, rivers, wind and freezing-thawing processes (Q. Yang & Zheng, 2004). Its 1 million km^2 of glaciers contains the largest ice volume found outside the polar regions

(Yao et al., 2019), and hence it has also been dubbed *The Third Pole*. The role of the TP in enhancing monsoon systems in the region (Ge et al., 2017; Ye & Wu, 1998; Broccoli & Manabe, 1992) together with the fact that major rivers such as the Yangtze River, the Yellow River and the Ganges River originates from the TP and supplies 1.4 billion people with freshwater has given it yet another name: *The Water Tower of Asia* (Yao et al., 2019).

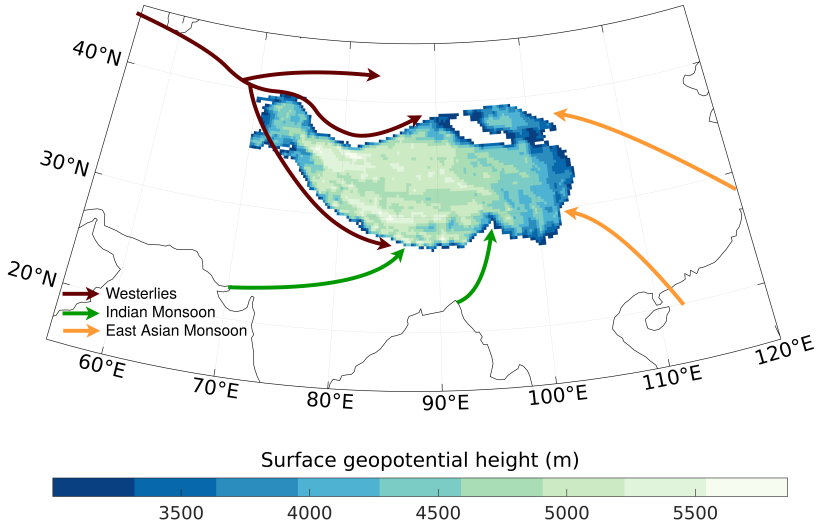

Figure 1: The Tibetan Plateau (TP). The TP, located in central Asia, is the largest and highest plateau on Earth. It is defined here as the region which lies within 70°E - 105°E and 27°N - 40°N and has an altitude of more than 3000 m above sea level. The colour map shows ERA5 surface geopotential height (≈ altitude) in metres. The arrows represents the three major circulation systems of relevance to the TP region, namely the westerlies (dark red arrows), the Indian monsoon (green arrows) and the East Asian monsoon (orange arrows), and were drawn after Figure 1 in Yao, Thompson, Yang, et al. (2012).

1.1.1 Climate of the Tibetan Plateau

General features of the TP climate include low air temperature, intense solar radiation, great diurnal temperature range, small annual temperature range and a distinctive dry and wet season (Q. Yang & Zheng, 2004; Bibi et al., 2018). However, large differences exist between different parts of the vast plateau. The western TP with its high elevations is generally 10° C colder than the eastern parts. Near-surface air temperatures across the TP are below 0° C during winter and range from 0° C in the west to 10° C in the east during summer (Frauenfeld, Zhang, & Serreze, 2005).

Based on data from monitoring stations and ice core reconstructions of regional precipitation regimes, it has been suggested that the TP can be divided into three domains: The area north of 35° N, in which the climate is dominated by the westerlies, the area south of 30° N, which is dominated by the Indian monsoon, and the region between 30° N and 35° N, which is a transition zone with shifting influences from both systems (Yao et al., 2013). It has also been suggested that the atmospheric circulation over the TP is primarily

dominated by the Indian monsoon during summer and the westerlies during winter. At the eastern margin of the plateau, the East Asian monsoon also has some influence (Yao, Thompson, Yang, et al., 2012). Overall, the TP precipitation has a large seasonal variation with a pronounced rainy season and the largest rainfall occurring in June, July and August (Tao & Ding, 1981). The interior of the plateau, which is less affected by the monsoons and westerlies than its margins, exhibits more continental climatic conditions with less precipitation (Yao, Thompson, Yang, et al., 2012).

1.1.2 Climate Change on the Tibetan Plateau

During recent decades, changes have been detected in the atmosphere, water cycle, cryosphere, land surface and ecosystems at the TP. Indeed, the TP region has been called "the most sensitive and readily visible indicator of climate change" (Yao, Thompson, Mosbrugger, et al., 2012, p. 52). X. Liu and Chen (2000) found linear temperature trends of around 0.16° C per decade in the annual mean and 0.32° C per decade in the winter mean during the 1955-1996 period. These rates exceeds the average for the Northern Hemisphere as well as the average for the latitudinal zone of the TP (X. Liu & Chen, 2000). A more recent study found that near-surface air temperatures at the TP increased by an average of 2° C during 1979-2016. They also found that the precipitation increased during this period, especially in summer (Zhu et al., 2019). However, precipitation trends differ between stations in different parts of the TP. Generally, stations in semi-arid and humid zones in the central plateau shows increasing trends while decreasing trends have been observed along the periphery (Bibi et al., 2018; X. Li, Wang, Guo, & Chen, 2017). In addition, elevation plays a role, and it has been found that increasing trends in temperature, surface specific humidity and precipitation, as well as decreasing trends in surface wind speed, are generally larger at higher elevations (X. Liu & Chen, 2000; X. Li et al., 2017; X. Guo, Wang, Tian, & Li, 2017).

Another climate variable which is exhibiting marked trends at the TP - and which is highly significant for the PBLH - is surface sensible heat flux (SH). SH is the heat transfer between the Earth's surface and the atmosphere (throughout this thesis, positive values denotes a net flux *from* the surface *to* the atmosphere). It is largely determined by the temperature difference between the surface and the atmosphere, the wind speed and the roughness of the surface. Despite the temperature increases at the TP, several studies have found declining trends for the SH at the plateau. Duan and Wu (2008) found decreasing SH trends of 14% (3.8 W/m2 per decade) for central-eastern TP from 1980 to 2003, with especially large declines during spring. K. Yang, Guo, and Wu (2011) agrees that the SH has weakened significantly across the TP, but only about 2% per decade (between 1984 and 2006). They attribute the differences between the respective estimates of the two studies to the method which is applied by Duan and Wu (2008) and argue that the declining SH trend may be overestimated in Duan and Wu (2008).

Interestingly, the trend in SH appears to have reversed during the last two decades. M. Wang et al. (2019) investigated the trend in spring SH using data from 77 stations in central-eastern TP for 1979-2014. They found that although there is indeed a significant decrease during the first two decades, the 2000-2014 period is instead characterised by a statistically significant *increasing* trend in spring SH. They identify declining wind speed as the main cause of the decreasing spring SH prior to 2000 and increased ground-air temperature difference (ΔT) as the reason for the increasing spring SH after 2000. Turning their attention to climate model output, they found that the increasing trend continues in future projections, and is larger in scenarios with stronger warming. As described below, the SH

is highly important for the thermal influence of the TP on regional weather and climate systems. Moreover, as discussed in Section 1.2, it is one of the factors which determines the PBLH.

1.1.3 Mechanical and Thermal Forcing Exerted by the Tibetan Plateau

The forcing of the TP influences weather and climate variability (Wu et al., 2014). Being a vast and elevated heat source protruding into the atmosphere, it directly affects the mid-troposphere (Koteswaram, 1958), and many studies have reported its influence on the Asian monsoon systems (Ye & Wu, 1998; Wu et al., 2014, 2007; Wu, He, Duan, Liu, & Yu, 2017; Wu et al., 2012; Flohn, 1957).

Yanai and Li (1994) declare that the TP maintains a thermally driven vertical circulation which, at the onset of the Indian Summer Monsoon (ISM), merges with the large-scale ascent associated with the monsoon. The ISM onset over Asia can thus be described as an interaction between TP induced circulation and the large-scale circulation associated with the northward migration of the monsoon rain-belt (Yanai, Li, & Song, 1992; Yanai & Li, 1994).

The thermal effects of the TP have been conceptualised as the TP sensible heat driving air pump, TP-SHAP (Wu et al., 2007). The "pump" is primarily driven by seasonally reversing forcing from SH on sloping lateral surfaces of the TP: During wintertime (November - February) the TP is a heat sink cooling the overlying air and causing it to descend and slide along the cooling sloping surfaces into surrounding areas. In summer (March - October) in contrast, the plateau acts as a heat source. The heated air ascends, and thereby lower tropospheric air is pulled from surrounding regions toward the TP and up along its heating sloping surfaces. The summertime "pulling" of the surrounding atmosphere by the TP-SHAP is stronger than its opposite wintertime effect, because during summer a positive feedback exists between small-scale convection over the TP and the large-scale convergent spiral of lower tropospheric circulation in the surrounding area (Wu et al., 2007, 2014).

Using numerical experiments to investigate the mechanical and thermal forcing of the Asian monsoon systems exerted by the Iranian Plateau (IP) and the TP, Wu et al. (2012) found that it is mainly *thermal* forcing that controls the summer monsoon. While the southern branch of the ISM is mainly driven by the thermal contrast between land and sea, the thermal forcing - or air pumping - of the IP and the TP is important for the northern branch of the ISM and for the EASM (Wu et al., 2012).

Although the thermal forcing of the TP dominates in summer, the mechanical forcing is significant in winter when the prevailing westerlies are deflected by the plateau. The resulting deviation produces a dipole with an anticyclone to the north of the TP and a cyclone to the south. At the western side of the anticyclone situated north of the TP, warm air is brought northward, while cold air is brought southward at its eastern side. The presence of the large anticyclone makes East Asia significantly colder than middle Asia. The cyclone situated south of TP transports dry air southward along its western rim and moist air northward along its eastern. By doing so it helps trigger the dry season in South Asia and the persistent rainfall in early spring in south China which precedes the monsoon onset (Wu et al., 2007, 2014).

In summary, the TP mechanically and thermally forces the atmosphere, producing notable effects on regional weather systems. In particular, the SH on the TP plays a crucial

part in driving the summer monsoon systems. During the winter, the deflection of the westerlies by the plateau influences temperature and precipitation in much of Asia.

1.2 The Planetary Boundary Layer

The PBL is the lowermost part of the troposphere, and as such it is directly influenced by the Earths' surface. The main processes of importance for PBL growth in the TP region are schematically represented in Figure 2 and will be discussed in the following paragraphs. Note that Figure 2 is a two-dimensional schematic of four-dimensional processes at a wide range of scales - hence, the relative importance or spatial and temporal scales of the processes represented here can not be derived from the figure.

The PBL can be defined as the part of the troposphere which is directly influenced by the underlying surface and responds to surface forcings quickly - generally within an hour. It is characterised by turbulence, which arises because of the frictional drag on the atmosphere as it flows over the uneven surfaces of the Earth and by the vertical motions of air being heated by the surface or losing heat to it. Therefore, topographic features, wind speed and wind shear (local variation in wind speed or direction in the atmosphere) as well as the energy exchanges at the surface affect the PBLH. In addition to locally produced conditions, the PBLH is influenced by large-scale weather systems (Oke, 2002; Sathyanadh, Prabhakaran, Patil, & Karipot, 2017). Cloud radiative effects also influence PBL growth, but quantification of their effects for specific geographical regions are scarce (Davis, Rajeev, & Mishra, 2020).

Unlike the overlying atmosphere, the temperatures in the PBL (over land regions) has a strong diurnal cycle following the daytime warming and nighttime cooling of the ground (Stull, 2012). The diurnal cycle is also reflected in the height of the PBL. Daytime PBLs can grow deep in response to convective unstable conditions. This particular type of PBL is often termed convective boundary layer (CBL) and is driven by convective thermals generated by heat transfer from the ground or radiative cooling from cloud tops. The CBL is characterised by vigorous turbulence resulting in a vertically well-mixed layer. At night in contrast, the surface layer becomes stable as the ground cools by emitting infrared radiation. As a result, nighttime PBLs are usually shallow, typically reaching less than 500 m (S. Liu & Liang, 2010; Stull, 2012). In addition to diurnal variations, the PBLH varies in response to seasonal differences in e.g. atmospheric stability and heat fluxes. The seasonal cycles differ greatly between regions. At extra-tropical latitudes, PBLH often peaks during late summer when the surface is warm and the static stability is low. Sub-tropical and tropical regions in contrast often have their maximum PBLH in the dry season when evaporation is low, since low evaporation favours SH, as explained below (Chan & Wood, 2013).

As outlined in the previous paragraph, the PBLH is strongly associated with convective activities within the PBL related to heating and cooling. In Figure 2, the large purple arrow represent the incoming shortwave solar radiation. The solar radiation is partly reflected and scattered by clouds and aerosols or absorbed in the atmosphere, and partly transmitted to the surface, where the energy (minus a fraction which is reflected off the surface) is absorbed and thereby transformed into other forms of energy. Some is partitioned into sensible heat giving rise to positive SH manifested as convection: as the ground absorbs the solar energy it may become warmer than the overlying atmosphere and heat up the lowermost air, causing it to rise in the form of turbulent eddies (Trenberth, Fasullo, & Kiehl, 2009; Oke, 2002). If cooler ground is instead underlying warmer air, the direction of the heat flux is from the air to the ground (negative SH). Positive SH is one of the most crucial factors behind the

deep TP PBL (K. Yang et al., 2004). Due to the presence of moisture, snow or ice in the surface layer, some energy is instead partitioned into latent heat flux. In contrast to sensible heat, the energy added to the surface is then partitioned into a change of *state* (e.g. snow melts or water evaporates) instead of a temperature change (Oke, 2002). Evaporated water that is carried as vapour into the atmosphere can strongly enhance the positive buoyancy of updrafts, since the energy that evaporated the water is released again when it condenses, providing extra heat for convection. Conversely, as water droplets evaporates in the atmosphere, the negative buoyancy of downdrafts is enhanced (American Meteorological Society, 2012).

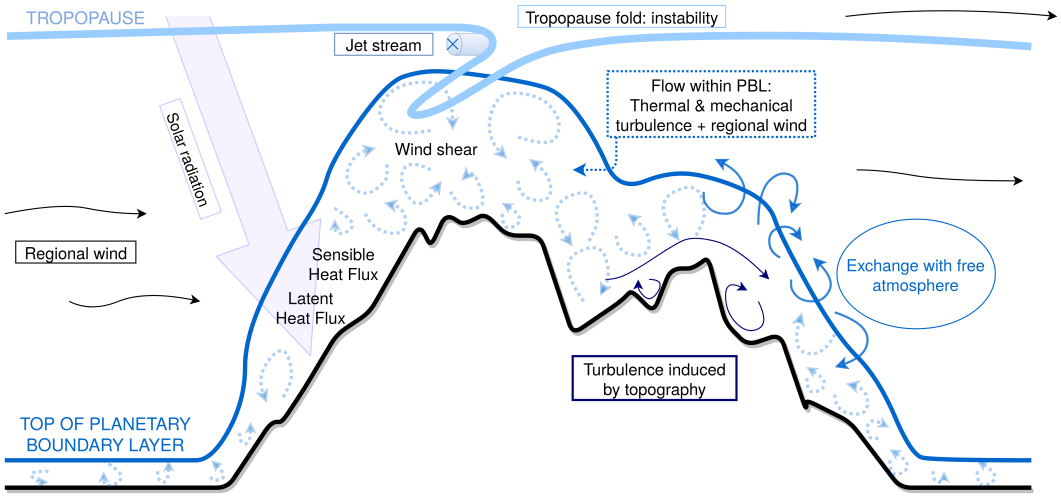

Figure 2: Planetary Boundary Layer (PBL) processes at the Tibetan Plateau. Solar radiation heating the ground gives rise to turbulent heat fluxes. Together with the turbulence from wind flowing over the rough surface of the plateau, these play a large role for the convection in the PBL and therefore its depth. In addition, wind shear between atmospheric layers with differing wind speed and large-scale meteorological variations in e.g. stability affects the PBL height (PBLH). The top of the PBL is where exchange between the PBL and the free atmosphere may occur. At the TP, high PBLs in combination with stratospheric intrusions in the form of tropopause folds along the subtropical jet stream causes exchanges between the stratosphere and the troposphere.

1.2.1 Planetary Boundary Layer Height at the Tibetan Plateau

PBLH varies greatly across time and space, ranging from a few hundred meters to several kilometres. At the TP, the PBL sometimes reaches unusual heights, especially during winter and spring. For example, X. Chen et al. (2013) studied radiosonde data from TP for the year 2008 and found that in winter days the PBL can reach approximately 9.5 km above sea level, corresponding to about 5 km above the ground. The high wintertime PBLs at the TP may be related to low atmospheric stability, allowing convection brought about by the surface heating to reach up to the upper troposphere during the afternoon. X. Chen et al. (2016) used measurements of the PBL and surface fluxes as well as numerical simulations and ERA-Interim reanalysis data, and found very high PBLs in late winter and early spring. They argue that the weak stability of the free atmosphere allows the PBL to reach depths it would not usually reach given the available energy at the surface. The authors further found that in ERA-Interim, the weak stability and resultant high wintertime PBLs are associated with high upper-level potential vorticity (PV, a measure of the capacity of

air to rotate) and a strong jet stream positioned relatively far to the south, right above the TP. As the monsoon season develops, the atmospheric stability increases, partly because of the weakening and northward shift of the upper-level jet stream, and the monsoon season PBLs reach much lower, generally 1 to 2 kilometres (X. Chen et al., 2016). X. Chen et al. (2013) suggests that the instability may be associated with tropopause folds, which are often formed beneath jet streams as they flow into a through (Reid & Vaughan, 2004).

1.2.2 Trends in Planetary Boundary Layer Height

Climate change may be affecting the PBLH. For example, studies using observations from radiosonde stations have found increasing daytime PBLH trends in Europe (Y. Zhang, Seidel, & Zhang, 2013) and weakly increasing PBLH trends in Japan (Y. Zhang & Li, 2019). J. Guo et al. (2019) studied PBLH in China from 1979 to 2016 and found a shift from increasing to decreasing trends around 2004. This is particularly interesting in the light of the shift in SH at the TP reported by M. Wang et al. (2019). They also found that the direction of the trend changed around this time, but in contrast to the shift from *increasing to decreasing* PBLH in J. Guo et al. (2019), the SH trend in M. Wang et al. (2019) changes from *decresing to increasing*. Given that SH is positively associated with PBLH it is puzzling that the signs of their respective trends are opposite, but it can be noted that M. Wang et al. (2019) only considered SH for the spring months. Moreover, only a few of the 89 radiosonde stations in J. Guo et al. (2019) are located in the TP region, and of these few the PBLH trend appears to reverse for about half of the stations. In summary, there seem to be a tendency for slight positive PBLH trends in many regions over the last decades. In the TP region however, this trend may have reversed, despite an opposite reversal of the SH trend.

1.3 Atmospheric Circulation Relevant to the Tibetan Plateau and its Planetary Boundary Layer Height

As seen in a previous section, the TP is highly affected by global climate variability, and at the same time the plateau itself has the potential to affect the climate and weather outside the TP by mechanically and thermally forcing the overlying atmosphere. Perhaps the most well studied example is the TP forcing on the Asian monsoon systems, but interconnections between TP and other large-scale systems such as the El Niño Southern Oscillation (ENSO) and the North Atlantic Oscillation (NAO) have also been reported. The following sections will briefly introduce these systems or oscillations and their connections to the TP and, when such can be found, to the TP PBLH.

1.3.1 Monsoons

Although the traditional definition of a monsoon only considers the annual reversal of surface winds, the term is often associated with pronounced seasonal changes in rainfall (B. Wang & Ho, 2002; Hamilton, 1987). This is of great importance for the inhabitants of the monsoon regions, where the agricultural practices often are tied to the regular variations in rainfall associated with the phases of the monsoon. Even small changes in the rainfall amount or the timing of the monsoon can have significant societal consequences, e.g. in the form of low crop yields or devastating floods (Webster et al., 1998). Understanding the effects of climate change upon linkages between the climate at the TP and the climate throughout the Asian monsoon region is therefore of great importance.

The overturning of the atmosphere throughout the tropics and sub-tropics is sometimes described as a global monsoon in which the regional monsoon systems are embedded, a definition which highlights that all regional monsoon systems are driven and synchronised by the annual cycle of solar radiation (Trenberth, Stepaniak, & Caron, 2000; B. Wang, Ding, & Liu, 2011). Still, there are distinct regional characteristics of the global monsoon as well as the mechanisms controlling its seasonal march. The strongest component of the global monsoon system is the Asian summer monsoon (ASM), bringing about the heaviest seasonal rainfall on Earth and affecting the lives of more than sixty percent of the world's population (B. Wang, 2006; Wu et al., 2012). The ASM in turn is commonly divided into three subsystems: The Indian summer monsoon (ISM, also known as the South Asian summer monsoon), the East Asian summer monsoon (EASM) and the Western North Pacific summer monsoon (Ha, Seo, Lee, Kripalani, & Yun, 2018; B. Wang, Wu, & Lau, 2001; B. Wang & Ho, 2002; Zhou, Hsu, & Matsumoto, 2011).

Wu et al. (2012) used climate model experiments to investigate the mechanisms influencing the ASM. They found that the thermal land-sea contrast and the thermal forcing of the TP and the Iranian Plateau (IP) are the main drivers of the ASM, while the mechanical forcing from these topographic barriers is not essential. Wu et al. (2012) divide the meridional circulation of the ISM into two separate branches. Its southern branch is located in the tropics, where water vapour is transported zonally along the "water vapour conveyer belt". Due to the thermal contrast between land and sea, the air within this branch ascends and forms monsoon rainfall. The northern branch is situated in the subtropics, along the southern margins of the IP and the TP. Part of its water vapour is pulled northward as it approaches the TP and lifted upwards due to the thermal forcing of the IP and the TP. As a result, heavy precipitation is formed in the monsoon through over India and along the foothills of the TP. Along the conveyer belt, the water vapour which has not been pulled northward continues northeastward to sustain the EASM, which is controlled by both the land–sea thermal contrast and the thermal forcing of the TP (Wu et al., 2012).

The effects of climate change on current and future characteristics of the monsoon are difficult to untangle. IPCC (2013) summarises that likely changes over the current century include an expansion of the total area which is encompassed by monsoon systems, weakening monsoon winds, intensified monsoon precipitation and, in many regions, a lengthening of the monsoon season. For some regions of East Asia, B. Wang, Bao, Hoskins, Wu, and Liu (2008) found significant correlations between the 5 year running mean rainfall and 5 year running mean TP surface air temperature. To further investigate the coupling between TP temperature and EASM rainfall, B. Wang et al. (2008) used an atmospheric general circulation model to run experiments in which the albedo at the TP was changed. They found that reducing the albedo (and thereby increasing the temperature) at the TP gives rise to precipitation increases along the southern margin of the TP and in some regions of East Asia. The pattern of enhanced precipitation in the low albedo simulation bears resemblance to the pattern of correlation between TP temperature and East Asian rainfall. Specifically, the precipitation is enhanced in much of China, Korea and Japan. The authors suggest that observed changes in East Asian summer rainfall may be linked to TP temperature increases and that future temperature increases at the TP may further enhance the rainfall.

While thermal effects of the TP itself on the monsoon are clear, it is harder to find studies regarding the connections between the TP PBLH and monsoon variations. However, a few studies have examined the relationship between PBLH and the ISM over the Indian subcontinent. Patil, Patil, Waghmare, and Dharmaraj (2013) investigated PBLH during extreme ISM years and found that the PBLH over North-Western India was anomalously

high during years with excess monsoon rainfall, while it was unusually low during years with deficient monsoon rainfall. They attribute their finding to the effects of the precipitation amount on soil moisture. In the case of excess monsoon rainfall, the soil moisture increases which leads to a decrease in surface albedo and thus an increase in net solar radiation at the surface. At the same time, the higher soil moisture decreases the Bowen ratio and increases the amount of water vapour within the PBL, which leads to an increase in terrestrial radiation at the surface. Taken together, this means that the net radiation at the surface and thereby the total heat flux (sensible and latent) from the surface increases, which in turn acts to raise the top of the PBL. For years with deficient rainfall, the result is the opposite: The low soil moisture leads to a higher surface albedo and thereby a decrease in total heat fluxes and thus the PBLH (Patil et al., 2013).

In a study examining seasonal PBLH variability in India with respect to the monsoon, Sathyanadh et al. (2017) also points to the effect of soil moisture. In contrast to Patil et al. (2013), their study relates *low* soil moisture to *high* PBLs. They identify two PBLH regimes over Indian land regions: dry and wet. The dry regime is typically found in arid regions and during the pre-monsoon period. It is generally associated with very low soil moisture, the presence of a dry continental air mass, clear sky conditions, intense surface heating, large scale subsidence and deep daily maximum PBL which is sustained until the evening before decreasing. During the wet regime, which is common during the monsoon season, the soil moisture is high and the atmospheric conditions cloudy and moist. The PBL is shallow and unlike dry regime PBLs, its daily cycle is characterised by a rapid decrease following its maximum daily height during the early afternoon hours. Overall, the evaporative fraction (the ratio of latent heat flux to the sum of latent and sensible heat flux) was found to be a dominant control on the PBLH, with large evaporative fraction corresponding to low PBLH. Still, as noted by the authors, multiple factors operating on different time scales may control the PBL growth. What factor that is most important in determining PBLH can thus vary greatly between seasons and regions.

1.3.2 The El Niño Southern Oscillation

The El Niño Southern Oscillation (ENSO) is a coupled ocean-atmosphere phenomenon with global repercussions. Its most well-known expression is the recurring El Niño events that cause higher than average sea surface temperatures in the eastern and central equatorial Pacific ocean, which in turn leads to dramatic weather changes including heavy rains and flooding in the central Pacific island states and along the west coast of South America as well as drought in Australia, Indonesia and neighbouring countries. El Niño, as well as the opposite manifestation of the ENSO, La Niña, typically occur every 2-7 years (McPhaden, Zebiak, & Glantz, 2006).

The ENSO has varied greatly in the past and it has been suggested that global warming is leading to stronger and more frequent El Niño events. However, apparent changes could also reflect influences of decadal variations of the background climate state (Fedorov & Philander, 2000; McPhaden et al., 2006). Climate model experiments have indicated that projected future ENSO changes are heavily model dependent and thus uncertain (C. Chen, Cane, Wittenberg, & Chen, 2017) and that the inherent ENSO variability is large, making it difficult to attribute projected changes to anthropogenic forcings (Maher, Matei, Milinski, & Marotzke, 2018). During the 1979-2018 period studied in this thesis, the strongest El Niño episodes occurred in 1982-83, 1997-98 and 2015-16, while the strongest La Niña episodes took place in 1988-89, 1998-1999, 2000-2001 and 2010-11 (*Multivariate ENSO Index Version 2 (MEI.v2)*, 2020).

Studies explicitly examining the connections between TP PBLH and ENSO appear to be lacking, but associations between ENSO and other climate variables at the TP, which in turn may affect the PBLH, exist. For example, several studies have reported effects on precipitation and drought conditions in the TP region. It has been found that El Niño events often are accompanied by deficit ISM rainfall and dry anomalies in India and China (Kumar, Rajagopalan, Hoerling, Bates, & Cane, 2006; Lei et al., 2019). These dry anomalies appear to be "bridged" by drier than usual conditions in the central TP, associated with anomalous sinking there. A dry zone is thus formed along the northwestern edge of the monsoon domain, so that the edge of the monsoon region in practice retreats equator-ward (Lei et al., 2019). While debated (Yuan, Tozuka, Miyasaka, & Yamagata, 2009), ENSO have also been associated with TP snow cover (Jiang et al., 2019; Shaman & Tziperman, 2005). Shaman and Tziperman (2005) found that El Niño leads to increased snowfall creating a large TP snowpack that persist through much of spring and summer and acts to weaken the monsoon. Through its effects on surface albedo and energy fluxes, the presence of snow in turn has the potential to influence PBLH.

1.3.3 The North Atlantic Oscillation

The NAO is one of the most prominent features of atmospheric variability over the middle and high latitudes of the Northern Hemisphere. Shifts between its phases are associated with changes in the wind field, transport of heat and moisture, and the characteristics of storms (Hurrell, Kushnir, Ottersen, & Visbeck, 2003). The NAO can be described as a large scale see-saw in atmospheric pressure between the low-pressure centre near Iceland and the high pressure centre near the Azores (Walker, G. T. and Bliss, E. W., 1932; Jianping & Wang, 2003). It is the dominant mode of variability in atmospheric circulation in the North Atlantic sector (Jianping & Wang, 2003; Barnston & Livezey, 1987) and through teleconnections, it may influence the climate in other parts of the world as well.

Similar to the ENSO, the NAO has been related to precipitation and snow cover variations at the TP. Positive NAO has been related to increased snowfall and snow cover (Y. Liu, Chen, Wang, & Qiu, 2018; You et al., 2011), but in summer the effect of the teleconnection appears to be opposite: Linderholm et al. (2011) found that the summer NAO is negatively correlated with precipitation in the TP region and Z. Wang, Duan, Yang, and Ullah (2017) suggests that a strong summer NAO leads to smaller moisture transport and less summer precipitation in the southern TP. In addition, Ding, Wang, and Lu (2018) investigated influences of the NAO on various extreme temperature indices in a TP sub-region spanning ≈ 89°- 102°E and 31°- 36°N. They found strong influences of the NAO on summer temperature extremes, manifested as negative correlations with warm extremes and positive correlations with most of their cold extreme indices. Although studies of connections between the PBLH in the TP region and the NAO appear to be lacking, its effect on temperature, precipitation and snow cover could perhaps play a role for PBLH variations.

1.4 The Tropopause

The tropopause is the transition between the troposphere, which is the lowest of the major layers in the Earth's atmosphere, and the overlying stratosphere. Most weather phenomena takes place in the troposphere, which is characterised by turbulent mixing and in which the temperature generally decreases with height. In the stratosphere in contrast, the temperature is more constant or increases with height due to the warming from UV absorption

by the ozone layer. This stably stratified temperature profile with warm, less dense air overlaying colder, more dense air, tends to suppress vertical movements and mixing in the stratosphere (Hoinka, 1998).

Several definitions of the tropopause exist, including the lapse rate tropopause (LRT) and the cold-point tropopause (CPT). The LRT is defined by a decrease in lapse rate, i.e. the rate of temperature decrease with height (World Meteorological Organization, 1957), and the cold-point tropopause (CPT) is defined as the level of minimum temperature in a vertical temperature profile (Highwood & Hoskins, 1998; Pan et al., 2018). Different tropopause definitions often produce dissimilar tropopause heights and may be suitable for different regions. Examining the differences between the LRT and CPT, Munchak and Pan (2014) found that while the seasonal average separation between the CPT and the LRT was small in the deep tropics, it increased to up to 1.5 km in the jet stream region. Moreover, they state that the LRT is applicable globally, while the CPT is confined to tropical regions. However, it is not clear at what latitude the CPT ceases to be meaningful as a tropopause definition (Munchak & Pan, 2014), and it has been applied to the TP region in previous studies (Feng, Fu, & Xiao, 2011; Khan & Jin, 2016).

The height of the global mean tropopause changes with climate. It has been argued that the tropopause altitude therefore may serve as a parameter for detecting climate variability (Schmidt, Wickert, Beyerle, & Reigber, 2004). During the last decades, the global mean altitude of the tropopause has increased (Santer et al., 2003). The increasing trend is a response to the warming of the troposphere, resulting from greenhouse gas emissions, and the cooling of the lower stratosphere, which is induced by changes in greenhouse gases and stratospheric ozone (Santer et al., 2003; Sausen & Santer, 2003). Despite the overall trend towards increasing altitude, the seasonal and regional trends may differ from the global mean. Moreover, temporary anomalies in the tropopause altitude can be connected to ENSO events (Gao, Xu, & Zhang, 2015) and explosive volcanic eruptions (Sausen & Santer, 2003).

The height of the tropopause also depends on the season and the latitude. On average, it has an altitude of around 16 km in the tropics and 8-12 km outside the tropics (Randel, Seidel, & Pan, 2007). The transition from the higher tropical tropopause to the lower extra-tropical tropopause is often not manifested as a smooth, continuous decrease in altitude. Instead, different tropopauses overlap so that, in terms of the LRT, the lapse rate increases again above the first tropopause (Kochanski, 1955; Randel et al., 2007). These double tropopauses frequently occur in the mid-latitudes near the subtropical jetstream. This latitude band can be seen as a transition region between the tropics and extratropics (Randel et al., 2007).

It has been found that the troposphere may reach unusually high over the TP. For example, Feng et al. (2011) used radio occultation data for 2006-2009 to examine the tropopause heights over the TP and found that the CPT was located approximately 18 km above the ground, while the LRT varied between 13 km in the winter and 19 km in the summer. They suggest that the TP acts as a heat source in the summer, forcing the LRT to an elevation about 2 km higher than that over low-elevation areas at similar latitudes. In the winter the effect of the TP is reversed: it acts to lower the LRT. In addition to TP thermal forcing, the LRT height is strongly affected by the subtropical jet. In contrast to the LRT (which is thermally lifted by the TP during summer), the CPT is lifted dynamically by the elevated topography of the TP all year round (Feng et al., 2011). A similar seasonal variation of the LRT was found by Jiang, Wang, Xu, Zhang, and Chiu (2017), who used sounding data

for 2008-2014. In their study, the LRT height over the TP varied from approximately 12 km in January to almost 17 km in June. They ascribe the pronounced seasonality to the seasonal occurrence of double tropopauses. When double tropopauses occur, which is common during the winter, the first tropopause is usually located at a lower altitude than it is during summer when only one tropopause is present. The tropopause height above the TP generally decreases with increasing latitude (Jiang et al., 2017), as expected from studies of global tropopause heights (e.g Santer et al., 2003).

1.5 Stratosphere-Troposphere Exchanges Through the Boundary Layer

Mixing between stratospheric and tropospheric air can take place in deep stratospheric intrusions like tropopause folds, which may occur along jet streams and fronts. Folds form in response to strong descent at the tropopause level and typically decay after 1-2 days. During the decay phase, diabatic heating and turbulence occur, and it is through these processes that the stratosphere-troposphere exchanges are achieved (Mohanakumar, 2008). Because stratospheric air is drier and contains more ozone than tropospheric air, these exchanges affect the atmospheric chemistry and may have climatic implications since water vapour and ozone are greenhouse gases (Škerlak, Sprenger, & Wernli, 2014; Stocker et al., 2001).

Usually, stratospheric air does not reach all the way to the surface, and when it does it is often very diluted by mixing (Škerlak, Pfahl, Sprenger, & Wernli, 2019). However, the vertical extent of the turbulent mixing, vertical diffusion and convective transport within the PBL as well as the level at which exchange with the free troposphere occurs is determined the PBLH (J. Guo et al., 2016; Seidel, Ao, & Li, 2010; Seibert et al., 2000) - and at the TP, PBLH may reach close to the tropopause (X. Chen et al., 2013). Therefore, air from stratospheric intrusions may be incorporated by the PBL and mixed toward the surface (Škerlak et al., 2019), while tropospheric air may enter the lower stratosphere and thereby influence global stratospheric water vapour concentration (Fu et al., 2006). The TP is noted for enhancing exchanges between the troposphere and the stratosphere and is deemed a "global hotspot" for *deep stratosphere–troposphere exchanges* (stratosphere–troposphere exchanges in which stratospheric air reaches the PBL within 4 days), especially during winter and spring (Škerlak et al., 2014).

Škerlak et al. (2019) used a model simulation with a stratospheric tracer to investigate stratosphere to troposphere transport during the occurrence of a prominent tropopause fold close to the TP in the summer 2006. They found that stratospheric air brought to the 300-500 hPa level by the tropopause fold was transported horizontally across the TP where it was incorporated by the growing PBL and mixed down to the surface. They point out that the diurnal cycle of the PBLH is important: there was virtually no stratospheric tracer at the surface during the early morning when the PBL was shallow, but during the day the PBL grew steadily up to around the 300 hPa level. This resulted in *entrainment*, a process in which turbulent air incorporates less turbulent air, causing the entrainment to proceed toward the less turbulent layer (in this case toward the stratospheric air originating from the fold). The incorporated stratospheric air was then mixed to the surface by the turbulence within the PBL. That stratospheric intrusions may reach the PBL top and be mixed downward by convection at the top of the PBL was previously identified by Johnson and Viezee (1981), but in contrast to their schematic, no vertical transport in the free troposphere was required in the case study by Škerlak et al. (2019) since the tropopause fold brought the stratospheric air to the vertical level of the PBL top.

X. Chen et al. (2013) also state that exchanges between the troposphere and the stratosphere are facilitated by the fact that the PBL sometimes reaches close to the tropopause. They suggest that the deep PBL is important for the vertical distribution of ozone at the TP, and like Škerlak et al. (2019), they point to the mechanism identified by Johnson and Viezee (1981).

1.6 Aim and Research Questions

Although several studies have shown that the PBLH reach unusually high altitudes over the TP (e.g. X. Chen et al., 2016, 2013; K. Yang et al., 2004), there is still much to explore about the seasonality and trends in these heights, and very little is known about whether their variations are related to regional atmospheric circulation features such as the westerlies or the East Asian and Indian monsoons. Moreover, the high PBL top may even reach to the vicinity of the tropopause, facilitating troposphere-stratosphere exchanges (X. Chen et al., 2013). Utilising 31 km resolution reanalysis data that are now available for the last four decades, this project aims to establish a PBLH climatology for the TP and asses PBLH variation and trends in relation to tropopause height and other climate variables as well as large-scale circulation indices. The project is focused around the following research questions:

- How has the PBLH over the TP varied during the last decades?
- How is the PBLH related to local climate variables and to circulation features such as the monsoon and westerlies?

2 Data and Methods

2.1 Dataset

Reanalysis makes it possible to study the climate in remote and data scarce regions like the TP using a consistent dataset. Reanalysis data are produced through data assimilation, a process which combines observations with numerical modelling using the laws of physics in order to obtain consistent estimates of atmospheric and land surface variables (ECMWF, n.d.). In this project, the 31 km (0.28°) resolution realisation (HRES) from the European Centre for Medium-Range Weather Forecasts (ECMWF) reanalysis dataset ERA5 is used (Copernicus Climate Change Service (C3S) , 2017). ERA5 is the fifth generation ECMWF atmospheric reanalysis, and is produced using 4D-Var data assimilation in ECMWF's Integrated Forecast System (IFS), which is coupled to a soil model as well as an ocean wave model (Hennermann & Berrisford, 2019). Compared to its predecessor ERA-Interim, it has a higher horizontal as well as vertical resolution and benefits from another decade of improvements and developments of the data assimilation and representation of model processes in IFS (Hersbach, 2018). Due to its relatively recent release, there is not yet a large amount of research evaluating ERA5 for different applications, but there are studies indicating e.g. that the overall quality of surface energy partitioning is better in ERA5 than in ERA-Interim (Martens et al., 2020) and that precipitation, surface energy, and water budgets appear realistic (Betts, Chan, & Desjardins, 2019). For the TP region specifically, Y. Chen and Ji (2019) states in a conference abstract that ERA5 in general reproduces the temporal and spatial variations of temperature and precipitation well.

2.2 Climate Variables and Indices

Descriptions of the climate variables and indices analysed for this project follow below. All ERA5 data were downloaded from the Climate Data Store (CDS; `https://cds.climate.copernicus.eu/cdsapp#!/home`). The climate variables and indices along with the abbreviations used for them throughout this thesis are listed in Table 1.

2.2.1 Climate Variables

PBLH (also called planetary boundary layer *depth*) is the height above ground level of the top of the PBL, i.e. a measure of the thickness of this layer, that is available as a diagnostic variable in ERA5. Since the PBLH can not be readily measured, it needs to be calculated from other measurements or variables. In IFS, it is computed using the bulk Richardson number (Ri_b), which is a measure of stability, and defining the PBLH as the level where Ri_b = 0.25 (ECMWF, 2017). This method follows the conclusions of Seidel et al. (2012), who evaluated methods for estimating the boundary layer height and found that an algorithm based on Ri_b (previously proposed by Vogelezang and Holtslag (1996)) is the most suitable for convective as well as stable boundary layers.

Surface sensible heat flux (SH) represents the heat transfer between the surface and the atmosphere through the effects of turbulent air motion (ECMWF, 2017). Since this project is concerned with the thermal forcing of the TP on the atmosphere rather than the other way around, the downloaded monthly mean SH was multiplied with -1 and thereby converted from the ECMWF convention "positive downwards" to "positive upwards".

Air temperature at 2 m above the surface (T2m) in ERA5 is calculated by interpolating between the lowest model level and the surface of the Earth, taking atmospheric conditions into account (ECMWF, 2017).

Total precipitation (Prc) represents the accumulated precipitation that falls to the surface. Prc is the sum of precipitation generated by large-scale weather patterns such as cold fronts or troughs, and precipitation from convection resulting from the ascent of warm air underlying colder air. After downloading the precipitation data, the units were changed from m/day to mm/day by multiplying each value with 1000. Thereafter, monthly sums were calculated by multiplying each value with the number of days in each month.

Wind is analysed in the form of wind speed at 500 hPa (WS500) as well as zonal wind (U) at the 100 and 300 hPa levels. Due to its high elevation, the 500 hPa level is close to the surface at the TP. The U component of wind is selected because the large-scale flow in the region is predominantly westerly. The zonal wind at the 300 hPa level (U300) is chosen to represent the westerly flow in the free atmosphere (i.e. above the PBL, where the effects of friction from the surface are negligible), and zonal wind at the 100 hPa level (U100) is selected because 100 hPa corresponds to altitudes where the tropopause may be found. The wind speed is calculated from the zonal and meridional wind components at 500 hPa (Equation 1).

$$WS = \sqrt{u^2 + v^2}. \tag{1}$$

The tropopause height, or pressure level, is not readily available in the ERA5 output. Instead it was calculated from hourly values of ERA5 temperature on 19 pressure levels; 20, 50, 70, 100, 125, 150, 175, 200, 225, 250, 300, 350, 400, 450, 500, 550, 600, 800 and 1000 hPa. The topmost level, 20 hPa, lies in the stratosphere at around 26-27 km height,

and the lowest level is close to the surface of the Earth. The levels were selected to obtain the full available resolution in the vicinity of the tropopause but reduce the amount of data for downloading by excluding some of the higher and lower levels. An assessment of the effect of the reduced resolution can be found in Appendix A. Since the temperature data is given on pressure levels, the tropopause values calculated here represent the pressure level at which the tropopause occur rather than its actual altitude above the ground. Since the atmospheric pressure decreases with height, low pressure corresponds to high altitude. The exact height of each pressure level depends on the atmospheric conditions at a specific time and location.

The tropopause can be defined in several ways, and different definitions often produce different tropopause heights (Pan et al., 2018). Here, two definitions are used: the LRT and the CPT. The LRT was defined according to the definition proposed by the WMO: "The first tropopause is defined as the lowest level at which the lapse rate decreases to 2°C/km or less, provided also the average lapse rate between this level and all higher levels within 2 km does not exceed 2°C/km." (World Meteorological Organization, 1957). Thus, in case of multiple tropopauses, only the lowest tropopause is accounted for here. The latter condition in the definition avoids the risk of defining a lower-level temperature inversion as the tropopause.

The LRT calculations were made using a modified version of "stattrop", the script underlying the function "trop_wmo" in the National Center for Atmospheric Research's command language NCL (The NCAR Command Language, 2017). The stattrop script was written by D. Brunner in 2000 and adapted for use within NCL by D. Shea in 2009. The trop_wmo computes the pressure at the tropopause, defined as the lowest level above 450 hPa which fulfills the WMO criterion. From the input pressure levels, the tropopause level is determined by interpolating the tropopause pressure linearly in log(pressure). In the trop_wmo code, any tropopause level that falls below 85 hPa is automatically set to 85 hPa. However, quite high tropopause altitudes (low pressure values) have been reported over the TP region. For example, Feng et al. (2011) found that when defining the tropopause using the WMO lapse rate criteria specified above, it could reach altitudes of approximately 19 km. This corresponds to around 55 hPa (depending on the atmospheric conditions). Therefore, the stattrop code, after being translated to MATLAB by D. Rayner & N. Slättberg (2019) to better fit the expertise of the author, was changed to allow a lower minimum value (55 hPa) but was otherwise kept unchanged.

The CPT is defined as the level of minimum temperature in a vertical temperature profile (Feng et al., 2011). Cubic spline interpolation was used to interpolate the tropopause pressure level from the relatively coarse input of 19 levels. A cubic spline is constructed of piece-wise third-order polynomials and returns interpolated values at a number of query points. In this case, ten query points was introduced between each input pressure level, so that the resolution of the tropopause level output is 10 times that of the input. To increase computational speed, the cold point level was first found among the 19 levels without using interpolation. Thereafter, the cold point level and the 3 levels directly above and below it were extracted and used to determine the interpolated cold point. For further details about the interpolation and the selection of the numbers of levels to include, see Appendix B.

2.2.2 Climate Indices

Climate indices of the EASM, the ISM, the NAO and the ENSO were used to assess the relationship between TP PBLH and these phenomena. To investigate spatial patterns of the associations, the time series of the indices were correlated with the PBLH at each specific grid point.

The ISM index was downloaded from the Asia-Pacific Data-Research Center of the International Pacific Research Center: `http://apdrc.soest.hawaii.edu/projects/monsoon/seasonal-monidx.html`. The ISM index is defined as the difference in zonal winds at the 850 hPa level between two regions (40-80°E,5-15°N and 70-90°E,20-30°N) as described in B. Wang et al. (2001). The ISM index spans to 2015, and therefore 2016-2018 was excluded in the correlations between PBLH and ISM.

The EASM index is defined as an area-averaged normalised seasonality of the 850 hPa wind field within the East Asian monsoon domain. The index thus utilises the strong seasonal variation of the monsoon to calculate the monsoon strength as measured by the magnitude of seasonal variation of the wind field (Jianping & Qingcun, 2003; J. Li & Zeng, 2002). It was downloaded from `http://ljp.gcess.cn/dct/page/65577`.

The ENSO has been described by several different quantitative definitions and indices. The index used here, MEI.v2, expands upon the original MEI developed by Wolter and Timlin (1993). It is the time series of the leading combined Empirical Orthogonal Function of five different variables: Sea level pressure, sea surface temperature, outgoing longwave radiation and zonal and meridional components of surface wind over the tropical Pacific. To take the seasonality of the ENSO into account and reduce the effects of intra-sesonal variability, the index is bi-monthly and thus consists of 12 overlapping "two-month seasons" (Dec-Jan, Jan-Feb, Feb-Mar, and so on). The ENSO index was downloaded from `https://www.esrl.noaa.gov/psd/enso/mei/`.

The NAO is generally quantified by indices based on variations in the sea level pressures of the Icelandic Low and the Azores High. The index used here was calculated on a basis of the Rotated Principal Component Analysis used by Barnston and Livezey (1987) applied to monthly standardised 500 hPa geopotential height anomalies. It was downloaded from the Climate Prediction Center of the National Oceanic and Atmospheric Administration (NOAA)/National Weather Service: `https://www.cpc.ncep.noaa.gov/products/precip/CWlink/pna/nao.shtml`.

In addition to the variables and indices mentioned above, there are a few additional variables (the logarithm of surface pressure, geopotential at the surface, temperature on all model levels and specific humidity on all model levels) that were not analysed but used to derive tropopause heights from the tropopause levels in a case study of a close encounter between the PBL top and the tropopause (as described in Section 2.5). Values of PV and specific humidity was also compared with temperature profiles in the aforementioned case study.

Table 1: Investigated climate variables and indices. All climate variables are derived from ERA5, but whereas the tropopause levels (LRTL and CPTL) were calculated from hourly mean atmospheric temperature and wind speed was calculated from monthly mean zonal and meridional wind components, the other climate variables are provided directly in the ERA5 output. For the climate indices, refer to the text for sources.

Climate variable	Abbreviation	Note (unit)
Planetary Boundary Layer Height	PBLH	Height above ground (m)
Surface Sensible Heat Flux	SH	Positive upwards (W/m^2)
Air Temperature at 2 m height	T2m	(K)
Total precipitation	Prc	(mm)
Wind Speed at the 500 hPa level	WS500	(m/s)
U component of wind at the 300 hPa level	U300	Zonal wind (m/s)
U component of wind at the 100 hPa level	U100	Zonal wind (m/s)
Lapse Rate Tropopause Level	LRTL	Pressure level (hPa)
Cold Point Tropopause Level	CPTL	Pressure level (hPa)
Climate index	**Abbreviation**	
Indian Summer Monsoon index	ISM	
East Asian Summer Monsoon index	EASM	
El Niño Southern Oscillation index	ENSO	
North Atlantic Oscillation index	NAO	

2.3 Temporal and Spatial Averaging

The data analysed in this project covers the period 1979-2018. ERA5 variables were downloaded with a monthly resolution except the tropopause levels, which was calculated from temperature with an hourly resolution, and PBLH, for which hourly data was analysed in a few regions (Figure 3) in addition to the monthly analyses. For seasonal analyses the monthly mean data were split into a dry season extending from October to April and a monsoon season spanning from May to September. The division was based on the plateau-wide average seasonal distribution of precipitation (Figure 13 C). Since the dry season always spans over two consecutive years, there are 39 full dry seasons and thus 39 time steps for the dry season while there are 40 for the monsoon season. For precipitation, the monthly means were converted to monthly sums prior to averaging over seasons. Seasonal precipitation means thus represent the mean monthly sum for the season in question. The bi-monthly ENSO index was divided into the dry and monsoon seasons as following: Each dry season consists of the values for Oct-Nov, Nov-Dec, Dec-Jan, Jan-Feb, Feb-Mar and Mar-Apr, while each monsoon season encompasses May-Jun, Jun-Jul, Jul-Aug and Aug-Sep.

The ERA5 data are given in Coordinated Universal Time (UTC). For the plots based on sub-daily values (PBLH diurnal cycles and the PBLH-LRTH case study), local time was calculated by adding $\text{lon}/360 \times 24$ (where lon is the longitude on which the region is centred and 360 represents the degrees of longitude around the Earth) and rounding to the nearest whole number.

The TP is defined here as the region which lies within 70 °E - 105 °E and 27 °N - 40 °N and has an altitude of more than 3000 m above sea level, following e.g. Kukulies, Chen, and Wang (2019). In order to obtain the specific elevation data with which the ERA5 data were produced, the altitudes were calculated by dividing the ERA5 parameter surface geopotential with the gravitational acceleration (g = 9.80665). Thus, the altitude here is

surface *geopotential* height.

Within the TP, two sub-regions were selected for analysis of PBLH with hourly resolution (Figure 3). The selection was based on spatial characteristics of the PBLH trend (Figure 5) using the following criteria: The central TP (CTP) region has a negative monsoon season trend which is stronger than 40 m/decade and significant at the 95% level. The southeastern TP (SETP) region has a positive dry season trend and is located east of 95 °E, south of 33 °N. The reason why the selection of the SETP region excludes values outside a certain geographical area is that the pattern of trends in the SETP region was not as spatially coherent and well defined as in the CTP region. In addition, a third region (labelled C in Figure 3) was selected for analysis of PBLH and tropopause height during a short period, as described in Section 2.5.

Spatial averages across regions were calculated using Climate Data Operators (CDO) "fldmean" which uses area weights derived from the grid cell area to account for the differences in grid cell size between different latitudes (Schulzweida, 2019).

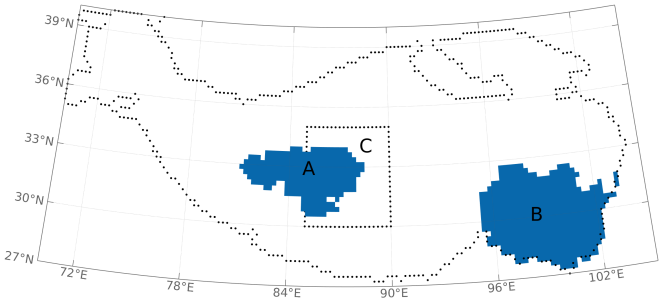

Figure 3: Tibetan Plateau (TP) regions for hourly analysis. The central TP region (A) and the southeastern TP region (B) were selected on a basis of differing characteristics of the Planetary Boundary Layer Height (PBLH) for hourly analysis of PBLH. The region indicated by the box (C) was selected because of its overlap of high planetary boundary layer and low tropopause. For this region, hourly PBLH and lapse rate tropopause height was investigated for a short period.

2.4 Statistical Methods

The data were analysed with the standard statistical methods described below. Statistical analyses and plotting was mainly performed using MATLAB (The MathWorks, 2018-2019).

2.4.1 Linear Regression

Linear regression was used to calculate trends. The regression model is shown in Equation 2

$$y = \beta_0 + \beta_1 x + \varepsilon \tag{2}$$

where y is the climate variable, β_0 is the y intercept (the value of y when the predictors are zero), β_1 is the slope coefficient for the predictor variable x (time) and the error factor ε is a stochastic variable (noise). The resulting slope coefficients thus indicate the strength and direction of the trend. Trends that were found to be within the 95% confidence interval

are denoted as statistically significant.

2.4.2 Linear Correlation

Linear correlation (Equation 3) was used to assess statistical relationships between different climate variables as well as between climate variables and climate indices.

$$r = \frac{\Sigma(x_i - \bar{x})(y_i - \bar{y})}{(\Sigma(x_i - \bar{x})^2(y_i - \bar{y})^2)^{1/2}} \tag{3}$$

In Equation (3), r is Pearson's correlation coefficient (a measure of the degree of linear relation between x and y) and $\bar{x}$ and $\bar{y}$ are the average of the observations of x and y, respectively. For PBLH and the other climate variables the correlations were calculated for each point in the gridded data, resulting in maps where the correlation coefficient at each point represent the correlation between the PBLH and the other climate variable at this particular point. The climate indices however are single time series which are not representative of a specific point. These index time series were therefore correlated with PBLH at each point, producing maps in which each point represent the correlation between the PBLH time series for this particular point and the single climate index time series. Following convention, correlations are denoted as statistically significant if the probability value p is smaller than 0.05, i.e., the correlation is significant at the 95% confidence level.

Correlations were also performed on data from which the linear trend had been removed, in order to be able to assess whether the correlated variables were primarily correlated in trend or in inter-annual variability. The detrending was calculated by removing the best straight-fit line (the line that best minimises the sum of the squares of the residuals) from the data. In addition, non-linear correlation (Spearman's rank correlation) was performed between PBLH and the other climate variables (although not the indices), but was excluded from the results because of the small differences between Pearson's and Spearman's correlation coefficients.

2.4.3 T-test and Planetary Boundary Layer Height in Relation to Notable Indices Values

The climate indices (ISM, EASM, ENSO and NAO) were further compared to PBLH through an assessment of PBLH differences between years when these indices had high values and years when they had low values. For each climate index, the upper and lower quartiles (Q3 and Q1) were counted as strong/positive years and weak/negative years, respectively. That is, for each respective index, Q3 consists of all values $\geq$ the 75th percentile, Q1 consists of all values $\leq$ the 25th percentile. These percentiles were derived from the mean June-August values for the monsoon indices, and for the monsoon and dry season for the ENSO and NAO indices. The Q3 and Q1 for each index consists of 10 values each, except for the somewhat shorter ISM time series for which there is only 9 values.

The PBLH corresponding to the Q3 and Q1 of each index was compared to see if there were consistent differences in PBLH when a particular index was strong and when the same index was weak. For this purpose, a paired sample t-test was performed. The t-test returns a test decision stating whether or not the null hypothesis can be rejected at a given significance level (95%). The null hypothesis states that there is no difference in the population of PBLH between the Q3 cases and the Q1 cases for a given index. Or, more formally, the null hypothesis states that the data in PBLH(Q3) – PBLH(Q1) comes from a normal distribution with mean = zero and unknown variance.

2.5 Tropopause Heights in a Small Region

Previous research indicates that the TP PBLH can reach very high in the cold season, which is when the tropopause reaches its seasonal minimum height, and that the short vertical distance between the PBL top and the tropopause facilitates exchanges between the troposphere and stratosphere (X. Chen et al., 2013). To be able to see how close to the tropopause that the PBL may actually reach, hourly tropopause heights were therefore calculated and compared with PBLH. Due to the large size of the data, the tropopause analysis is only performed for the LRT (since the CPT is generally higher) and only for a small region and short period which were selected from the monthly data using the criterion LRTL $>$ 260 hPa and PBLH $>$ 1600 meter as a means to find time steps and grid points were low tropopause and high PBL overlap. The criterion was true for January 2008, at 87.5°E, 32.5°N. To be able to catch some of the spatial variability between nearby grid cells, data was downloaded for a small region around this point (85-90°E, 30-35°N, Figure 3).

The LRTL was calculated using the modified version of the stattrop as described above. LRT height (LRTH) was then derived from the LRTL in order to be able to investigate the distance between the PBL top and the tropopause. For this purpose, the logarithm of surface pressure, geopotential at the surface and temperature as well as specific humidity on all vertical levels were used to obtain the geopotential for each vertical level at the selected grid points and time steps. The geopotential was then divided with the gravity constant (g = 9.80665) to obtain the height of each level in metres. Using these data, the height of each calculated LRTL could be found. The scripts for downloading the required data and calculating the heights were modified from ECMWFs example python scripts which are freely available at `https://confluence.ecmwf.int/display/CKB/ERA5%3A+compute+geopotential+on+model+levels`. The calculation was performed on the 137 model levels rather than the pressure levels utilised in the rest of this project. This allows more accurate representation of the tropopause heights, and that the scripts made available by ECMWF could be downloaded and used without the need for translating the model levels into corresponding pressure levels.

3 Results and Discussion

In the following sections, the results are presented and discussed. The first part (Section 3.1) constitutes a PBLH climatology while the second part (Section 3.2) explore the connections with other climate variables in order to find explanations for the PBLH variations.

3.1 Planetary Boundary Layer Height Climatology

The following sections deal with spatiotemporal variations in TP PBLH. First the time series and seasonal cycles (Section 3.1.1) as well as spatial patterns (Section 3.1.2) for the entire plateau are considered. Thereafter special attention is given to two regions with very different inter-annual, seasonal and diurnal PBLH characteristics (Section 3.1.3).

3.1.1 Tibetan Plateau-Average Planetary Boundary Layer Height

The seasonal cycle, calculated from monthly mean PBLH averaged across the TP, is displayed in Figure 4 A. The monthly mean PBLH is greatest in spring and early summer, when the median of all the years in the period reaches well over 600 m above ground. The maximum monthly value (879 m) is found for March 1985, although the highest median

values are found in May and June. The spread among the individual years, reflected in the interquartile range (the 75th percentile minus the 25th percentile) as well as the extreme values, is considerably larger during the dry season than during the monsoon season. The overall seasonal pattern of PBLH is somewhat similar to previous studies, even though the monthly means used here can not be directly compared to the sub-daily values in e.g. X. Chen et al. (2016), which are not averaged over time or space like the values here. Still, the presence of high PBLs in late winter and early spring found in e.g. X. Chen et al. (2016) can be discerned here in the extreme values reaching their maximum in March.

The inter-annual variation and linear trends in TP PBLH are shown for the monsoon season (dashed, purple line), the dry season (dash-dotted, blue-green line) and for the annual means (solid, black line) in Figure 4 B. The year-to-year variability is considerable, especially for the dry season. A notable peak occurs in 1984-1985 and a large dip is seen for the dry season 1997-1998. The seasonal means display trends of roughly equal size but opposite directions - the monsoon season PBLH decreases with 5.3 m per decade while the dry season PBLH increases with 6.6 m per decade. The annual means exhibit a weak upward trend of 0.9 m per decade. None of the trends are statistically significant at the 95% level.

J. Guo et al. (2019) found that the sign of PBLH trends at some stations in the TP region had shifted from positive to negative around 2004, while M. Wang et al. (2019) in contrast found that the trends in SH - which is strongly correlated with PBLH - shifted from negative to positive around 2000. Trends were therefore calculated separately for the first and second half of the PBLH time series. For the monsoon season, the trend is 10 m per decade during the first 20 years and -0.4 m per decade during the latter 20 years. The dry season PBLH in contrast has a trend of -28 m per decade in the first half and a positive trend of 17 m per decade during the second half. In the annual means, the half-period trends are -12 and 4.5 m per decade, respectively. It thus appears that the PBLH trends indeed change sign during the investigated period. It can also be noted that their direction during the half-periods depends on the season, so that the behaviour of the monsoon season trend resembles the shift from increasing to decreasing PBLH found by J. Guo et al. (2019) while the dry season shift from decreasing to increasing rather resembles what may be expected from the shift in SH found by M. Wang et al. (2019).

However, a few remarks can be made here. First, none of the half-period trends found here are statistically significant, and at least for the second half-period of the monsoon season trend, the magnitude is very small. Moreover, the time span is very short, which means that individual years with extreme values have a large influence on the trend. It can be questioned if it makes much sense to calculate trends over a 20 year period within a time span of just 40 years. Lacking data further back in time, there is no clue to the average size of the PBLH variability on decadal time scales, and therefore no way of telling whether any "shift" seen here indicates a longer term change in the PBLH trend.

To summarise the main features of the PBLH variations explored here, it can be stated that the monthly mean PBLH is greatest during spring and summer and generally reaches its annual peak in June, although the larger inter-annual difference during the dry season allows for the individual greatest monthly mean PBLH in the entire 1979-2018 period to be found in March. Trends differ between seasons and between the first and second half of the period. When considering the full time span, the decreasing monsoon season trend and the increasing dry season trend result in a weak positive trend in the annual means. However, none of the trends are statistically significant.

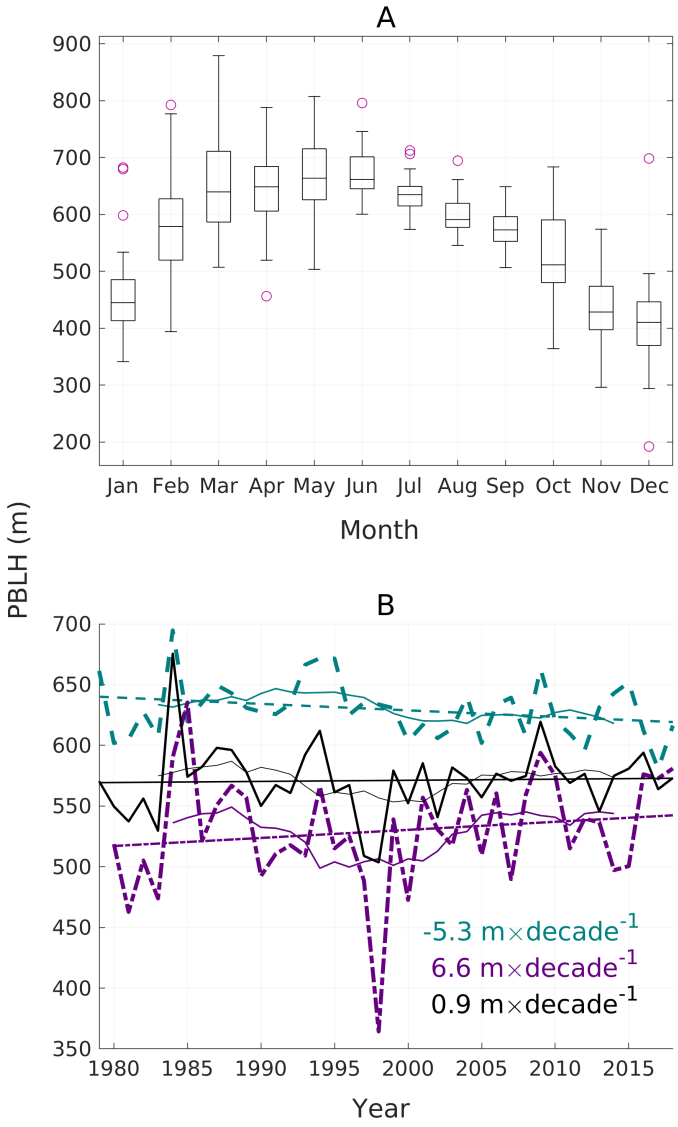

Figure 4: Tibetan Plateau (TP) Planetary Boundary Layer Height (PBLH). A: Seasonal Cycle. For each month, summary statistics of the monthly mean 1979-2018 PBLH are displayed. Each box gives the median (central line in each box), the 25th percentile (bottom of each box), the 75th percentile (top of each box), the most extreme value that is not considered an outlier (the "whiskers", i.e. black lines above and below boxes) and possible outliers (pink circles). Outliers are values more than 1.5 times the interquartile range (the 75th percentile minus the 25th percentile) away from the top or the bottom of the box. **B: Annual time series with trends.** Mean PBLH, running 9 year average and linear trends are shown for the monsoon season (dashed blue-green line), the dry season (dash-dotted purple line) and the full year (solid black line). The values of the linear trends are given in the bottom right corner. None of the trends are significant at the 95% level. All values in A and B are spatially averaged across the entire TP.

3.1.2 Spatial patterns in Planetary Boundary Layer Height

How does the PBLH and its trends vary across the vast plateau? The mean 1979-2018 PBLH and the linear trend are displayed for each grid cell in the TP region in Figure 5. In addition to the seasonal means and trends, the annual values are included in order to show the result of the combined seasonal contributions.

In the left column of Figure 5, the mean PBLH is shown for the monsoon season (A), the dry season (B) and the annual means (C). For both seasons, the greatest PBLH is found in the central plateau and the lowest PBLH along its rims. The contrast between regions with great and small PBLH, respectively, is most pronounced in the dry season (Figure 5 B). The interior of the plateau, where the greatest PBLHs are found, overall has a higher elevation than the rims and the western and eastern parts. However, the PBLH differences *within* this region does not suggest that PBLH increases with height. Rather, there is a tendency for higher PBLH where the elevation is lower. For example, there is a pronounced region of lower PBLH in the northwestern TP in the monsoon season which is co-located with a high-elevation area which is likely to be at least partly glaciated (for elevation see Figure 1, for glacial extent, albeit not in ERA5, see Yao, Thompson, Yang, et al., 2012, their Figure 1). The low PBLH in this region could be a result of cold conditions and low surface sensible heat fluxes related to the high elevation and the presence of snow and ice.

In the right column of Figure 5, the trends are shown for the monsoon season (D), the dry season (E) and the annual means (F). Black stripes are drawn over regions for which the trend is not significant at the 95% level. The perhaps most striking feature of the trends is a large region of statistically significant decreasing monsoon season trends in the central plateau. In this region, which is largely overlapping with the area in which the means are the highest, the strongest trends reach up to around -65 m per decade (Figure 5 D). The dry season PBLH trend in contrast is largely positive in this region, albeit statistical significance is lacking. In fact, within the TP, statistical significance for the dry season trends can only be discerned in small, scattered regions, some of which are present in the monsoon season as well as smaller regions of positive trend in the western and eastern TP. For the dry season, the most pronounced such regions display positive trends of up to around 70 m per decade and are mainly found in the southeastern plateau (Figure 5 E). Some of these regions of statistically significant positive trends are visible in the annual means, in which the central TP region monsoon season decline can also be discerned, although non-significant (Figure 5 F).

In summary, the PBLH is greater in the interior of the TP and lower toward its rims in both seasons. The monsoon season trend is dominated by a large region of significantly decreasing PBLH in the central TP while the dry season exhibits only smaller regions of significant trends, which are mostly positive.

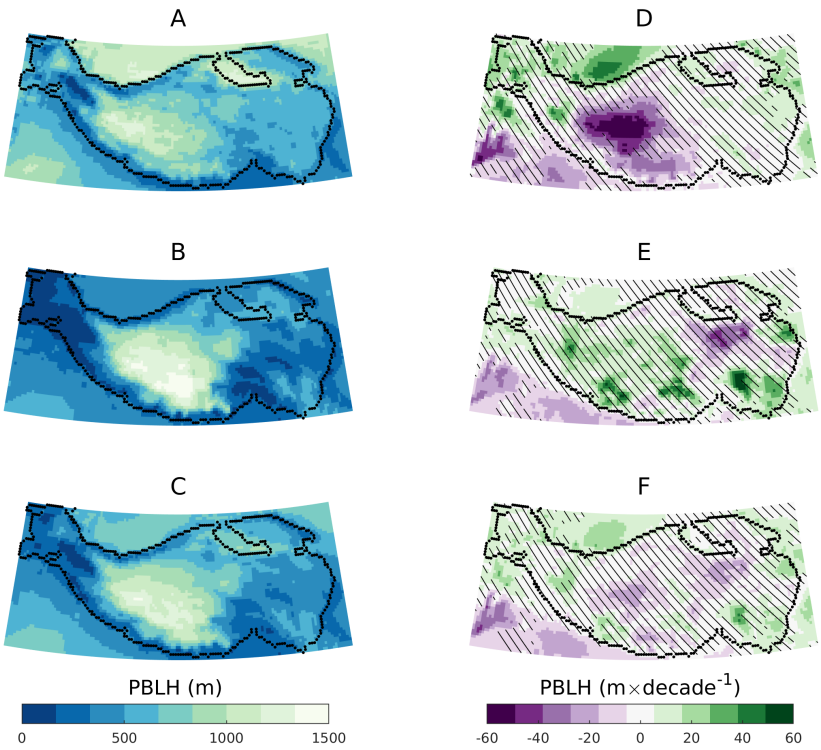

Figure 5: 1979-2018 mean (left column) and linear trends (right column) in Planetary Boundary Layer Height (PBLH). A: Monsoon season (May-September) mean PBLH, given in metres above ground level. **B:** As A, but for the dry season (October-April). **C:** As A, but for annual mean PBLH. **D:** Linear trend in monsoon season mean PBLH, given in metres per decade. The thin lines mark areas for which the trend is *not* statistically significant at the 95% level. **E:** As in D, but for the dry season. **F:** As in D, but for annual mean PBLH.

3.1.3 A comparison Between a Central and a Southeastern Tibetan Plateau Region

As seen in the previous sections, characteristics of the TP PBLH varies greatly over time and space. Therefore, the seasonal cycles, trends and diurnal cycles of two different regions will be compared in the following section. The two regions were selected on a basis of the spatial distribution of PBLH trends as described in Section 2.3 and their areal extent is shown in Figure 3.

3.1.3.1 Seasonal cycles In the CTP region, the seasonal PBLH cycle has a pronounced peak in spring, with its highest median (about 1600 m) in April and the highest extreme in March (Figure 6 A). Thereafter the PBLH declines to reach its seasonal minimum in August, when the median lies around 680 m. A second and lower seasonal peak is reached in October, thereafter the median declines slightly before starting to rise in January. X. Chen et al. (2016) investigated the seasonal cycle of PBLH in ERA-Interim, for the grid point nearest to a measurement station located at 84.03°E, 32.17°N, which is within the CTP region. The heights are not directly comparable since their data is not spatially averaged, and because they use daily values for 14:00 and 20:00 rather than monthly means. Still, the

patterns of seasonal variability are similar. The median PBLH in X. Chen et al., (2016, their Figure 1) also peaks in April and then decreases until August. Their second and smaller peak, however, is found in September rather than October, and their minimum median is found in December.

In the SETP region, the greatest values are found in the monsoon season, throughout which the median PBLH lies around 500 m (Figure 6 B). The seasonality in the spread is more pronounced for the SETP region, which has considerably smaller interquartile ranges and variation in extremes during the monsoon season (except May, which has the highest maximum) than during the dry season.

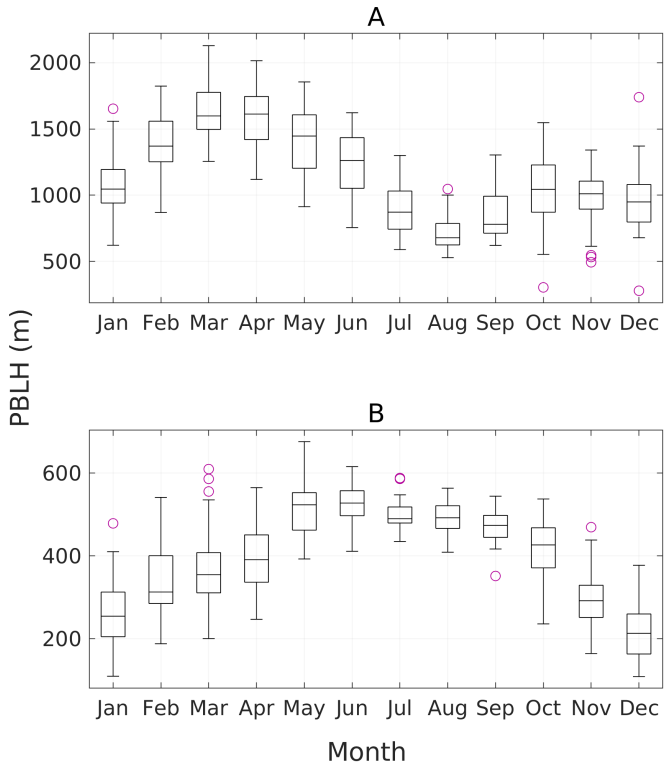

Figure 6: Seasonal Cycles in two different Tibetan Plateau (TP) regions. A: Seasonal Cycle in the central Tibetan Plateau region. For each month, summary statistics of the monthly mean 1979-2018 PBLH are displayed. Each box gives the median (central line in each box), the 25th percentile (bottom of each box), the 75th percentile (top of each box), the most extreme value that is not considered an outlier (the whiskers) and possible outliers (pink circles). Outliers are values more than 1.5 times the interquartile range away from the top or bottom of the box. **B**: As A, but for the southeastern TP region.

3.1.3.2 Time series and trends Figure 7 shows the time series and linear trends of spatially averaged PBLH in the two regions. The 1997-1998 dry season dip that was found in the time series for the entire plateau is present for the CTP region but not discernible for the SETP region. The trends also differ: Region A features a statistically significant negative monsoon season trend of 51 m per decade and a non-significant positive dry season trend of

13 m per decade. Together the seasonal contributions result in an annual (non-significant) trend of 13 m per decade. Region B in contrast has a positive non-significant monsoon season trend of just 2 m per decade and a positive, statistically significant dry season trend of 18 m per decade. The annual mean trend is a statistically significant increase of 10 m/decade. The directions of the seasonal trends thus resembles what can be expected for these regions from the trend maps in Figure 5 D, E and F.

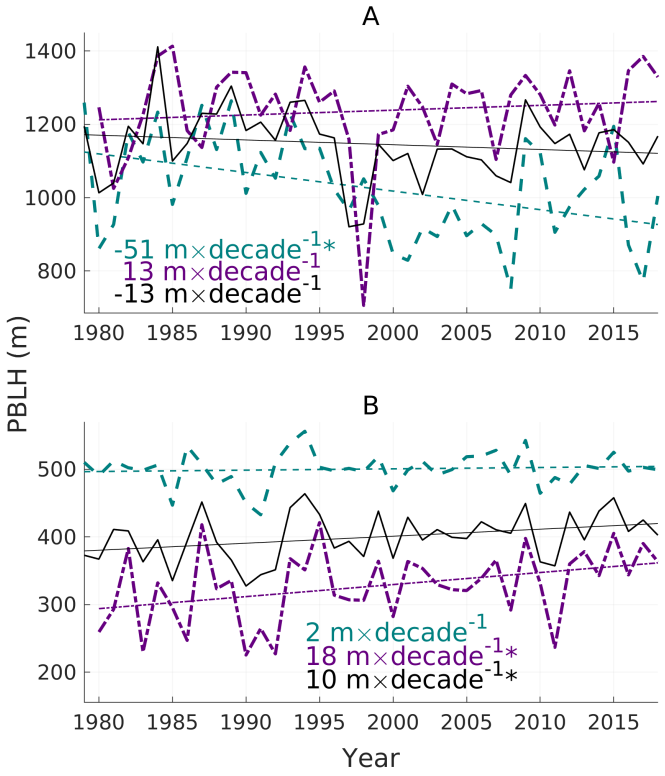

Figure 7: Time series and trends of Planetary Boundary Layer Height (PBLH) in two Tibetan Plateau (TP) regions. A: Central TP mean PBLH and linear trend lines for the monsoon season (blue-green dashed lines), the dry season (purple dash-dotted lines) and the full year (black solid lines). The values of the linear trends are also given in the plot, a star indicates significance at the 95% level. **B:** As, A, but for the southeastern TP region.

3.1.3.3 Diurnal cycles To see how the PBLH may vary across the day in different parts of the plateau, diurnal cycles for spatially averaged PBLH in the central and southeastern TP regions are plotted in Figure 8 and Figure 9, respectively. These are shown for both seasons, but the annual mean diurnal cycles, which were relatively similar to the seasonal mean diurnal cycles, are not included.

In the CTP region, the afternoon (local time) PBL can reach extremely high in both seasons, with outliers above 6 km. In fact, without the spatial averaging, individual grid points features even higher PBLH, over 7.5 km (not shown). In the monsoon season, the median PBLH in the region stays above 2 km from 13.00 to 17.00, with a few outliers reaching above 6 km in the late afternoon (Figure 8 A). Thereafter if falls, with the median reaching only around 100 m in the early morning. In the dry season, the median reaches above 3 km in

the afternoon, and extreme values around 5-6 km are more common than in the monsoon season (Figure 8 B). The lowest daytime values are also lower in the dry season, in some cases the PBLH is just a few hundred m even in the afternoon hours, indicating that the variability is higher in the dry season. Nighttime median values are relatively low in both seasons, but the spread is larger in the dry season, when individual nighttime values can reach well above 2 km despite the low median. The annual means include both seasons and therefore shows the extreme values of both, while the medians resemble the dry season median more closely than the monsoon season median (not shown).

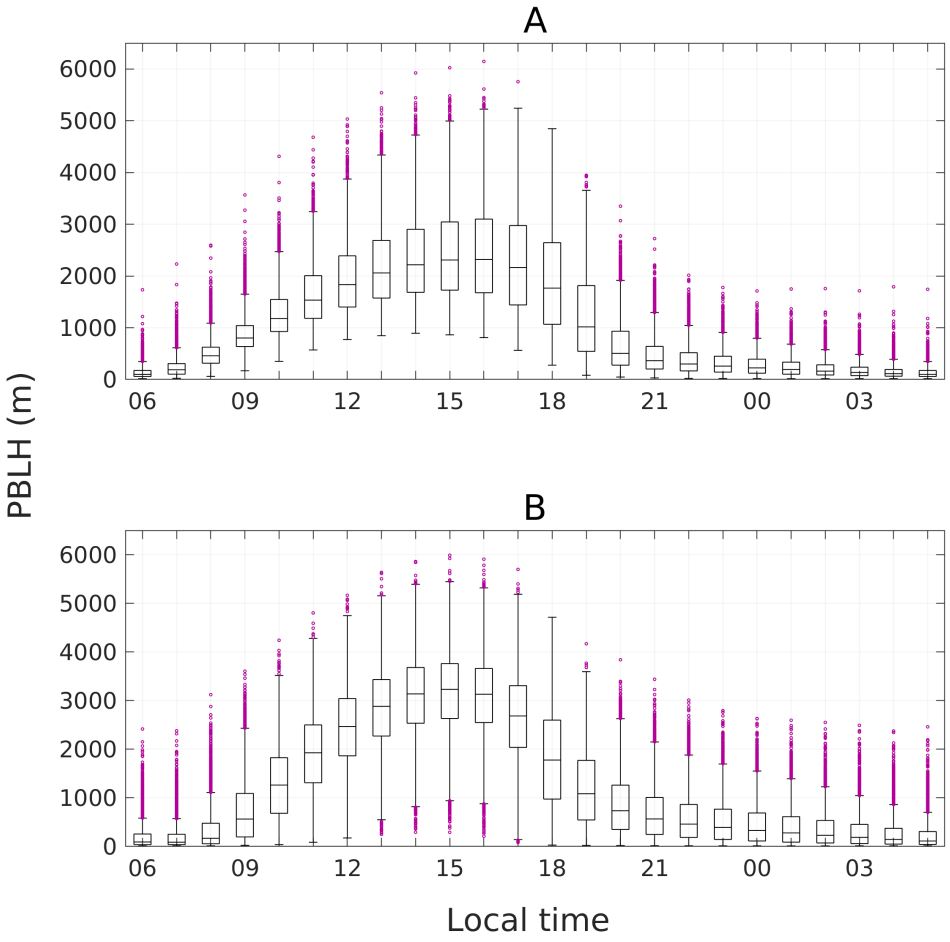

Figure 8: Diurnal Cycles of Planetary Boundary Layer Height (PBLH) in a Central Tibetan Plateau (CTP) region. Summary statistics of 1979-2018 PBLH is shown for each hour of the day (in local time, valid at the centre of the region). The boxes give the median (central line in each box), the 25th percentile (bottom of each box), the 75th percentile (top of each box), the most extreme value that is not considered an outlier (the whiskers) and possible outliers (pink circles). Outliers are values more than 1.5 times the interquartile range away from the top or bottom of the box. **A:** Monsoon season. **B:** Dry season.

In the SETP region, the PBL does not reach nearly as high. Afternoon median values (local time) reach up to around 1.2 km during the diurnal peak at 14:00 in the monsoon season (Figure 9 A) and barely 1 km during the diurnal peak at 15:00 in the dry season (Figure 9 B). The greatest maximum value lies around 2.5 km in the dry season and a few hundred m higher in the monsoon season. Night-time values lie around 100 m in the monsoon season and below 50 m in the dry season. Annual medians vary from around 50-60 m in the night to around 1.1 km in the afternoon (not shown).

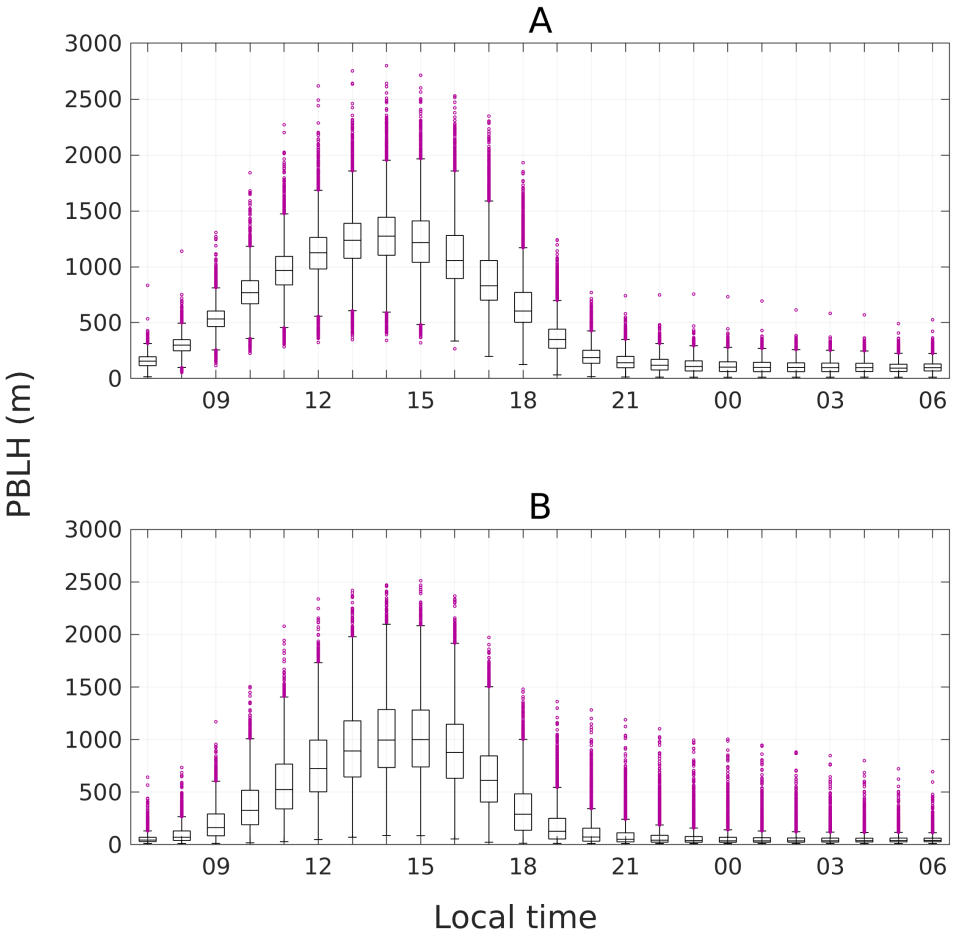

Figure 9: Diurnal Cycles of Planetary Boundary Layer Height (PBLH) in a Southeastern Tibetan Plateau (SETP) region. Summary statistics of 1979-2018 PBLH is shown for each hour of the day (in local time, valid at the centre of the region). The boxes give the median (central line in each box), the 25th percentile (bottom of each box), the 75th percentile (top of each box), the most extreme value that is not considered an outlier (the whiskers) and possible outliers (pink circles). Outliers are values more than 1.5 times the interquartile range away from the top or bottom of the box. **A:** Monsoon season. **B:** Dry season.

Increasing PBLH through the morning hours and peak heights in the afternoon as found for both the CTP region and the SETP region is the general pattern that can be expected

in response to the solar cycle. Direct comparisons with previous studies is difficult given differences in location, temporal data coverage, PBLH calculation method etc. Still, it can be noted that the diurnal patterns of variation are somewhat in agreement with K. Yang et al. (2004) who found that the PBLH (estimated for 11 rain free days in June) increases rapidly during mid-morning to mid-afternoon and stabilises in the late afternoon.

As for the heights themselves, K. Yang et al. (2004), whose study area is located between the CTP region and the SETP region, found peak values of 3 km around 15.00 (local standard time). This is much lower than the high extremes in the CTP region in both seasons, but higher than the monsoon season median reaches. In the SETP region, 3 km PBLH is never reached. PBLH in the CTP region can also be compared to X. Chen et al. (2016), who found that PBLs at 19:00 exceeded 4 km for 9 out of 24 soundings during their observation period (25th February to 19th March 2008) at a radiosonde station in the CTP region. Their measurements were taken at 19:00 Beijing standard time, which corresponds to 17.00 in local time as calculated here. For the dry season, the spatially averaged PBLH at 17:00 exceeds 4 km on 600 occasions, which gives a frequency of about 15 times per season on average. PBLs above 4 km thus appear to be less common than in the study by X. Chen et al. (2016), but again, it should be noted that a single-point measurement is not directly comparable with a spatial average.

3.1.4 Climatology Summary

As shown in the previous sections, TP PBLH exhibits great variability over time and space. In agreement with previous studies the PBL may reach very high, although the heights greatly depend on time and location. The central plateau features the greatest PBLH, especially in spring. The direction and magnitude in trends differ much between regions and seasons, resulting in a very weak TP-average annual trend. A common feature of TP PBLH is the tendency for higher variability during the dry season. In the next part of this thesis, potential reasons behind the PBLH characteristics explored here are examined.

3.2 Connections with Climate Variables

In the following sections, PBLH is compared to other climate variables in order to explain the PBLH variations that are displayed in the previous sections. First the TP-average PBLH time series is analysed along with the other climate variables (Section 3.2.1) and thereafter the seasonal cycles are investigated (Section 3.2.2). Spatial patterns in correlations (Section 3.2.3) as well as means and trends (Section 3.2.4) in the climate variables are then examined in order to find potential reasons behind the spatial PBLH variations. Thereafter, PBLH and LRT is analysed for a short period in a small region and the possibility of stratosphere-troposphere exchanges is discussed (Section 3.2.5). Finally, PBLH is analysed in relation to the climate indices for ISM, EASM, NAO and ENSO (Section 3.2.6).

3.2.1 Time Series and Correlations

To what extent may the TP-average PBLH be affected by variations in the investigated climate variables? In order to answer this question, PBLH is plotted along with each of the other variables, and correlations are computed between the time series of PBLH and the climate variables.

For the monsoon season, significant correlations are found for Prc (-0.44), WS500 (0.41) and U300 (0.40) (Figure 10 C, D and F). U100 shows a non-significant correlation of 0.28

(Figure 10 F). The correlation with SH is of a similar size (0.27, not statistically significant) which is surprisingly low given the supposedly large influence of SH on TP PBLH. Performing the correlation on detrended PBLH and SH however yields a significant correlation of 0.36. The low correlation for the non-detrended data may therefore be mainly due to the differences in trend or multi-year variability, which appears to be very pronounced from the 1990s and onward (Figure 10 A). The remaining correlations are close to zero: Correlation with T2m is -0.08, and again the longer term variation diverge in the 1990s as the T2m continues climbing upwards during a period when PBLH decreases (Figure 10 B). Correlations with the tropopause levels LRTL and CPTL are -0.05 and 0.03, respectively (Figure 10 G and H).

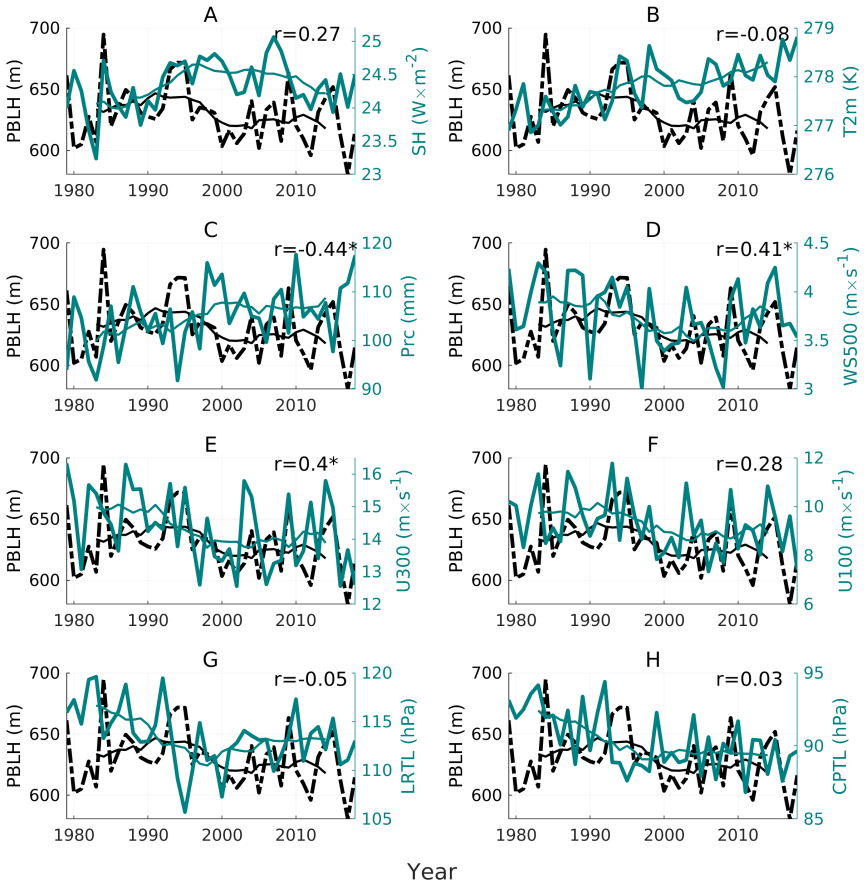

Figure 10: Monsoon season time series for Tibetan Plateau (TP) Planetary Boundary Layer (PBLH) and selected climate variables. TP-average PBLH (left axes, black dash-dot lines) is plotted along with the climate variables (right axes, blue-green solid lines). The thin lines show the 9 year moving average. The correlation between the PBLH and each climate variable is given in the top right corner of each subplot, stars denote correlations that are statistically significant at the 95% confidence level. **A**: Sensible Heat flux (SH), **B**: 2 meter air temperature (T2m), **C:** Precipitation (Prc), **D**: Wind Speed at the 500 hPa level (WS500), **E**: Zonal wind component at the 300 hPa level (U300), **F**: Zonal wind component at the 100 hPa level (U100), **G**: Lapse Rate Tropopause Level (LRTL) and **H**: Cold Point Tropopause Level (CPTL).

In the dry season, all climate variables except Prc are significantly correlated with PBLH (Figure 11). In particular the correlation with SH is very high (0.82), and both shorter and longer term variations are similar to those of PBLH (Figure 11 A). T2m is also quite highly correlated with PBLH (0.69), although its 9 year moving average is quite dissimilar to that of PBLH during the first half of the period (Figure 11 B). The wind variables are positively correlated with PBLH (Figure 11 D, E and F) and the strongest correlation among them is found for U300 (0.61). Their inter-annual variability is somewhat larger than in the monsoon season. It is therefore conceivable that the seasonal differences in wind speed variability may play a role for the seasonal differences in PBLH variability. The tropopause levels are anticorrelated with PBLH, indicating that the heights are positively correlated (Figure 11 G and H). This is perhaps not because PBLH and tropopause heights affect each other, but likely due to the fact that conditions favouring high PBLs may also favour high tropopauses and vice versa. For example, Feng et al. (2011) suggests that LRTH above the TP is related to the thermal forcing from the plateau. However, it can be noted that while they did not see a similar effect on the height of the CPT, the correlation with CPTL is stronger than the correlation with LRTL in Figure 11.

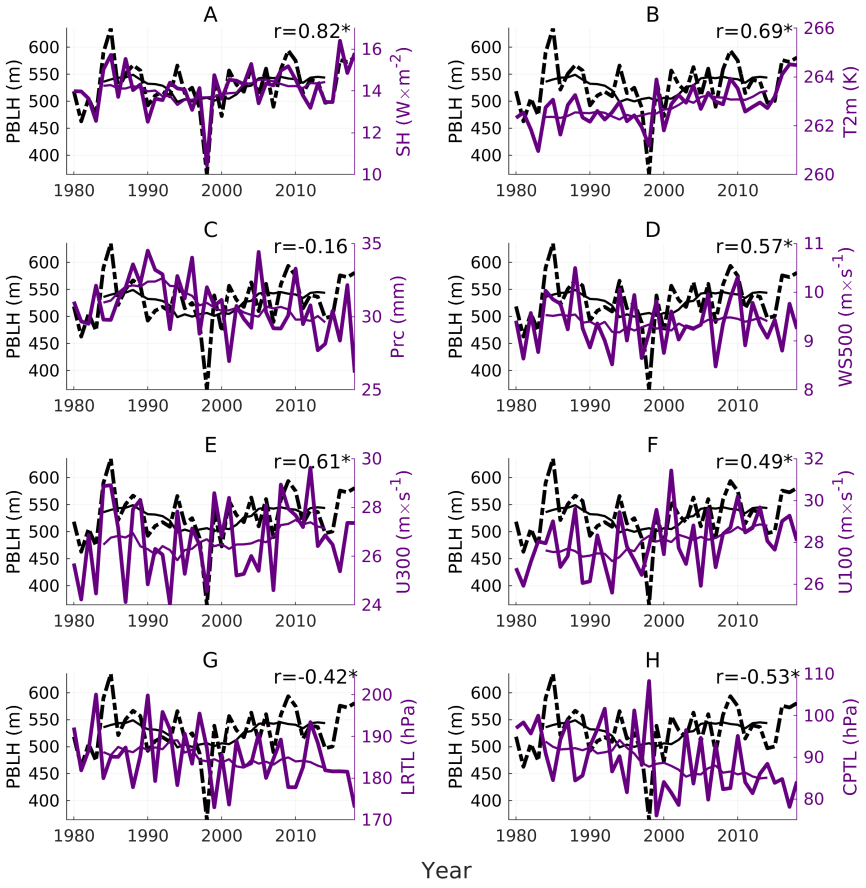

Figure 11: Dry season time series for Tibetan Plateau (TP) Planetary Boundary Layer (PBLH) and selected climate variables. TP-average PBLH (left axes, black dash-dot lines) is plotted along with the climate variables (right axes, purple solid lines). The thin lines show the 9 year moving average. The correlation between the PBLH and each climate variable is given in the top right corner of each subplot, stars denote correlations that are statistically significant at the 95% confidence level. **A**: Sensible Heat flux (SH), **B**: 2 meter air temperature (T2m), **C:** Precipitation (Prc), **D**: Wind Speed at the 500 hPa level (WS500), **E**: Zonal wind component at the 300 hPa level (U300), **F**: Zonal wind component at the 100 hPa level (U100), **G**: Lapse Rate Tropopause Level (LRTL) and **H**: Cold Point Tropopause Level (CPTL).

The correlation for the annual means appear to be more influenced by the dry season than the monsoon season, perhaps because of the stronger dry season correlations, or because the dry season encompasses 7 months and the monsoon season only 5 months. All variables are significantly correlated with PBLH except Prc and CPTL (although the correlation with CPTL is significant when performed on detrended data) and the strongest correlation is found for WS500 (0.69).

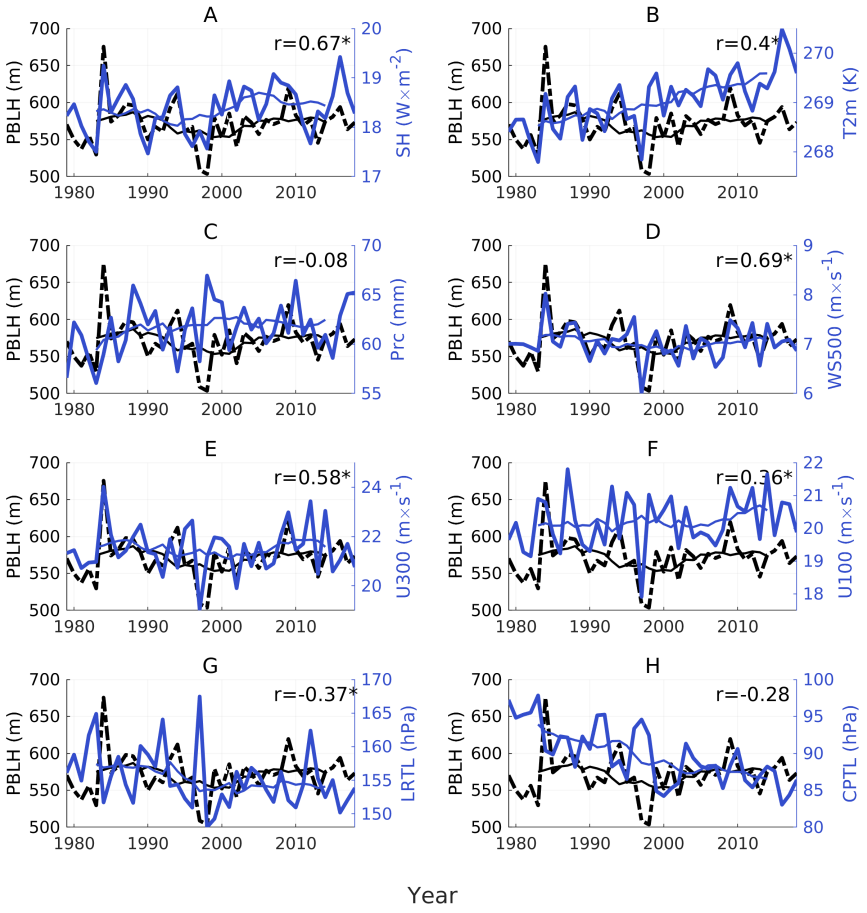

Figure 12: Annual mean time series for Tibetan Plateau (TP) Planetary Boundary Layer (PBLH) and selected climate variables. TP-average PBLH (left axes, black dash-dot lines) is plotted along with the climate variables (right axes, blue solid lines). The thin lines show the 9 year moving average. The correlation between the PBLH and each climate variable is given in the top right corner of each subplot, stars denote correlations that are statistically significant at the 95% confidence level. **A**: Sensible Heat flux (SH), **B**: 2 meter air temperature (T2m), **C:** Precipitation (Prc), **D**: Wind Speed at the 500 hPa level (WS500), **E**: Zonal wind component at the 300 hPa level (U300), **F**: Zonal wind component at the 100 hPa level (U100), **G**: Lapse Rate Tropopause Level (LRTL) and **H**: Cold Point Tropopause Level (CPTL).

In summary, WS500 and U300 are the only variables here that are significantly correlated with PBLH in both seasons. In addition, SH and T2m are significantly correlated for the dry season and the annual means, while Prc is significantly anticorrelated in the monsoon season. These results indicate that wind speed may play a large role in both seasons, while the influences of SH, T2m and Prc may have a more pronounced seasonal dependency. Still, the correlation with detrended SH is significant for the monsoon season as well, indicating that it is relatively important in both seasons.

3.2.2 Seasonal Cycles

In order to assess the seasonal variation of PBLH in relation to that of the other climate variables, the seasonal cycles of each variable was plotted along with PBLH for the whole TP as well as the CTP and SETP regions. It should be kept in mind that all variables examined here vary with the seasons, and that their variation is ultimately determined by a common factor: the seasonal variation in incoming solar radiation as the tilted Earth orbits the sun. However, given the interplay among these variables and their effects on PBLH, a comparison of their seasonal cycles may offer some clues to the PBLH variations.

3.2.2.1 TP-average seasonal cycles As seen in a previous section, the PBLH grows rapidly between January and March, remains high until June and then starts to decline. In contrast, both SH (Figure 13 A) and T2m (Figure 13 B) increases more slowly during spring and summer and reach their annual maxima in late summer, which indicates that their seasonal march is mainly coordinated by the seasonal cycle of incoming solar radiation. It thus appears that the high winter-spring PBLs can not be explained by thermal forcing from high SH or T2m. The seasonal patterns of the strength in the wind variables is opposite to that of PBLH (Figure 13 D, E and F). In late winter and early spring, the wind variables exhibit relatively large values, which may contribute to the high PBLs. The Prc remains fairly low during winter and spring as the PBLH climbs toward its annual peak - but it should be kept in mind that the dry season anticorrelation with Prc is not significant (Figure 14 C). During the monsoon season, when the Prc is high, PBLH starts to drop. Since PBLH is significantly anticorrelated with precipitation in the monsoon season, it could be argued that the PBLH starts decreasing during the summer due to the presence of clouds and precipitation, which could act to reduce the SH and thus the PBLH. However, as noted above, the seasonal cycle of SH appears to be coordinated by the seasonal cycle of incoming solar radiation, and SH does not drop as the Prc peaks.

As for the tropopause levels, it is perhaps not plausible that their seasonal variations directly influence the PBLH, but their variations are nevertheless interesting from a stratosphere-troposphere exchange perspective (Figure 13 G-H). The LRT displays lower pressure (higher altitude) during the summer months as expected since heating and mixing is greater in summer. The CPT in contrast reaches the lowest pressure in spring.

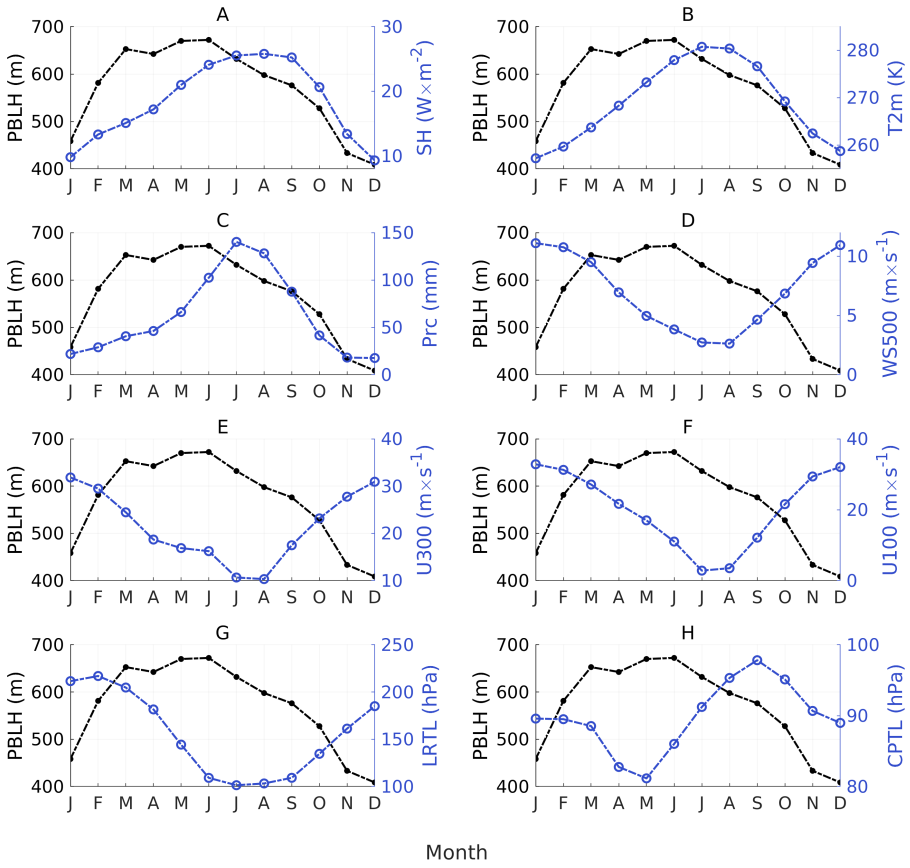

Figure 13: Seasonal cycles of Planetary Boundary Layer (PBLH) and selected climate variables at the Tibetan Plateau (TP). For each month, the mean over the entire 1979-2018 period is shown for PBLH (black, left axis) and the other climate variables (blue, right axis). **A:** Sensible Heat flux (SH), **B:** 2 meter air temperature (T2m), **C:** Precipitation (Prc), **D:** Wind Speed at the 500 hPa level (WS500), **E:** Zonal wind component at the 300 hPa level (U300), **F:** Zonal wind component at the 100 hPa level (U100), **G:** Lapse Rate Tropopause Level (LRTL), **H:** Cold Point Tropopause Level (CPTL).

3.2.2.2 Seasonal cycles in the central Tibetan Plateau region As seen in a previous section, the seasonal PBLH cycle in the CTP region is quite different from the TP-average. After peaking in early spring, it plunges to a minimum in August before reaching a second and much smaller peak in October. The seasonal SH cycle in the CTP region is also very different from its TP-average counterpart (Figure 14 A). From January to February it increases rapidly and then remains at around 26 W/m^2 throughout the monsoon season before decreasing to its minimum of around 19 W/m^2 in December. Thus, the SH is roughly as strong when PBLH peaks in March as it is during its minimum in August. As for the T2m, it increases more than 20 K from late winter to late summer, when PBLH is at its lowest (Figure 14 B). Clearly, thermal forcing from SH or T2m is not able to explain neither the high spring PBL or the low summer PBL.

The seasonal cycle of Prc, however may seem to offer an explanation, since the Prc is low when the PBL is high and vice versa (Figure 14 C). On the other hand, it is difficult to see how Prc would affect the PBLH *without* affecting the SH: If high Prc and associated cloudiness indeed corresponds to a small amount of energy at the surface and a higher fraction of the energy that is available going into evaporation (latent heat), then it is hard to explain why SH remains high and relatively constant as Prc changes.

As for the wind variables, they all exhibit similar patterns of higher speed in the dry season months and lower in the monsoon season months (Figure 14 D-F). Given that high wind speed favours PBL growth it is notable that the PBLH decreases along with the wind speeds as the monsoon season progresses and then starts climbing toward its second peak as the wind variables starts increasing again. From October to December the PBLH decreases again while the wind variables keep increasing, but as seen above, the SH and T2m decreases during this time. It could therefore be argued that PBLH in the CTP region may be highly determined by wind speed from spring to autumn, while the low thermal forcing results in small PBLH during the winter in spite of higher wind speeds. However, this remains a speculation.

The LRTL once again displays lower pressure (higher altitude) in summer as expected (Figure 14 G). The seasonal pattern of CPTL is inversely similar to the pattern of PBLH in this region, with lower pressure during spring and higher pressure in summer (Figure 14 H).

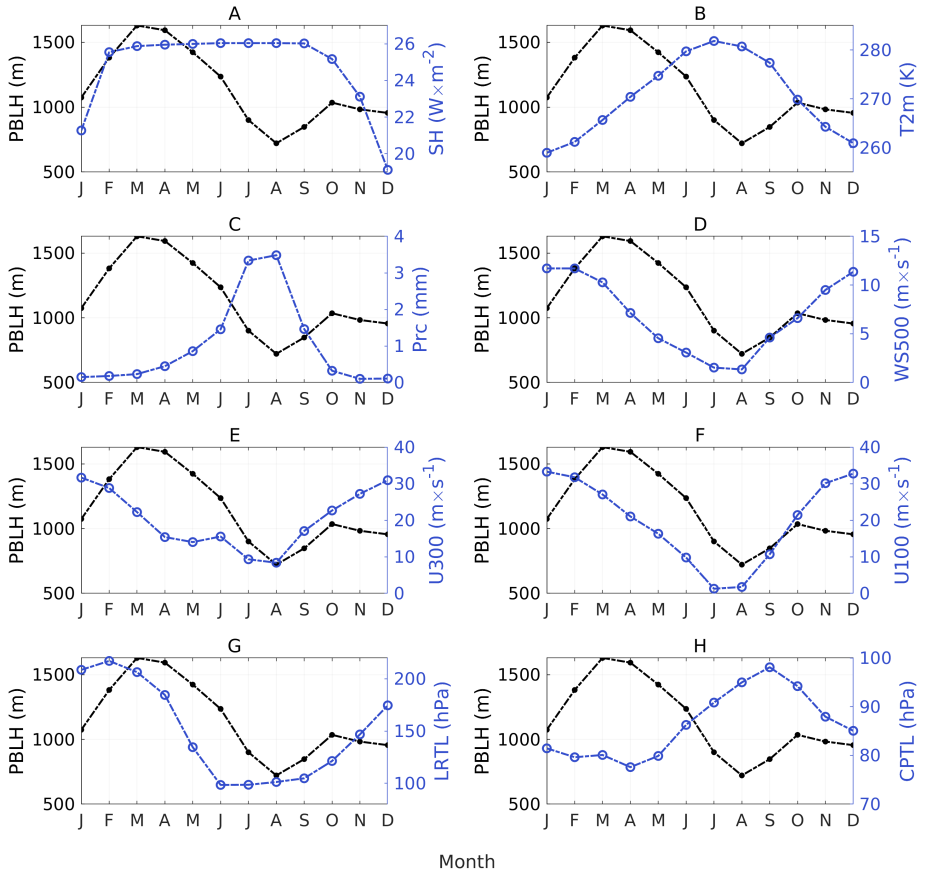

Figure 14: Seasonal cycles of Planetary Boundary Layer (PBLH) and selected climate variables in the central Tibetan Plateau (CTP) region. For each month, the mean over the entire 1979-2018 period is shown for PBLH (black, left axis) and the other climate variables (blue, right axis). **A:** Sensible Heat flux (SH), **B:** 2 meter air temperature (T2m), **C:** Precipitation (Prc), **D:** Wind Speed at the 500 hPa level (WS500), **E:** Zonal wind component at the 300 hPa level (U300), **F:** Zonal wind component at the 100 hPa level (U100), **G:** Lapse Rate Tropopause Level (LRTL), **H:** Cold Point Tropopause Level (CPTL).

3.2.2.3 Seasonal cycles in the southeastern Tibetan Plateau region The SETP region PBLH cycle, as seen in a previous section, is characterised by much lower PBLH and lacks the late summer dip that is seen for the CTP region. In fact, it appears to follow the seasonal evolution of SH and T2m quite well, although it starts decreasing slightly after June in spite of the fact that the other two variables are still increasing (Figure 15 A-B). The small decrease may perhaps be partly explained by the high Prc amount, but as noticed above the mechanism by which this is achieved is unclear, since the Prc seems to influence the PBLH without noticeably affecting the SH (Figure 15 C). As for the wind variables, their seasonal pattern is more or less the opposite of the PBLH cycle (Figure 15 D-F). The seasonal patterns in the tropopause levels is relatively similar to that in the CTP region and the TP-average (Figure 15 G-H).

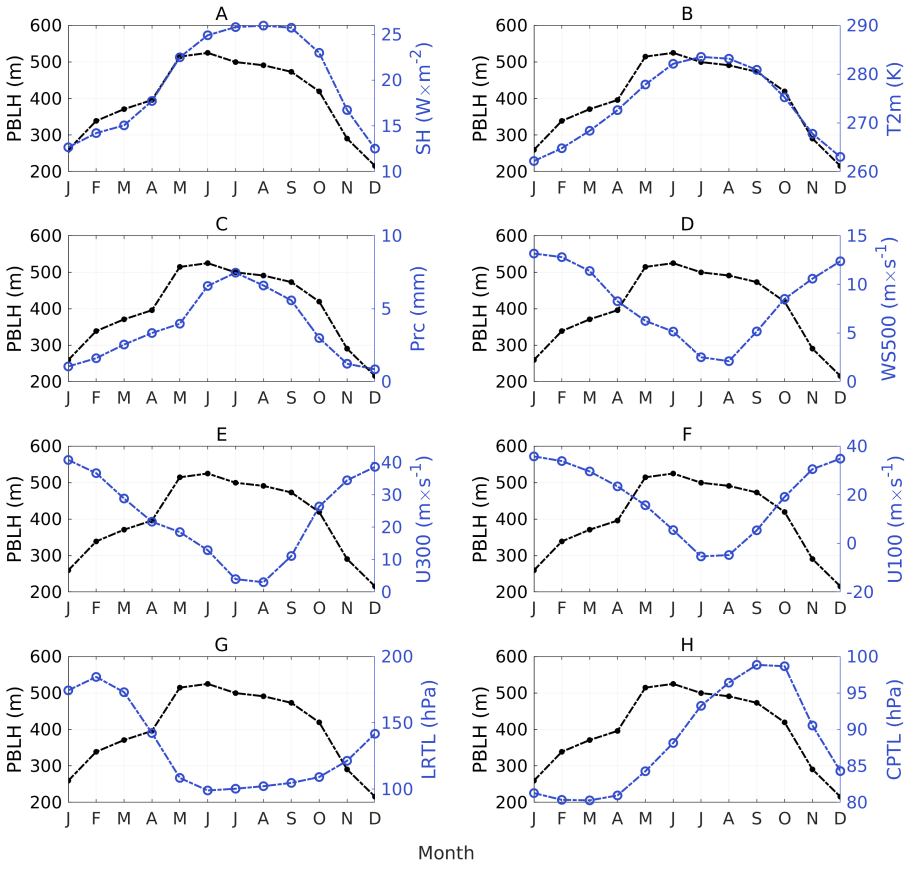

Figure 15: Seasonal cycles of Planetary Boundary Layer (PBLH) and selected climate variables in the southeastern Tibetan Plateau (SETP) region. For each month, the mean over the entire 1979-2018 period is shown for PBLH (black, left axis) and the other climate variables (blue, right axis). **A:** Sensible Heat flux (SH), **B:** 2 meter air temperature (T2m), **C:** Precipitation (Prc), **D:** Wind Speed at the 500 hPa level (WS500), **E:** Zonal wind component at the 300 hPa level (U300), **F:** Zonal wind component at the 100 hPa level (U100), **G:** Lapse Rate Tropopause Level (LRTL), **H:** Cold Point Tropopause Level (CPTL).

3.2.2.4 Seasonal cycles discussion and summary It can be noted that the seasonal cycles of PBLH in the two regions somewhat resembles the difference in seasonality between extra-tropical latitudes (>40°) and tropical to sub-tropical latitudes (35°S - 35°N) described by Chan and Wood (2013): While extra-tropical PBLHs have their seasonal maximum in late summer when the surface is warm and the static stability low, the subtropical and tropical PBLH are to a large degree controlled by the availability of surface moisture. In the monsoon season when more water is available for evaporation, a larger fraction of the solar heating is partitioned into latent heat flux, at the expense of the sensible heat flux. Therefore, the seasonal cycle of PBLH in tropical and subtropical regions often display their maximum during the dry season.

The increase in moisture as the monsoon season develops could explain the seasonal PBLH variation in the CTP region if it was not for the fact that SH remains high throughout the monsoon season. However, thermal convection is not affected by SH alone. The effects of clouds on radiation and heat fluxes complicate the matter because in addition to reducing the ground heating and thereby the SH, clouds may warm the atmosphere in higher layers, e.g. during cloud formation when latent heat is released (Davis et al., 2020). If the temperature higher up exceeds that of the underlying air, convection will not be able to penetrate through the warmer layer. It is conceivable that such a temperature inversion could inhibit PBL growth past a certain height in spite of high SH.

As for the SETP region, it is also positioned in sub-tropical latitudes, but does not show a very pronounced monsoon season dip. Instead it exhibits a seasonal PBLH cycle that may suggest combined influences from the controlling factors deemed as typical for extra-tropical regions and those deemed as typical for subtropical regions by Chan and Wood (2013).

The PBLH is likely significantly affected by multiple factors, including variables that were not assessed here, such as the effects of clouds. In addition, X. Chen et al. (2016), who found very deep PBLs in late winter, argues that dry conditions alone are not sufficient for extremely great wintertime PBLH. They state that the stability of the free atmosphere also plays a key role, and that the weak wintertime stability allowing the PBL to grow high is associated with high PV values corresponding to a strong and southerly positioned jet stream. This may help explain why the CTP and TP-average PBLH are so great in late winter and early spring.

If the seasonal cycles can be affected by moisture availability and clouds as well as atmospheric stability conditions related to the position of the subtropical jet stream, it is plausible that the positioning of the intertropical convergence zone as well as the jet stream in relation to the two regions play a role in creating the differences in PBLH.

In summary, it is hard to determine to what extent the PBLH cycle may in fact be explained by the seasonal variation in the other variables. In the CTP region, wind speed may play a role for great PBLH in late winter-early spring and perhaps for the smaller peak in autumn, while Prc (or clouds) may be responsible for the small PBLH in summer. The TP-average PBLH could be interpreted similarly, but it should be noted that the autumn PBLH peak is not present in the TP-average despite similar wind speeds. In the SETP region, the PBLH rather appears to follow the seasonal cycles of SH and T2m, although the small decrease during summer may be related to high Prc. As for the tropopause levels, the cycles differ between LRTL and CPTL, but the variation in each tropopause level is relatively similar in both regions in spite of varying PBLH. This could perhaps be taken as an indication that the seasonal evolution of tropopause height and PBLH, respectively, is not very closely coupled.

3.2.3 Spatial Correlations

In order to examine the spatial variations across the TP, correlations between PBLH and the other climate variables were calculated for each respective grid point. The correlations were performed on both raw and detrended data, in order to assess whether or not the trend plays a large role for the correlations. It can be noted that for T2m, especially for the monsoon season, the correlation was stronger and the region of significance more widespread when the trends were removed. This can be seen as an indication that the opposite direction of the trends in PBLH and T2m, respectively, decreased the correlation slightly when using

the raw data. However, in general the results were similar and therefore only correlations using the raw data are included here. Correlations using annual means were also calculated but are excluded here because of their general similarity with the seasonal correlations. Since the correlations with LRTL and CPTL are partly opposite when comparing the two seasons, it may still be worth briefly mentioning how these appear in the annual means: the LRTL correlations are predominantly negative while the CPTL correlations, although mainly negative, have some regions of positive correlation, mainly in the southern TP. Statistical significance is lacking over much of the plateau, especially for CPTL.

3.2.3.1 Monsoon season correlations The monsoon season correlation between SH and PBLH is positive, statistically significant and very strong across the TP (Figure 16 A). This is line with previous findings about the large role of SH for TP PBLH (K. Yang et al., 2004). The spatial correlation with T2m is weaker and not consistently significant, but it remains positive except along the southern rim of the plateau (Figure 16 B). Prc in contrast is anticorrelated with PBLH except in a few smaller regions. The strongest anticorrelation is seen in a large region in the central TP (Figure 16 C). As noted above, a negative relationship with Prc can arise due to the associated cloudiness which may inhibit surface heating by blocking incoming solar radiation and due to moister conditions leading to a larger latent heat flux on behalf of the SH. Both the clouds and the Prc itself may thus act to dampen the SH and PBLH.

WS500 is significantly and positively correlated with PBLH throughout the central plateau but smaller areas of significant anticorrelation are also found in the west, east and southeast (Figure 16 D). It is hard to say why the association with wind variables is mainly confined to the central TP. Potentially, this is related to topographic variations or the interplay between the different variables in this region. As for U300 and U100 (Figure 16 E and F, respectively) they both have spatial patterns similar to those of U500, although their correlations are somewhat weaker.

If LRTL respond to the thermal forcing from the surface of the plateau (Feng et al., 2011) and PBLH also does so, this would manifest in a negative correlation, since higher pressure levels correspond to lower altitudes. However, both LRTL and CPTL (Figure 16 G and H, respectively) exhibit regions of significant positive correlation in south-central TP. Some significant anticorrelation is present as well, mainly in the northwest for LRTL and the east and northeast for CPTL.

As for the two regions for which the PBLH was analysed in a previous section, it can be noted that in the CTP region, there are strong significant relationships with SH, Prc, WS500 and to a lesser extent T2m, U300 and U100. In most of the SETP region however, significant correlations are only found for SH and, to a somewhat lesser extent, T2m and Prc.

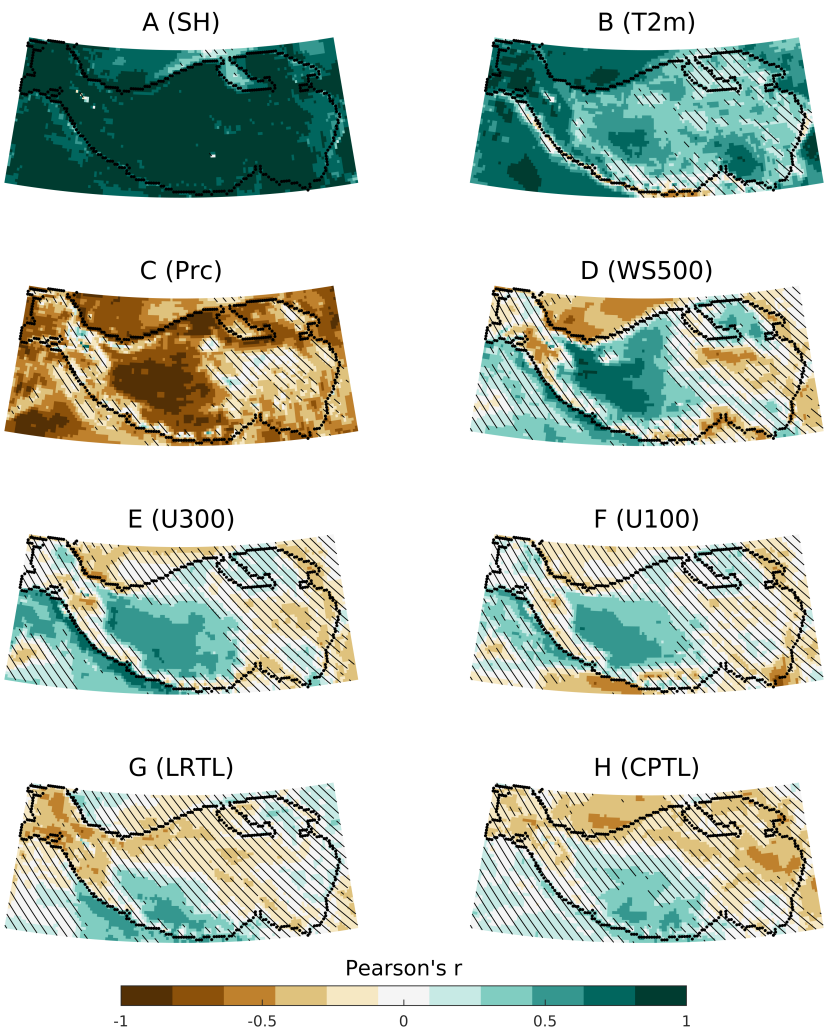

Figure 16: Monsoon Season Spatial Correlations between Planetary Boundary Layer Height (PBLH) and selected climate variables. Correlation coefficients (Pearson's r) are shown for **A**: Sensible Heat flux (SH), **B**: 2 meter air temperature (T2m), **C:** Precipitation (Prc), **D**: Wind Speed at the 500 hPa level (WS500), **E**: Zonal wind component at the 300 hPa level (U300), **F**: Zonal wind component at the 100 hPa level (U100), **G**: Lapse Rate Tropopause Level (LRTL) and **H**: Cold Point Tropopause Level (CPTL). Black lines are drawn over regions where the correlation is *not* significant at the 95% confidence level.

3.2.3.2 Dry season correlations In the dry season, the correlations between PBLH and SH are statistically significant, positive and strong, although slightly less consistently than in the monsoon season (Figure 17 A). With T2m on the other hand, the positive correlation is stronger for the dry season, and significant nearly everywhere. The narrow region of anticorrelation which was shown for the monsoon season is not present (Figure 17 B).

For Prc, the correlation resembles that of the monsoon season, with statistically significant anticorrelation in central TP (Figure 17 C). A spurious feature of the correlation with Prc is the presence of small regions of *positive* correlation. It can be noted that Prc affects the soil moisture, which has implications not just for the energy partitioning but also for the surface albedo. Wetter soil has a lower albedo (more solar radiation is absorbed) which in itself acts to raise the temperature of the land surface. Patil et al. (2013) found that PBLH in northwestern India was positively related to soil moisture, because of the increase in total heat flux (sensible and latent) from the surface as well as the reduced albedo. This is in sharp contrast to other studies, like Sathyanadh et al. (2017) who related high soil moisture with a large evaporative fraction and shallow PBLs or Eltahir (1998), who hypothesised that higher soil moisture leading to a cooler surface and thus smaller SH acts to decrease the PBLH in spite of the higher total heat flux. However, the most pronounced region of positive correlation in Figure 17 C is the northwestern TP high-elevation area which is likely partly glaciated. Dry season precipitation in such a region should result in more snow, higher albedo, and a thinner PBL. It is therefore not clear why the correlation is positive in this particular region.

For WS500, positive correlation is present over most of the plateau, although significance is lacking along the rims and in much of the western and eastern TP (Figure 17 D). A similar pattern is found for U300 and U100, although for the latter, the region of statistically significant positive correlation is smaller (Figure 17 E and F, respectively).

LRTL is anticorrelated with PBLH over most of the TP, but in most regions the correlations lack significance (Figure 17 G). With CPTL the correlation is also predominantly negative, although regions with positive correlation can be discerned in the westernmost and easternmost parts of the TP. Significance is mainly found in central and southeastern TP (Figure 17 H).

Again, it can be noted that the CTP region exhibits more pronounced relationships with several of the climate variables than the SETP region does. In particular, this is true for the wind variables and Prc. With SH and T2m however, the relationship is similar in both regions.

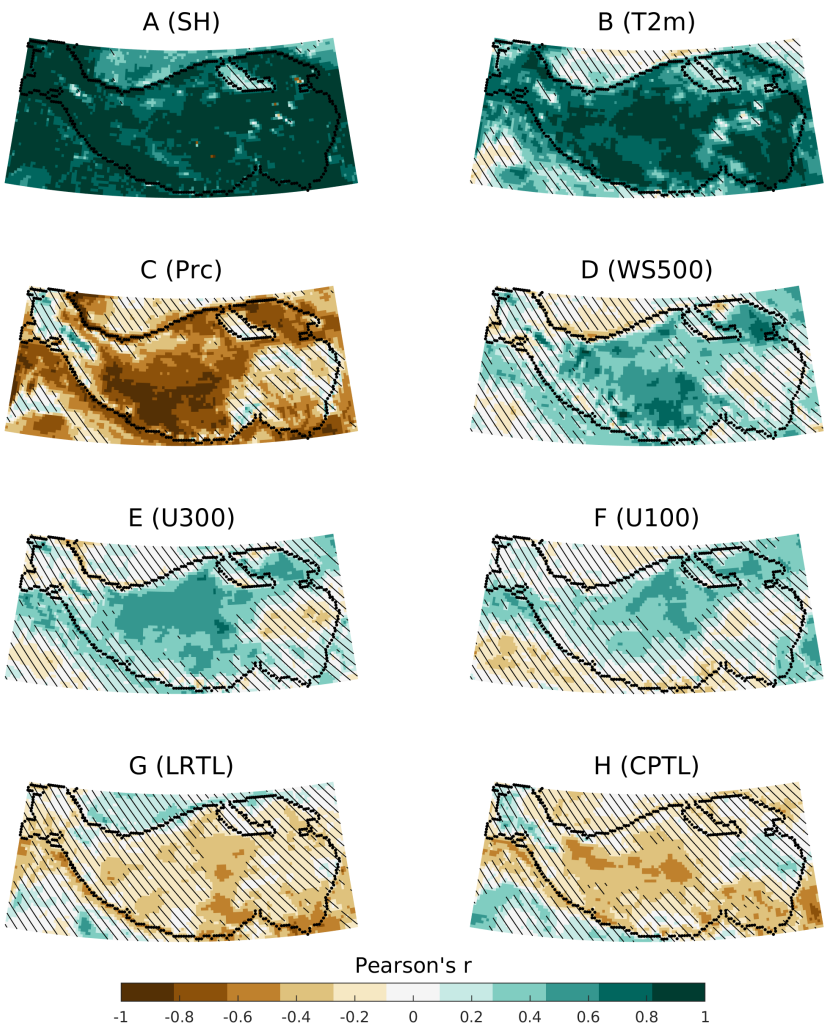

Figure 17: Dry Season Spatial Correlations between Planetary Boundary Layer Height (PBLH) and climate variables. Correlation coefficients (Pearson's r) are shown for **A**: Sensible Heat flux (SH), **B**: 2 meter air temperature (T2m), **C:** Precipitation (Prc), **D**: Wind Speed at the 500 hPa level (WS500), **E**: Zonal wind component at the 300 hPa level (U300), **F**: Zonal wind component at the 100 hPa level (U100), **G**: Lapse Rate Tropopause Level (LRTL) and **H**: Cold Point Tropopause Level (CPTL). Black lines are drawn over regions where the correlation is *not* significant at the 95% confidence level.

3.2.3.3 Spatial correlations summary The analysis above indicates that thermal conditions are crucial across the TP. In addition, Prc and WS500 appears to play a large role in the interior of the plateau. The strongest correlations are found for SH, which is significantly positively correlated with PBLH across the TP in both seasons. Since SH is generally of great importance for PBLH, and has been deemed one of the most crucial factors between high TP PBLH (K. Yang et al., 2004), the strong positive relationship is not unexpected. Over almost the entire plateau T2m is also positively correlated with

PBLH, although, especially in the monsoon season, the magnitude varies and significance is lacking in some regions. It can be noted that high T2m is not necessarily favourable for PBL development, since warm air temperatures promote negative SH if the ground is cooler than the air. Still, warmer air near the surface can promote convection and thereby PBL growth, and the consistently positive correlation between PBLH and T2m suggest that high air temperature is related to high PBL and vice versa.

Prc is strongly anticorrelated with PBLH in the central TP, especially in the monsoon season. The anticorrelation may be explained by effects of rain and cloudiness on the surface energy budget leading to smaller SH. Why PBLH is *not* anticorrelated over parts of the western and eastern TP could potentially be explained by a competing influence on the surface energy budget: the albedo increase associated with higher soil moisture following rainfall. However, this interpretation makes it difficult to explain the presence of positive correlations in a high altitude area in northwestern TP in the dry season. Here, precipitation is likely to take the form of snow, and should thus be associated with an *increased* albedo, which in turn should correspond to lower surface heat fluxes and smaller PBLH.

As for the tropopause levels, the correlations are mainly not significant or very strong. This is not surprising, since the tropopause is not generally a determining factor behind PBLH or vice versa. However, it is plausible that they can both respond to the same thermal forcing from the surface of the plateau and therefore exhibit a correlation. Therefore, it is puzzling that the correlations with the tropopause levels goes in both directions. However, the general weakness and lack of significance indicates that there may not be a notable association at all between PBLH and the tropopause levels.

3.2.4 Spatial Means and Trends

Means and trends across the TP were plotted in order to allow comparison between the spatial patterns of the climate variables and those of PBLH. For the four near-surface variables - SH, T2m, Prc and WS500 - some features of the spatial patterns can be found which may offer clues to the mean and trend patterns of PBLH. Therefore, the means and trends of these four variables are displayed for the monsoon season (Figure 18), the dry season (Figure 19) and the annual means (Figure 20). Note that the colour scale limits differ between seasons. For Prc, the extreme values in both means and trends along the southern border of the eastern TP are not visible, since setting the colour scale to include these would hide the variations over the rest of the TP. Due to large differences in magnitude, values outside the TP were removed from the means in order to allow better representation of the values at the TP.

3.2.4.1 Monsoon season spatial means and trends The spatial patterns of the monsoon season means and trends of PBLH (Figure 5 A and D) and SH (Figure 18 A and B) are strikingly similar. The mean SH is highest in the southwestern parts of the central TP and lower towards the outskirts of the plateau, especially in the high-elevation area in northwestern TP, in great similarity with PBLH. The pattern of SH trends, with a pronounced significant decreasing trends in the central plateau and smaller regions of significant increase in the western parts is also extremely similar to the pattern of the PBLH trends. In fact the only clearly distinguishable feature of the monsoon season PBLH trend that is not mirrored in the SH trend is a smaller region of relatively weak but statistically significant increasing PBLH in the eastern TP which is not present for SH.

The mean T2m (Figure 18 C) is somewhat similar to the SH mean and very similar to

the elevation (Figure 1), with lower temperatures in high-altitude regions. The central TP region of pronounced decreasing trends in PBLH and SH is discernible in the T2m trend as well, as the only larger region where T2m is *not* significantly increasing (Figure 18 D).

For Prc, the difference in mean conditions is quite large between the wet southeastern TP and the drier western parts, but the spatial patterns are not very similar to those of PBLH, although Prc remains relatively low in central TP where the PBLH is high (Figure 18 E). The central TP features statistically significant increasing Prc trends over a large region which corresponds well to the region of decreasing SH and PBLH (Figure 18 F). This also agrees with Bibi et al. (2018) and X. Li et al. (2017), who describes a tendency for increasing precipitation trends in the semi-arid and humid central TP. As noted in other studies, e.g. Q. Zhang, Zhang, Qiao, and Wang (2011), more arid conditions favour PBL growth because of the dry surface and absence of clouds. The increasing Prc trend in the central plateau where the SH and PBLH exhibits decreasing trend is therefore notable, particularly in the light of the strong negative correlation between PBLH and Prc in this region. In magnitude however, the central TP trend is dwarfed by those found along the southern rim, where negative trends of 60 m per decade as well as positive trends of 35 m per decade are found. Right outside the TP, as it is defined here, even larger trends are found. (Note that the Prc colour scales were set to make the variations within the plateau clear, which means that the magnitude of the largest trends and means along the rim are not captured in the figure).

Regarding WS500, its patterns in mean and trend are not very similar to those of PBLH. (Figure 18 G and H). Still, it can be noted that the trends is declining over most of the region where PBLH has a decreasing trend, although significance is lacking except over northern and northeastern TP.

In summary, the SH appears to be the most dominating factor for the monsoon season PBLH, as seen in both the correlations in the previous section and the spatial patterns of means and trends. The altitude plays a large role for the SH not only because of the high average elevation leading to intense solar radiation and thereby large SH, but also because the highest altitudes with glaciated surfaces (such as the elongated high elevation-feature in northwestern TP) has *smaller* SH and therefore lower PBLH. The fingerprints of the other variables are not as clear in the mean conditions. In trends however, the central TP region of PBLH decrease is visible not only as SH decrease, but also as a lack of significance in the T2m trends and as increasing Prc trends. This, together with the fact that Prc is strongly anticorrelated with PBLH in this region, leads to the suspicion that increased Prc has led to colder conditions and smaller SH resulting in lower PBLH. It is plausible that the SH decrease was brought about by a shadowing effect of a cloud cover increase associated with the increasing Prc, and/or that more of the available energy at the surface was partitioned into latent heat flux, at the expense of SH. Whether or not WS500 changes has played an additional role in the PBLH trends is hard to say, but the general decrease may have contributed to the negative trends in PBLH.

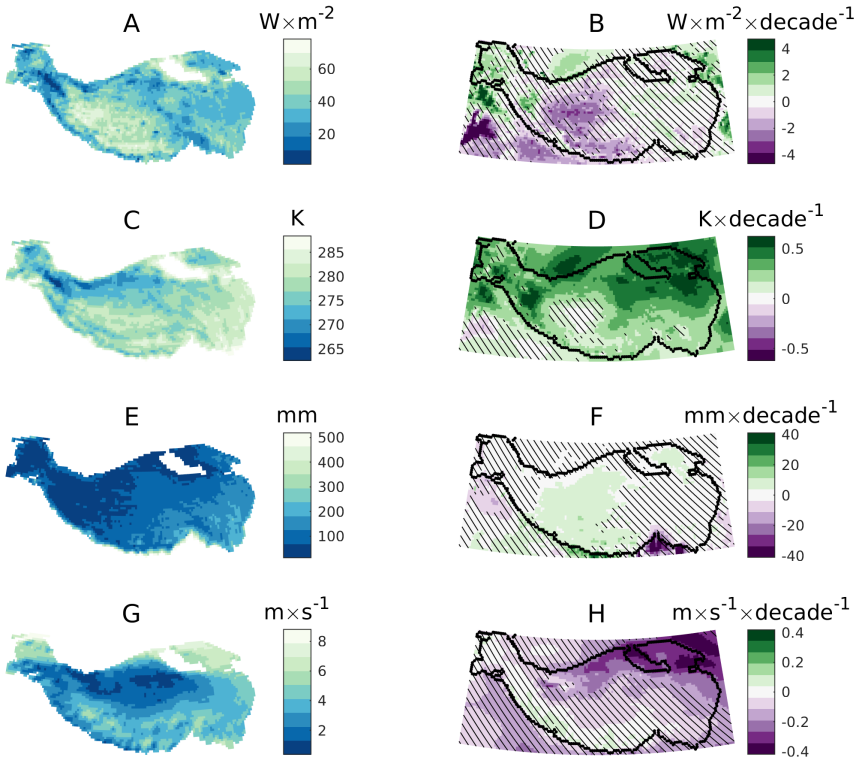

Figure 18: Monsoon season 1979-2018 means and linear trends in selected climate variables. Left column shows the means, right column shows the trends. **A**: Mean Sensible Heat flux (SH), **B**: SH trends, **C:** Mean 2 meter air temperature (T2m), **D**: T2m trends, **E:** Mean Precipitation (Prc), **F:** Prc trends, **G:** Mean Wind Speed at the 500 hPa level (WS500), **H:** WS500 trends. Black lines are drawn over regions where the trend is *not* significant at the 95% confidence level.

3.2.4.2 Dry season spatial means and trends The spatial patterns of the SH mean and, in particular, trends, (Figure 19 A and B) are similar to the corresponding patterns in PBLH (Figure 5 E) for the dry season as well. The altitude effects are once again clearer in the mean T2m means (Figure 19) than in the SH or PBLH means, although the high elevation region in northwestern TP is discernible in both T2m and SH. Although the similarity is not as pronounced as for SH, strong T2m trends (Figure 19 D) and PBLH trends (Figure 5 E) generally appear to be co-located.

The interior of the TP is quite dry, while the northwestern parts, the southern rim and the southeastern parts again receive more precipitation than can be visualised without losing the differences at the rest of the plateau (Figure 19 E). The Prc trend lacks significance over almost the entire plateau, but in similarity with the monsoon season trend, there are strong decreases along the southern rim of the eastern TP (Figure 19 F). The WS500 means are higher in the northern, westerlies-dominated part, as well as the eastern (Figure 19 G). In central TP, it appears to follow the topography to some extent (for comparison, see Figure

1), possibly as wind is channelled through large west-east oriented valleys. However, despite significant positive correlation with PBLH in this area, the same elevation-following patterns are not evident in the PBLH means. WS500 trends are not significant or particularly strong, and although some similarities with PBLH can be discerned in the decreases in the north and east and increases in the central TP, the patterns do not agree well (Figure 19 H).

In similarity to the monsoon season, SH appears to be the strongest factor behind the spatial distribution of mean PBLH as well as its trends. As for Prc, the clear fingerprint in the spatial pattern of the trend that was seen for the monsoon season is lacking in the dry season. Given the relatively strong anticorrelation with Prc in central TP, the lack of common patterns in the trends should perhaps not be taken to indicate that the Prc trend is unimportant for the PBLH trend. Instead it can be attributed to the lack of significant trends in both PBLH and Prc over most of the TP.

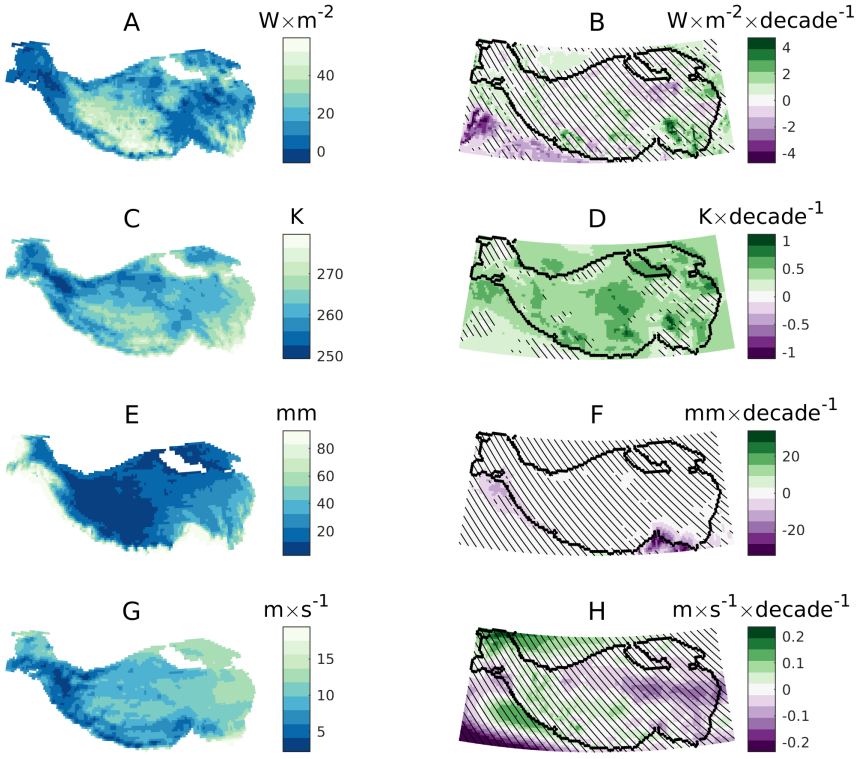

Figure 19: Dry season 1979-2018 means and linear trends in selected climate variables. Left column shows the means, right column shows the trends. **A**: Mean Sensible Heat flux (SH), **B**: SH trends, **C:** Mean 2 meter air temperature (T2m), **D**: T2m trends, **E:** Mean Precipitation (Prc), **F:** Prc trends, **G:** Mean Wind Speed at the 500 hPa level (WS500), **H:** WS500 trends. Black lines are drawn over regions where the trend is *not* significant at the 95% confidence level.

3.2.4.3 Annual spatial means and trends Given that the seasonal values are quite different from each other, annual means and trends are also included, to show the combined result of the seasonal components. In the annual trends, once more the similarities between the SH trends (Figure 20 A) and the PBLH trends (Figure 5 F) are strongly pronounced. This is not the case for T2m (Figure 20 D), although smaller regions of strong T2m increase (e.g. parts of the southeastern TP) are co-located with PBLH increases. The annual Prc trend is dominated by the monsoon season trends, with increases in central TP and strong decreases along the southern rim of eastern TP (Figure 20 F). WS500 increases in the north-east and decreases in parts of western TP, but most of its trends lack significance, and have no noteworthy similarities to the annual PBLH trends.

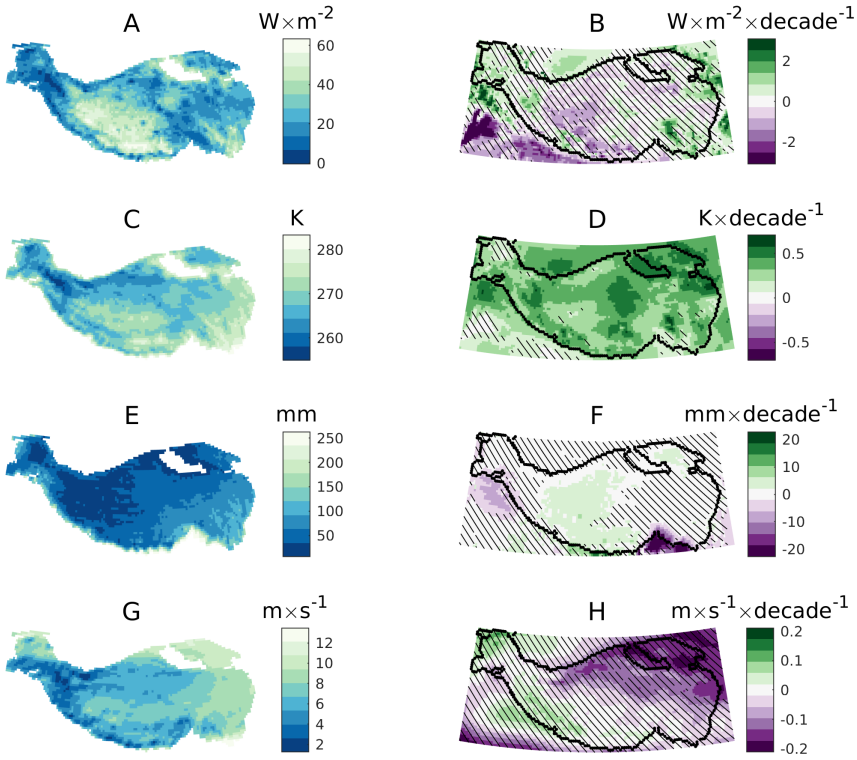

Figure 20: Annual 1979-2018 means and linear trends in selected climate variables. Left column shows the means, right column shows the trends. **A**: Mean Sensible Heat flux (SH), **B**: SH trends, **C:** Mean 2 meter air temperature (T2m), **D**: T2m trends, **E:** Mean Precipitation (Prc), **F:** Prc trends, **G:** Mean Wind Speed at the 500 hPa level (WS500), **H:** WS500 trends. Black lines are drawn over regions where the trend is *not* significant at the 95% confidence level.

3.2.4.4 Spatial trends summary and discussion The spatial patterns in the mean conditions show that the high PBLH in the interior of the TP are co-located with high SH and relatively dry conditions, while the lower PBLH in the east, west and along the rims are situated where SH is lower and precipitation higher. In some cases, especially low PBLH is

seen at high-elevation features. The pronounced similarity in the spatial patterns of PBLH trends and SH trends indicates that PBLH trends in both seasons are strongly coupled to SH changes. While a detailed analysis of the underlying causes behind the SH trends is beyond the scope of this thesis, it can be noted that SH increases are somewhat co-located with T2m increases. While higher air temperature does not necessarily mean higher SH (if the air is warmer than the underlying surface the SH will even be negative, i.e., heat is transferred from the warmer air to the colder surface), warmer conditions *could* be a sign of surface heating and thus larger SH. At the same time, *decreasing* SH is co-located with weaker-than average warming and in the monsoon season also with significantly increasing precipitation trends. Therefore, it is plausible that changes in Prc and T2m has led to changes in SH which has in turn affected the PBLH.

The large difference in mean Prc between the seasons may play a role behind the seasonal contrast in PBLH variability. In the dry season, PBLH exhibits more variability both in the seasonal cycles, the annual time series and, in the case of the CTP region, the diurnal cycle. Drier conditions with less clouds may mean larger and more rapid short-term variations in surface heating and thus PBLH.

3.2.5 Close to the Tropopause? A case of small difference between the Planetary Boundary Layer and the Tropopause

Previous research has indicated that TP PBLs reaching close to the tropopause facilitates interaction between the PBLH and the tropopause and exchanges between the troposphere and the stratosphere (X. Chen et al., 2013). But how close to the tropopause does the PBL top reach? Based on a criterion aiming to find when and where low tropopause and high PBL coincides in the monthly data, a 85-90°E, 30-35°N region and the period January 2008 were selected for calculation of hourly LRTH (see Section 2.5 for details).

3.2.5.1 Tropopause characteristics In the selected data, LRTH was actually lower than PBLH in some cases, and even dropped to the ground level at a few instances. This is likely an artefact of the tropopause calculation, either arising from the calculation of tropopause pressure levels or their conversion to metric heights. However, comparisons for a subset of the data indicate that the difference is small between tropopause levels obtained from the original NCL function and tropopause levels from the modified version used here (except that tropopause levels above the 85 hPa limit are set to 85 hPa in the NCL calculation, as described in Section 2.2.1). Neither can the strange values be traced to the conversion from height above sea level to height above ground level (through subtraction of the elevation). In any case, the extremely low values are relatively few: While 2.26% of the January values are lower than 4 km above the ground level (corresponding to around 9 m above sea level, which is not necessarily unreasonably low for a wintertime tropopause) only 0.36% of the January values are lower than 1 km above ground level. Still, since the reason for the strange values has not been ascertained, the tropopause heights should be treated with some caution.

When omitting all LRTH lower than 4000 metres above ground level in order to exclude all values suspected of being erroneously low, the smallest difference between PBLH and LRTH (108 m) was found for 28th January 2008, at 14:00, local time. LRTH (blue, dash-dot) and PBLH (black, solid) is plotted for the grid point for which this minimum difference was found, from January 26, 22:00 to January 30, 06:00 (local time) in Figure 21. In addition, the area average is shown as stars, and all the individual grid points as

dots. The plot indicates that the LRTH varies rapidly over time and space between a higher level situated around 10-14 km above the ground and a lower level, around 4-6 km above the ground, which is close to the afternoon PBL tops. Although interactions between the PBLH top and the tropopause or troposphere-stratosphere exchanges can not be assessed from Figure 21, it is still noteworthy that the PBL and the tropopause are in such proximity.

The apparent tropopause fluctuations of several km from one hour to another lack a physical explanation. Instead, the existence of two preferred tropopause heights seem to suggest either a double tropopause or a tropopause fold. However, the tropopause calculation used here does not account for double tropopauses or folds. So why do two distinct levels emerge in Figure 21?

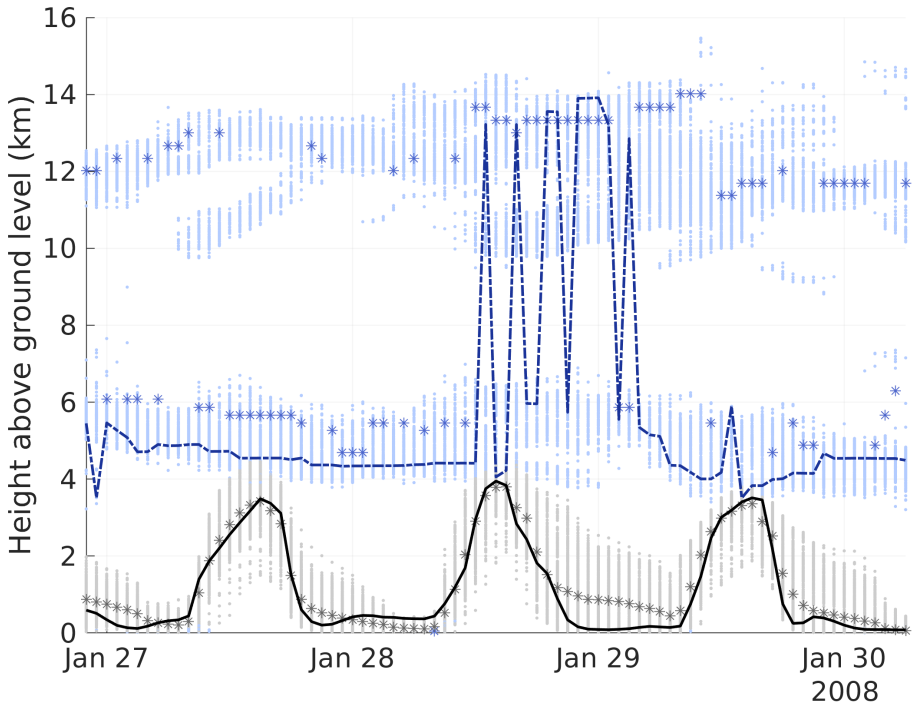

Figure 21: Planetary Boundary Layer Height (PBLH) and Lapse Rate Tropopause Height (LRTH). Hourly values of LRTH was calculated and compared with PBLH for a small region (85-90°E, 30-35°N, Figure 3) and a short time frame (January 2008). The selection is based on where a low tropopause level coincides with a large PBLH in the monthly data (see Section 2.5). PBLH (black) and LRTL (blue) is shown for a few days in January 2008, centred around the time of minimum height difference (28th January, 14:00 local time). Black solid and blue dash-dot lines show PBLH and LRTH, respectively, for the single grid point for which the smallest difference was found (after excluding low LRTHs suspected of being erroneous). The grey and light blue dots show PBLH and LRTH, respectively, for each of the other grid points in the aforementioned region, and the grey and blue stars show the average of all the grid points in the region. The x axis shows local time in the middle of the region, rounded to the nearest whole hour.

3.2.5.2 Why did two levels emerge? In order to examine why the calculations have returned two preferred tropopause levels, the area-averaged temperature profiles are shown for each time step in the period that is displayed in Figure 21. Temperature profiles for time steps in which the LRTH was higher than 9 km are shown in red and temperature profiles for time steps in which the LRTH was lower than 7 km are shown in black (Figure 22).

The temperature profiles display two atmospheric regions characterised by variation among the individual profiles and small or negative (temperature increases with height) lapse rates. The first such region is reached around 4 km above the ground, when the profiles starts differing more from each other and displaying smaller and then negative lapse rates. Above 6 km, the lapse rates increase again, although they remain smaller than they were below 4 km. From around 11 km and above, the profiles once again differ more from each other, and at various levels in the 11-16 km region their lapse rates becomes negative. Clearly, these regions correspond to the two tropopause regions in Figure 21.

However, the profiles in Figure 22 that produced a high tropopause (red lines) and the profiles that produced a low tropopause (black lines) all display a similar pattern in which both "tropopause candidates", i.e. layers of low or negative lapse rates, are seen. The tropopause definition underlying the function used for calculating the LRTL states that the tropopause is the lowest level above 450 hPa at which the lapse rate is 2°C (or K) per km or less, given that the average lapse rate between this level and all higher levels within 2 km above it does not exceed 2°C (World Meteorological Organization, 1957; The NCAR Command Language, 2017). Keeping this in mind, it could be that in some cases (red lines), the average lapse rate within 2 km above the lower tropopause candidate exceeds 2 K, so that the second criterion in the tropopause definition is not met, the lower tropopause candidate is disregarded as an inversion and the calculation returns the higher tropopause level. In other cases (black lines), the average lapse rate in the 2 km above the lower tropopause candidate remains below 2 K, and the lower candidate is counted as a tropopause. These differences are not clear from the figure, and may be therefore be very small, which leads to the suspicion that the choice of tropopause candidate is in fact quite arbitrary. In any case, it seems to have led to the fact that despite the calculation only returning one tropopause, both tropopause candidates can indeed be seen, if looking across several adjacent time steps.

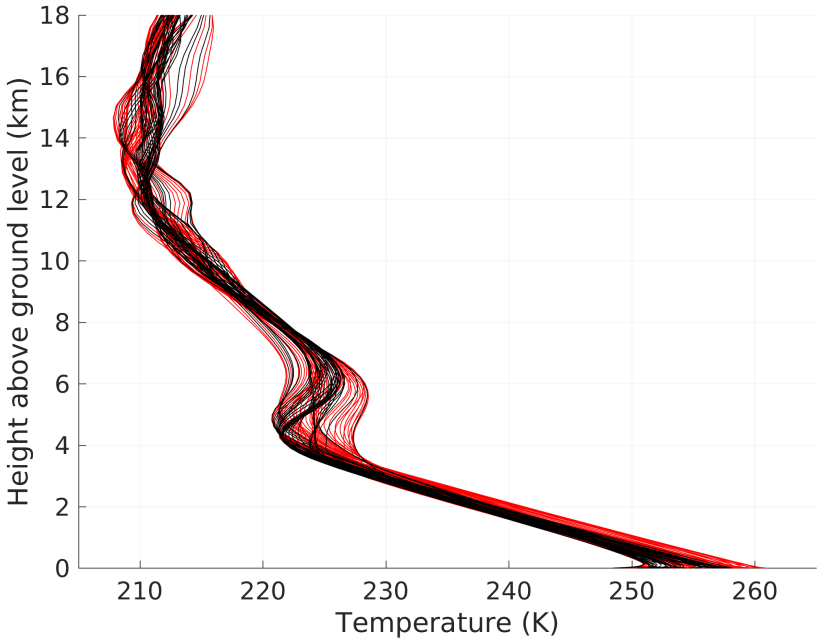

Figure 22: Area averaged temperature profiles for the 85-90°E, 30-35°N region. Each line represents one hourly time step in the period spanning January 26, 22:00 to January 30, 06:00 (local time). Red lines show the temperature profiles which yielded lapse rate tropopause heights (LRTH) higher than 9 km, black lines show the temperature profiles that yielded LRTH lower than 7 km.

3.2.5.3 What do the two levels correspond to? What may be the physical reason behind the existence of two separate atmospheric regions of temperature inversion? Tropopause folds, which frequently occur along the subtropical jetstream (Mohanakumar, 2008) and which has been found over the TP in other studies (X. Chen et al., 2013), may result in temperature profiles like those in Figure 22: a negative lapse rate may persist through the fold, while a positive lapse rate is found above the fold, and a negative lapse rate occurs again as the stratosphere is finally entered. Although it is conceivable that a tropopause fold could give rise to alternating tropopause heights between closely situated regions, or perhaps even from hour to hour due to movements in the fold, the fact that two levels are seen during the entire month (not shown) makes tropopause folding a highly unlikely cause, since folds usually decay after 1-2 days (Mohanakumar, 2008).

A more plausible explanation is that this region is situated below the transition from a lower (extra-tropical) to a higher (tropical) tropopause. Rather than a continuous decrease, the transition from tropical to extra-tropical tropopause height is often characterised by a region of overlapping tropopauses, which is generally found between 35°N and 45°N. (Kochanski, 1955; Randel et al., 2007). The latitudinal position (30°N-35°N) of the region analysed here suggests that it may be situated at the southern edge of the overlap. In that case, the southern parts of the region could be below the tropical tropopause and the northern parts of it below an underlying extra-tropical tropopause. However, the maximum value exceeds 12 km above ground level at each grid point (not shown) - i.e., the higher tropopause candidate is present at every grid point at some time during the investigated period. At the same time, the minimum over the period is lower than 5 km at all the grid points - so

the lower tropopause candidate also appears to be present everywhere. Rather than being situated at the border of the transition region and only having double tropopauses present in the southern parts, the region investigated here could therefore be fully positioned under the overlap region, i.e. below both tropopauses. The fact that the higher level is seen at all in the output from the tropopause calculation is because the lower tropopause is sometimes not regarded as a tropopause in the calculation.

3.2.5.4 May exchanges occur? If the study region is indeed situated under a double tropopause and the lower tropopause candidate truly is the extra-tropical tropopause as argued in the preceding section, the afternoon PBL tops are quite close to the extra-tropical tropopause, even without stratospheric intrusions like tropopause folds bringing the stratospheric air closer to the PBL. Given that the proximity between the PBL top and the tropopause is interesting because of its potential role in stratosphere-troposphere exchanges, the important remaining question is: can stratospheric air be reached by the PBL top? While the small distance seems to indicate that it can, it should be kept in mind that the tropopause as such represents a transport boundary because of the temperature inversion which hampers vertical transport. Therefore, mixing stratospheric air across the tropopause in a "normal" situation should be more difficult than mixing it from an intrusion in the form of a fold given the turbulence associated with fold decay (Mohanakumar, 2008), even if a turbulent layer - the PBL - reaches high enough.

To conclusively determine the lowest level where stratospheric air can actually be found or the degree of mixing at the interface between the troposphere and the stratosphere, a more thorough analysis would be required. However, what the preceding analysis has shown is that an inversion layer which is likely to be the extra-tropical tropopause does at least occasionally reach close to the top of high afternoon PBLs. In addition, it can be noted that the specific humidity drops rapidly in the region between 2 and 7 km and thereafter remains low and relatively constant, which is interesting since stratospheric air is generally much drier than tropospheric air (not shown). Moreover, PV, which is often used when determining the *dynamic tropopause*, increases above the commonly used tropopause threshold value of 2 PV units around the 300 hPa level, which is roughly 9 km above sea level in a standard atmosphere, corresponding to about 4 km above ground level (not shown). While specific humidity is not a general method for determining the tropopause height and the choice of threshold value for the dynamic tropopause is somewhat subjective and not necessarily useful on a smaller than synoptic scale (Maddox & Mullendore, 2018), the fact that both these variables also exhibit pronounced changes in the vicinity of the lower tropopause candidate lends further support to the idea that this is indeed a tropopause. Therefore, it is possible that stratospheric air can be entrained at the top of extremely deep TP PBLs or that tropospheric air may reach the stratosphere even in the absence of tropopause folding, despite the fact that stratosphere-troposphere exchanges over the TP have mainly been attributed to tropopause folds in previous studies (e.g. X. Chen et al., 2013; X. Chen, Ma, Kelder, Su, & Yang, 2011). Although outside the scope of this project, such a possibility merits further investigation elsewhere.

3.2.5.5 Close to the tropopause summary The small case study carried out her indicates that the PBL top can reach very close to a layer of negative lapse rates which likely represents the extra-tropical LRT, even without the aid of a stratospheric intrusion such as a tropopause fold. This layer is situated just above the afternoon PBLH peaks, roughly 4-6 km above ground level, and is overlain by a second region of negative lapse rates at an altitude of around 10-14 km, which is interpreted here as the tropical tropopause. Looking

across several time steps and adjacent grid points, it thus appear that a double tropopause can indeed be discerned despite the fact that the calculation performed her does not include detection of a second tropopause.

However, whether or not this proximity between PBL top and the tropopause has implications for stratosphere-troposphere exchanges can not be determined here. Although the vertical region above the presumed extra-tropical tropopause displays lower specific humidity and higher PV values than the region below, it is not further assessed whether the air above the presumed extra-tropical tropopause is truly stratospheric. Moreover, it is not certain that mixing can be achieved across the transport boundary that the tropopause constitutes without the turbulence brought about by an intrusion.

3.2.6 Connections with Climate Indices

In addition to the gridded climate variables investigated above, PBLH is investigated in relation to ISM, EASM, ENSO and NAO indices. First, correlation results are presented for TP-average PBLH (Section 3.2.6.1) and thereafter for PBLH in the CTP and SETP regions (Section 3.2.6.2). Next, a comparison is made between PBLH when the indices have high values and PBLH when the indices have low values (Section 3.2.6.3). Finally, results from correlations between gridded PBLH and the indices are shown (3.2.6.4).

3.2.6.1 TP-average planetary boundary layer height vs climate indices Correlations were computed between TP-average PBLH and the climate indices. With ENSO and NAO, the correlations were computed monthly (note that the ENSO "months" represent 2-month means) and seasonally. For the monsoon indices the correlations were performed for June, July, August and the June-July-August mean. The correlations are generally weak, regardless of whether they were performed on raw or detrended data. Correlations (for raw values) with the monsoon indices are shown for the summer months and correlations with ENSO and NAO for the dry and monsoon season in Table 2. Although a few individual months display significant correlations for ENSO and NAO, the only statistically significant correlation for the seasonal means is a negative correlation of 0.37 with ENSO in the dry season. The monsoon season correlation with ENSO is positive and weaker, 0.22, and for the other indices, the correlations are weaker still.

Table 2: Correlations between Tibetan Plateau (TP) Planetary Boundary Layer Height (PBLH) and climate indices. Correlation coefficients (Pearson's r) are shown for correlations between Tibetan Plateau area-averaged seasonal and monthly mean Planetary Boundary Layer Height (PBLH) and climate indices of the El Niño Southern Oscillation (ENSO), the North Atlantic Oscillation (NAO), the Indian Summer Monsoon (ISM) and the East Asian Summer Monsoon (EASM). The correlations with ENSO and NAO were performed for monsoon season (May-September) means and dry season (October-April) means. Due to the monsoon indices being available (and most relevant) for the summer, correlations with EASM and ISM were calculated for June, July, August and the summer (JJA) mean. A star denotes that the p value was < 0.05.

Climate Index	Monsoon season	Dry season		
ENSO	0.22	-0.37*		
NAO	0.16	0.06		
Climate Index	**June**	**July**	**August**	**JJA mean**
EASM	-0.02	0.17	0.20	0.03
ISM	0.04	-0.03	0.08	-0.14

Given that ENSO exhibited a statistically significant anticorrelation with PBLH in the dry season, may ENSO explain some of the inter-annual TP-average PBLH variability that was seen in Figure 4 B? Figure 23 show dry season mean PBLH and dry season mean ENSO. Strong El Niño are indicated by vertical dashed lines and strong La Niña by vertical dotted lines. (These are valid for the *dry season* ENSO time series and therefore the strongest El Niño and La Niña differs slightly from those of annual mean ENSO time series). At least for part of the time series, the anticorrelation is discernible. Most notable is the large PBLH dip in the 1997-1998 dry season, which coincides with a strong El Niño. However, no especially pronounced dips are shown for 1982-1983 or 2015-2016, when other strong El Niño episodes occurred. Neither can the strongest La Niña events (1988-1989, 1999-2000, 2010-2011) be discerned as any noteworthy PBLH anomalies.

It is possible that the seasonal aggregation hides shorter-term ENSO influences or that such influences are drowned in inter-annual variability resulting from other factors. Moreover, there may be delayed effects. To investigate this, correlations were performed between PBLH for individual months and ENSO bi-monthly means, with and without time lags. Statistically significant correlations occurred - however, they went in both directions, and in several cases they were approximately equally strong regardless of whether or not a time lag was introduced. For example, correlating the January time series of TP PBLH against the December-January time series of ENSO gives a statistically significant correlation of 0.5. Lagging PBLH behind by one month in order to allow detection of a delayed ENSO effect (i.e., correlating the December-January time series of ENSO against the February time series of PBLH) gives a slightly weaker but still significant correlation of 0.37. However, reversing the time lag so that January PBLH is correlated against January-February ENSO gives a statistically significant correlation of 0.48. It is therefore likely that ENSO does not exert a particularly large influence over the TP PBLH and that the monthly correlations found here may be attributed mainly to chance and should be treated with much caution.

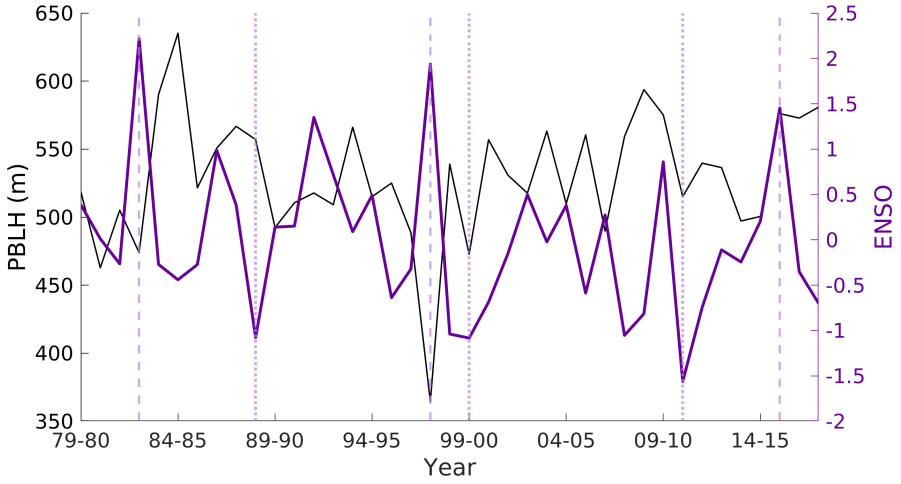

Figure 23: Time series of Tibetan Plateau (TP) Planetary Boundary Layer Height (PBLH) and the El Niño Southern Oscillation (ENSO) Index. Dry season (October-April) means are shown for PBLH (thin black line, left axis) and ENSO (purple thick line, right axis). Strong El Niño episodes are marked with dashed vertical lines, strong La Niña episodes are marked with dotted vertical lines.

3.2.6.2 Correlations with climate indices in the central and southeastern regions Potential influences exerted by the climate indices may differ in strength or even magnitude at different parts of the TP, so that existing influences disappear when correlating against the TP-average PBLH. Correlations were therefore computed for area-averaged PBLH in the two subregions.

No statistically significant correlations are found for the raw monsoon indices in the CPT region, but on the detrended data, the correlation with mean June-August ISM is negative and significant. For ENSO, significant negative correlations arise for January and February as well as the dry season mean, while significant positive correlations are found for July, August and September. With NAO, significant positive correlations are found in August and November.

In the SETP region, ISM is significantly positively correlated in August. EASMI exhibits a significant negative correlation in June, and a significant positive correlation in August. None of the correlations with ENSO are statistically significant, but positive significant correlations with NAO are found for June and December.

Regarding the ENSO correlations for the two regions, it can be noted that previous research has shown that El Niño events are often associated with deficit ISM rainfall and anomalously dry conditions in central TP (Kumar et al., 2006; Lei et al., 2019). Such conditions, especially given the significant anticorrelation between PBLH and Prc in central TP shown in Section 3.2.3, are likely to be associated with high PBL. While the monsoon season correlation with ENSO was indeed positive for the CTP region, it was not statistically significant, and the magnitude (0.27) was similar to that of the SETP region (0.30). For the dry season however, a significant correlation of -0.34 was found for the CTP region. It can also be noted that the CTP region, in contrast to the SETP region, exhibits a large dip in PBLH during the dry season 1997-1998 (Figure 7 A), which also suggest that in the dry

season, El Niño may act to reduce TP PBLH at least in some cases. Possibly, this could be achieved by the proposed ENSO effects on TP snow cover. Shaman and Tziperman (2005) argues that El Niño leads to increased snowfall which creates a large TP snowpack. It is conceivable that the snowpack in turn may be related to anomalously low PBLs, since it alters the surface energy balance by increasing the albedo and reducing the SH.

3.2.6.3 Planetary boundary layer height corresponding to notable indices values For each of the investigated climate indices, Q3 and Q1 (the upper and lower quartiles, i.e values $\geq$ the 75th percentile and values $\leq$ the 25th percentile) were counted as strong/-positive years and weak/negative years, respectively (Section 2.4.3). The mean PBLH in the corresponding years was then compared to see if there were consistent differences in mean PBLH during years when a particular index was strong and years when the same index was weak (Table 3). By this simple comparison of the single mean values, it can be noted that there is consistency to the differences: The mean PBLH in strong ISM years is lower than the mean PBLH in weak ISM years, for the CTP and SETP regions as well as the entire TP, both when looking at the annual PBLH means and the monsoon season PBLH means. The opposite is true for the EASM, for which the mean PBLH is instead consistently higher in the strong EASM years than in the weak EASM years. For the ENSO, the difference is dependent on the season. The dry season mean PBL is lower in strong ENSO dry seasons (i.e. El Niño-like conditions), while the monsoon season mean PBL is higher in strong ENSO monsoon seasons. The positive NAO years in contrast, corresponds to higher PBLH in both seasons.

To see if the often small but entirely consistent differences in mean PBLH corresponds to statistically significant differences between all PBLH in the Q3 and Q1 cases, respectively, paired sample t-tests were performed. However, the tests did not indicate significant differences for any of the indices. It can be noted that Q3 and Q1 were selected to generate equally sized groups of strong/positive and weak/negative values for all the indices and not with respect to what is generally considered a particularly high or low value of each index. Q3 and Q1 may therefore not correspond to values generally taken to be e.g. "El Niño and La Niña" , or "strong monsoon and weak monsoon".

Table 3: Planetary Boundary Layer Height (PBLH) in years or seasons with higher than average (+) and lower than average (-) values for the climate indices. Annual mean PBLH (A), monsoon season mean PBLH (M) and dry season mean PBLH (D) is shown for the central Tibetan Plateau (TP) region (CTP), the southeastern TP region (SETP) and the entire plateau (TP). For each respective climate index, the + sign denotes mean PBLH calculated over all the years/seasons for which that index had a value at or above the 75th percentile. The - sign denotes mean PBLH over the years/seasons when the index had a value at or below the 25th percentile. The indices are for the Indian Summer Monsoon (ISM), the East Asian Summer Monsoon (EASM), the El Niño Southern Oscillation (ENSO) and the North Atlantic Oscillation (NAO).

Index	PBLH (m)					
ISM	CTP (A)	SETP (A)	TP (A)	CTP (M)	SETP (M)	TP (M)
+	1164	382	567	1026	494	624
-	1174	423	583	1060	507	635
EASM	CTP (A)	SETP (A)	TP (A)	CTP (M)	SETP (M)	TP (M)
+	1148	401	577	1013	499	633
-	1106	390	557	997	493	622
ENSO	CTP (D)	SETP (D)	TP (D)	CTP (M)	SETP (M)	TP (M)
+	1182	323	512	1115	512	640
-	1278	331	544	990	496	623
NAO	CTP (D)	SETP (D)	TP (D)	CTP (M)	SETP (M)	TP (M)
+	1282	334	535	1106	505	641
-	1184	319	525	989	499	623

3.2.6.4 Spatial correlations with climate indices Given the large differences in PBLH characteristics across the TP, correlations were also performed between the climate indices and PBLH at each grid point. Correlations were performed using monthly as well as seasonal means, on raw and detrended data, but were mostly weak. Only a selection of the resulting correlation maps are included here.

In August the ISM is anticorrelated with PBLH in a small part of western TP, while positive correlation dominates in the south and east (Figure 24 A). However, significance is lacking over most of the plateau. In the JJA mean, there is mainly negative correlation in central TP and positive correlation towards its edges, especially along the southern rim (Figure 24 B). The correlations are generally weak and significance is absent to an even larger degree than for August. However, the ISM correlations were stronger and significance more extensive when the trend was removed, indicating that the correlation (anticorrelation) between PBLH and ISM arises due to correlation in shorter term variations rather than trends (Figure 24 C and D).

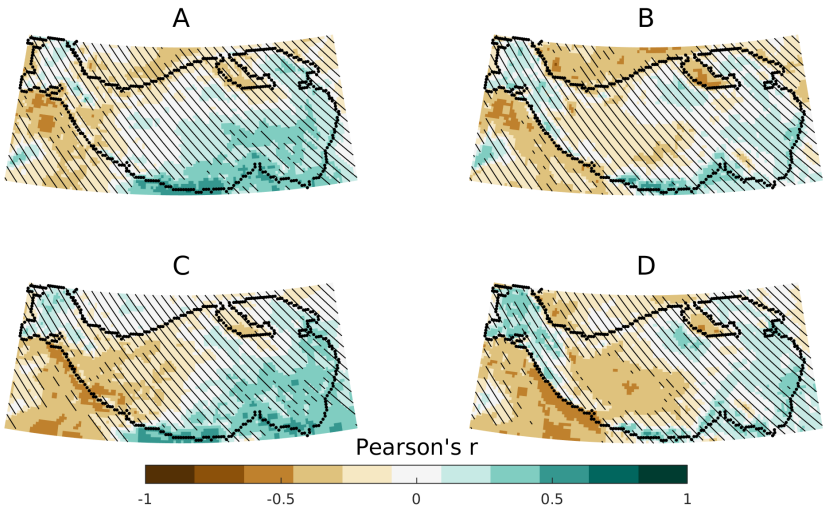

Figure 24: Spatial Correlation between Planetary Boundary Layer Height (PBLH) and the Indian Summer Monsoon (ISM). Black lines are drawn over regions where the correlation is *not* significant at the 95% confidence level. **A:** August. **B:** June-July-August mean. **C:** As A, but the correlation was performed on detrended data. **D:** As B, but the correlation was performed on detrended data.

EASMI and PBLH were correlated for June, July, August and the June-July-August mean. The correlations were mainly weak and without significance, and there was not much difference between correlations computed for the raw and detrended data, respectively. For June however, some anticorrelation is found in the eastern parts along with correlation at and outside of southwestern TP (Figure 25 A). For August, positive correlation is present along the southeastern rim of the plateau (Figure 25 B). The difference in sign between June and August in southeastern TP may possibly be related to the seasonal march of the EASM, but given that the region should be affected by the EASM in both months it is hard to say how or why. Given that the correlations are mostly weak, it is also possible that no notable relationship exist between the EASM and TP PBLH. The correlations may then be more related to influences of a common factor on both variables than to an effect of the EASM on PBLH or vice versa.

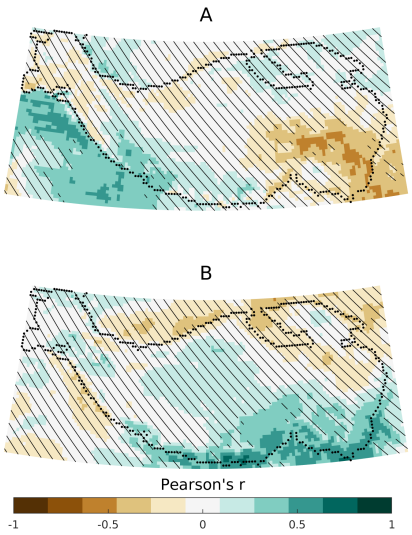

Figure 25: Correlation between Planetary Boundary Layer Height (PBLH) and the East Asian Summer Monsoon (EASM). Black lines are drawn over regions where the correlation is *not* significant at the 95% confidence level. **A:** June **B:** August.

Season-wise correlations with the ENSO yielded weak and mainly non-singnificant correlations, with a tendency towards positive correlation during the monsoon season and negative correlation during the dry season (not shown). Correlations on the monthly means revealed that January had the largest region of statistically significant anticorrelation, while July, August and September featured prominent positive correlations (not shown). Therefore, correlations were computed for the July-September mean (Figure 26). Significant positive correlation of around 0.5 is present over the central plateau and along its southern rim, while the rest of the TP exhibits very weak and non-significant correlation.

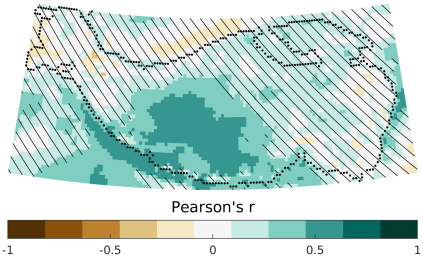

Figure 26: Spatial correlation between Planetary Boundary Layer Height and the El Niño Southern Oscillation (ENSO) Index, for June-September mean values. Black lines are drawn over regions where the correlation is *not* significant at the 95% confidence level.

Monthly as well as seasonal correlations with the NAO were non-significant over most of the TP (not shown). In both seasons, positive but fairly weak correlation is present in central-western TP, along with equally weak anticorrelation in a small northeastern TP region. The effects on TP precipitation and snow cover found in previous studies (Linderholm

et al., 2011; Z. Wang et al., 2017; Y. Liu et al., 2018) could explain why correlations with PBLH arise at all, but given that the correlations are generally weak and goes in both directions even within the same season it is likely that there is no particularly strong relationship between TP PBLH and NAO.

3.2.6.5 Indices summary The correlations with the climate indices for ISM, EASM, ENSO and NAO are in most cases not very strong. TP-average PBLH and ENSO are significantly anticorrelated for the dry season, but no general influences of individual El Niño or La Niña events are discernible in the PBLH dry season time series. On a monthly time scale the ENSO correlations yields similar results whether or not a time lag was introduced, indicating that at least for this time scale, the ENSO is not particularly relevant for TP PBLH in spite of some significant correlations.

Consistent differences in mean PBLH is found between years with low and high values, respectively, for all the indices, but statistically significant differences are not present for any of the indices.

Spatial correlation results differ between seasons and regions. Anticorrelations with ISM are present in central TP and show improved significance when performed on detrended data, indicating that ISM and PBLH are anticorrelated in inter-annual variability but that the decreasing trends in both variables diminish the anticorrelation signal if the ISM trend is not removed. In contrast to the dry season, ENSO exhibits positive correlations in central TP in summer. EASMI may play a role in smaller regions, particularly in the southeastern TP. For the NAO, strong or consistent relationships with TP PBLH appear to be lacking.

3.2.7 Connections with Climate Variables Summary

While SH appears to be the most dominating factor behind PBLH and its trends, the relative contribution of each forcing may differ greatly between regions. For example, it is plausible that the seasonal variations in the SETP region are determined by the annual cycle of insolation and heating to a larger degree than the seasonal cycle in the CTP region, which appears to be more sensitive to changes in moisture conditions. Further, the analysis of the proximity between the PBL top and the tropopause indicates that high wintertime PBLs can indeed reach very close to the tropopause, as suggested by previous research (X. Chen et al., 2013), and that tropopause folding is not necessary to bring about this proximity. As for the climate indices quantifying the ISM, EASMI, ENSO and NAO, their relationships with the PBLH appears to be generally weak, although significant in certain regions and for particular time spans.

3.3 Scientific Contributions and Relevance

The results presented and discussed in the previous sections describe the main spatial and temporal characteristics of plateau-wide PBLH during the last four decades, and some suggestions are made regarding the factors determining the PBLH. What is to be gained from this knowledge?

While the findings may not be directly applicable for any practical purposes, they help shed some light over a data-scarce and interconnected region about which there is still much to learn. Firstly, this study complements previous research which has largely relied on measurements conducted at a single location and for a much shorter time span. As seen in the previous sections, there is great spatial variability within the TP, for PBLH as well as

the other investigated climate variables. Using a homogeneous gridded dataset covering a comparatively long period therefore helps to fill the gaps and provides an overview which may serve as a useful starting point for further and more detailed studies. Especially, the results highlight the large spatial differences and makes it clear that single location studies of TP PBLH should never be assumed to represent a larger area.

Secondly, the differences in the strength and even direction of the trends indicate that so far, TP PBLH has not responded to climate change in a uniform way. This complicates projections of the future PBLH evolution and makes it clear that climate change studies in which TP PBLH is included need to be very careful when making assumptions about future PBLH trends.

Lastly, it appears that the PBL top and the tropopause may be found at roughly the same altitude, even in the absence of tropopause folding. This suggests that interactions and exchanges between the PBL top and the tropopause as well as the stratosphere should be examined.

3.4 Limitations

There are a number of limitations to this study that should be addressed. Firstly, there are many factors contributing to PBL development that are ignored, and secondly, the analysis as well as the data on which it is performed has limitations leading to uncertainties concerning some of the results.

3.4.1 Ignored Factors

Many factors that may contribute to PBL development are not explicitly considered here. Therefore, their contributions can not be assessed separately, even if their effects are still present since they are involved in the calculations in IFS. For example, data on cloud cover or type are not included despite the fact that clouds play a large role for radiation in the atmosphere as well as the surface, and thus for the SH and PBLH. Although the presence of clouds can be inferred from precipitation, which is included here, there are no means of separating the effects of precipitation from the effects of cloudiness, or, in the absence of rain, cloudy conditions from clear conditions. Moreover, PBLH variations are not statistically analysed in relation to topographic variations. Due to the complex topography of the TP such variations may cause spatial differences in PBLH characteristics that could not be explained here. For example, local wind systems such as mountain-valley circulations was found to influence deep convection in K. Yang et al. (2004). Neither is the type (grass, glacier, snow, etc) or moisture content of the land surface analysed, despite the fact that these are important in determining PBLH because of their effects on surface albedo and heat fluxes. Another factor which is crucial for SH and therefore PBLH is ΔT, the difference between land surface temperature and air temperature. In addition, previous research (X. Chen et al., 2013, 2016) has indicated that the high PBLs in late winter and early spring can be attributed to favourable atmospheric stability, which in turn may be related to jet stream strength and position and upper-level PV. Although PBLH is determined by the Ri_b, which is a form of stability measure, the stability in higher layers may also play a role.

3.4.2 Limitations of the Analysis

Some limitations are inherent to statistical analyses such as those performed here. While e.g. correlations can readily be computed, it is more difficult to decide in what cases the

results should be ascribed to chance, and when they should be taken to indicate that the investigated variables are indeed connected. In the case of a complex and interconnected system like the climate system, it is not obvious whether two variables a and b have a similar (or opposite) variation because a influences b, because b influences a, or because they are both influenced by a common factor c. Physical knowledge about the climate system must therefore always be carefully considered when interpreting the results.

Whereas the first research question - *how* the PBLH has varied - can be answered well within a framework of statistics and visualisation, the second research question, inquiring into the relation between PBLH and other variables, is more challenging. Although it can be shown how PBLH varies in relation to other variables, such an analysis would have benefited from modelling experiments run in parallel with the statistical analysis.

In addition, the results may be sensitive to the temporal aggregation and it is not obvious which approach is the best. While analysing shorter periods like individual months separately may leave more noise in the result, aggregating over longer periods may enhance the risk that opposite signals cancel each other out. Including a pre-monsoon period may have allowed better interpretation of the high PBLs in late winter and early spring.

Although tropopause height was analysed along with PBLH in a small region for a very short time frame, no assessments could be made about how often high PBL coincide with low tropopause, or how close they generally reach. Although the region and time frame was selected because the monthly values of PBLH and LRTL indicated a short distance, the analysis in Section 3.2.5 should be treated as an example and not be taken to be generally applicable.

3.4.3 Data Limitations and Uncertainties

Although reanalysis data do present an exciting opportunity to study the climate of any region, it should be kept in mind that evaluation of data quality is difficult for regions like the TP. First, there are few observations available and secondly, the complex terrain means that the scarce observations that exist may not be representative for any larger region. Further investigation into the reliability and accuracy in ERA5 PBLH and related variables for the TP region are thus much needed.

3.4.3.1 Spatial resolution As stated above, a detailed analysis of PBLH variations in relation to topography, preferably using data with higher resolution than ERA5, might have contributed to understanding the spatial PBLH variability. However, for a plateau-wide investigation, homogeneous data coverage over the entire TP is arguably more important than high resolution.

3.4.3.2 ERA5 limitations and uncertainties in planetary boundary layer height and associated variables No data validation was performed within this project, and due to its relatively recent release, there is not yet a large amount of research evaluating ERA5 for different applications. The few studies that have been made generally indicate significant improvements from its predecessor, ERA-Interim (e.g. Martens et al., 2020), but a few shortcomings have been reported that may have implications for the PBLH. M. Wang et al. (2019) looked at the spring trend in SH at the central and eastern TP and found an increasing trend in ERA5 (as well as in JRA-55, the other reanalysis data which was included

in their study) which does not agree with the observations or simulations they compared it against. Moreover, a recent study found a tendency for over-estimations of surface turbulent fluxes and therefore the amount of energy that was transported into the PBL during sunny days in the central TP, for the June-September 2011 period they studied. However, as the authors point out, the difference in spatial resolution complicates comparisons with single-point observations (Sun et al., 2020).

The PBLH is not a variable that can be readily measured and simply read from an instrument. Instead it relies on other variables, and estimating it involves calculations and therefore approximations as well as assumptions, which may introduce errors. How PBLH and other parameterised variables are calculated in relation to each other may also impact their statistical relationships. It should therefore be noted that the results obtained here applies to ERA5 and can not be assumed to be valid for other datasets.

3.4.3.3 Uncertainties in the tropopause calculations The tropopause levels are not readily available in the ERA5 output but was calculated from the temperature data (See Section 2 and Appendix A and B for further information). In the case of the LRT, this was performed using a modified version of the NCL function trop_wmo (The NCAR Command Language, 2017). While a comparison indicated that LRTL calculated with the modified version agrees well with the LRTL values calculated with the original function, spurious low values were present when analysing hourly LRTH. It is not entirely clear whether these arose from the LRTL calculation or the conversion to LRTH. It can be noted that the calculation of LRTH involves simplifications, since it does not account for the effects of cloud ice and water or precipitation.

As for the CPTL, it was calculated using cubic spline interpolation. Although an evaluation that was made for a small sample of the data indicates that the calculation performs well, it can not be ruled out that the interpolation introduces artefacts. It is possible that fitting a lower order polynomial would reduce the risk of such artefacts.

3.5 Future Outlook and Research Challenges

Atmospheric stability in higher layers, which has been deemed important in previous studies dealing with individual stations and short time spans, could be a lacking factor which could help to explain the high winter-spring PBLH in this study. Future studies should therefore utilise reanalysis data to investigate if this is indeed the case. Moreover, tropopause PBLH interactions and stratosphere-troposphere exchanges across the TP should be further assessed given the indications found here that the distance can be extremely small.

Studies should be carried out that aim to untangle the TP PBLH responses to climate change and predict future PBLH changes under different climate scenarios. Modelling should be carried out to investigate the causality behind statistical results. Finally, the practical implications of PBLH changes -if such exist- should be analysed. While it is plausible that important features of the regional climate such as the monsoon systems affect the PBLH rather than the other way around, the TP climate is known for its far-reaching influences. Therefore it should be assessed if recent and future changes in PBLH will in turn lead to other changes in the climate, at the TP and elsewhere.

4 Summary and Conclusions

In this thesis, the reanalysis dataset ERA5 is used to investigate PBLH variations at the TP for the 1979-2018 period. The first part of the analysis consists of a PBLH climatology displaying inter-annual and seasonal variations as well as spatial patterns and, for two focus regions, diurnal variations. This part of the analysis is focused around the research question: *How has the PBLH over the TP varied during the last decades?* The main conclusions are listed below.

- The PBLH exhibits great spatial variations across the TP in terms of seasonal cycles, trends, mean heights and maximum heights.
- TP-average PBLH reaches its seasonal maximum heights in spring, with its highest median in May and its highest maximum in March. Comparing two different regions however reveals differing seasonal patterns in different regions: In the CTP region, PBLH peaks in March and April and has its annual minimum in August, while PBLH in the SETP region peaks in May and June and remains high throughout the summer.
- The PBLH trend is ambiguous. While statistically significant decreasing trends of up to 65 m per decade dominates the interior of the plateau during the monsoon season, non-significant positive trends of varying magnitude is present across most of the plateau in the dry season. The area-averaged plateau-wide trends are not statistically significant, and the declining monsoon season trend of 5.3 m per decade along with the increasing dry season trend of 6.6 m per decade together result in a very weak annual trend of 0.9 m per decade.
- TP PBLs can grow extremely high. In parts of the central plateau the dry season mean PBLH reaches about 1.5 km. Area-averaged CTP PBL occasionally reaches heights of 6 km in the afternoon, while individual grid points in this region features PBLH greater than 7.5 km.

In the second part of the analysis the PBLH variations are put in to a context of variations in local climate variables and indices describing ISM, EASM, ENSO and NAO. This part is focused around the question: *How is the PBLH related to local climate variables and to circulation features such as the monsoon and westerlies?* The main conclusions follow below.

- Overall, the SH exerts a dominating influence on TP PBLH. In addition to being strongly positively correlated with PBLH over most of the plateau, its spatial patterns in means and trends closely resembles the PBLH patterns, indicating that changes in SH is the dominating cause behind PBLH trends.
- In addition to SH, PBLH in most parts of the TP is positively correlated with T2m and negatively correlated with Prc. Some positive correlation with WS500, U100 and U300 is also present.
- In the CTP region, it is plausible that the increasing monsoon season precipitation trend acts to reduce the SH and thereby the PBLH. This reduction may be brought about by alterations to the surface energy budget, resulting from the increased precipitation as well as the associated cloudiness.
- The positive PBLH trends in the SETP region during the dry season are found where SH and T2m have their strongest trends, indicating that the PBLH has increased in response to increasing SH and T2m in this region.

- The reasons for differences in the seasonal PBLH cycle between the CTP region and the SETP could not be fully untangled here, but precipitation and wind speed may partly explain the variation in the CTP region while thermal conditions appear to be more important in the SETP region.
- An analysis of PBLH and LRTH in a small region indicates that the low extra-tropical tropopause may reach very close to the high wintertime PBL tops, even in the absence of stratospheric intrusions like tropopause folds. Whether or not the proximity between the PBL top and the LRT is enough for stratosphere-troposphere exchanges to occur even without the aid of tropopause folding has not been assessed in this study but remains an interesting possibility and should be studied further.
- The ISM, EASM, ENSO and NAO indices are generally not strongly correlated with TP PBLH. The weak correlations indicate the dominant influence of local factors in determining the PBLH over the TP. However, there is a negative correlation with ENSO in the dry season, although no clear influence of El Niño or La Niña events can be discerned in the PBLH time series. The monsoon indices show correlations of both signs in certain regions, which in the case of ISM is stronger when the trend is removed prior to correlation.
- Variables that were not included in this analysis, such as atmospheric stability, cloud radiative effects and land surface characteristics should be considered in future studies aiming to explain the PBLH characteristics over the TP. Statistical analysis should be combined with modelling to better understand the processes involved in PBL growth and potential implications of future changes in TP PBLH should be examined.

5 Acknowledgements

First and foremost, I would like to thank my supervisor Deliang Chen for suggesting this project and helping me along the way by sharing knowledge and ideas. I would also like to thank my co-supervisor David Rayner for help, suggestions and discussions, not least regarding code and statistical methods. In addition, I want to thank my examiner Sofia Thorsson and my opponent Sara Jäger for helpful suggestions and comments.

Moreover, I would like to thank Julia Kukulies for encouragement and help with data download, Peng Zhang for letting me know about the NCL function trop_wmo, and Tinghai Ou for help with technical issues regarding work on the remote server.

I would also like to express my gratitude to Johan Lund for all the discussions, encouragement and coding tips. Last but not least, I would like to thank my fellow students in Ventifakten. It was great sharing laughter, frustration and coffee with you!

6 Glossary

Albedo The ratio of reflected radiant energy to incident radiant energy. For example, bright surfaces such as snow or ice have a high albedo in the visible spectrum (high reflection of visible light) while the opposite is true for dark surfaces.

Atmospheric stability There are several different types of stability, giving rise to a variety of motions. For example, *static stability* is the tendency of a fluid at rest to become turbulent or laminar due to the effects of buoyancy, while *dynamic stability* is the propensity of

a fluid to resist or recover from perturbations, induced by e.g. wind shear. Most generally, air is unstable if very small perturbations tend to grow. Lapse rate (temperature decrease with height) is often used as an indicator of (static) stability, since it determines whether vertical movements are suppressed or enhanced.

Bowen ratio The ratio of sensible heat flux to latent heat flux (from the Earth's surface into the atmosphere). Higher values thus correspond to more arid conditions.

Buoyancy The buoyancy (of e.g. a parcel of air) allows it to ascend and remain suspended in a fluid (such as the atmosphere). Thus, in the atmosphere, the *buoyancy force* is the upward force exerted upon the parcel because of the density difference between the parcel and the surrounding air: A heated air parcel ascends because its density is lower than that of the surrounding air.

Cryosphere The fraction of the Earths surface which is made up of frozen water, such as ice sheets, glaciers, permafrost, seasonal snow cover, river ice, lake ice, sea ice and solid precipitation.

Diabatic A diabatic process involves an energy exchange by virtue of a temperature difference (as opposed to an *adiabatic* process, in which no heat or mass is exchanged).

Latent Heat Flux Energy addition or subtraction manifested as a change of state, e.g., from liquid to gas, while the temperature is unchanged (compare with sensible heat flux).

Intertropical convergence zone A region encircling the Earth in which the trade winds from both hemispheres converge and warm humid air rises.

Planetary boundary layer (PBL) The PBL is the part of the troposphere which is directly influenced by the surface of the Earth. It's height and characteristics are therefore dependent on properties of the underlying surface, such as its temperature, moisture and roughness.

Potential Vorticity Potential vorticity is a vector field giving a measure of rotation at any point in a fluid, or a measure of the capacity for air to rotate. It is a quantity that it conserved (if the effects of heating and friction are ignored), putting thermodynamic constraints on motion in the fluid, since momentum fields must evolve in a way that preserves the potential vorticity following the motion. Potential vorticity can be used to locate regions in the atmosphere where large storms may develop. In addition, potential vorticity increases strongly above the tropopause and can therefore also be used when determining the tropopause or investigating stratosphere-troposphere exchanges.

Sensible Heat Flux Energy addition or subtraction manifested as a change in temperature (compare with latent heat flux).

Stratosphere The layer of the Earths atmosphere overlying the troposphere. The stratosphere spans from the tropopause at altitudes of approximately 10-17 km up to an altitude of roughly 50 km.

Tropopause The transition zone between the troposphere and the stratosphere.

Troposphere The troposphere is the lowest part of the Earth's atmosphere, extending

to heights of about 10-17 km depending on season and region. Almost all weather phenomena takes places in the troposphere.

References

American Meteorological Society. (2012). *Glossary of meteorology.* Retrieved from `http://glossary.ametsoc.org/wiki/Latent_heat` (Accessed 2020-03)

Barnston, A. G., & Livezey, R. E. (1987). Classification, seasonality and persistence of low-frequency atmospheric circulation patterns. *Monthly weather review*, *115*(6), 1083–1126.

Betts, A. K., Chan, D. Z., & Desjardins, R. L. (2019). Near-surface biases in ERA5 over the Canadian Prairies. *Frontiers in Environmental Science*, *7*, 129.

Bibi, S., Wang, L., Li, X., Zhou, J., Chen, D., & Yao, T. (2018). Climatic and associated cryospheric, biospheric, and hydrological changes on the Tibetan Plateau: a review. *International Journal of Climatology*, *38*, e1–e17.

Broccoli, A. J., & Manabe, S. (1992). The effects of orography on midlatitude Northern Hemisphere dry climates. *Journal of Climate*, *5*(11), 1181–1201.

Chan, K. M., & Wood, R. (2013). The seasonal cycle of planetary boundary layer depth determined using COSMIC radio occultation data. *Journal of Geophysical Research: Atmospheres*, *118*(22), 12–422.

Chen, C., Cane, M. A., Wittenberg, A. T., & Chen, D. (2017). ENSO in the CMIP5 simulations: life cycles, diversity, and responses to climate change. *Journal of Climate*, *30*(2), 775–801.

Chen, X., Anel, J. A., Su, Z., de la Torre, L., Kelder, H., van Peet, J., & Ma, Y. (2013). The deep atmospheric boundary layer and its significance to the stratosphere and troposphere exchange over the Tibetan Plateau. *PloS one*, *8*(2), e56909.

Chen, X., Ma, Y., Kelder, H., Su, Z., & Yang, K. (2011). On the behaviour of the tropopause folding events over the Tibetan Plateau. *Atmospheric Chemistry and Physics*, *11*(10), 5113.

Chen, X., Škerlak, B., Rotach, M. W., Añel, J. A., Su, Z., Ma, Y., & Li, M. (2016). Reasons for the extremely high-ranging planetary boundary layer over the western Tibetan Plateau in winter. *Journal of the atmospheric sciences*, *73*(5), 2021–2038.

Chen, Y., & Ji, D. (2019). Evaluation of ERA5 Atmospheric Reanalysis Datasets for Surface Climatology over the Tibetan Plateau. *AGUFM*, *2019*, A13R–3100.

Copernicus Climate Change Service (C3S) . (2017). *ERA5: Fifth generation of ECMWF atmospheric reanalyses of the global climate. Copernicus Climate Change Service Climate Data Store (CDS).* `https://cds.climate.copernicus.eu/cdsapp#!/home`. (Acessed: 2019)

Davis, E. V., Rajeev, K., & Mishra, M. K. (2020). Effect of Clouds on the Diurnal Evolution of the Atmospheric Boundary-Layer Height Over a Tropical Coastal Station. *Boundary-Layer Meteorology*, 1–18.

Ding, Z., Wang, Y., & Lu, R. (2018). An analysis of changes in temperature extremes in the Three River Headwaters region of the Tibetan Plateau during 1961–2016. *Atmospheric research*, *209*, 103–114.

Duan, A., & Wu, G. (2008). Weakening trend in the atmospheric heat source over the Tibetan Plateau during recent decades. Part I: Observations. *Journal of Climate*, *21*(13), 3149–3164.

ECMWF. (n.d.). *ERA5 hourly data on single levels from 1979 to present.* `https://cds-dev.copernicus-climate.eu/cdsapp#!/dataset/reanalysis-era5-single-levels?tab=overview`. (Accessed: 2019-09-16)

ECMWF. (2017). Part iv: Physical processes. In *IFS Documentation CY43R3.* ECMWF. Retrieved from `https://www.ecmwf.int/node/17736`

Eltahir, E. A. (1998). A soil moisture–rainfall feedback mechanism: 1. Theory and observations. *Water resources research*, *34*(4), 765–776.

Fedorov, A. V., & Philander, S. G. (2000). Is El Niño changing? *Science*, *288*(5473), 1997–2002.

Feng, S., Fu, Y., & Xiao, Q. (2011). Is the tropopause higher over the Tibetan Plateau? Observational evidence from Constellation Observing System for Meteorology, Ionosphere, and Climate (COSMIC) data. *Journal of Geophysical Research (Atmospheres)*, *116*, 21121-. doi: 10.1029/2011JD016140

Flohn, H. (1957). Large-scale aspects of the "summer monsoon" in South and East Asia. *Journal of the Meteorological Society of Japan. Ser. II*, *35*, 180–186.

Frauenfeld, O. W., Zhang, T., & Serreze, M. C. (2005). Climate change and variability using European Centre for Medium-Range Weather Forecasts reanalysis (ERA-40) temperatures on the Tibetan Plateau. *Journal of Geophysical Research: Atmospheres*, *110*(D2).

Fu, R., Hu, Y., Wright, J. S., Jiang, J. H., Dickinson, R. E., Chen, M., ... Wu, D. L. (2006). Short circuit of water vapor and polluted air to the global stratosphere by convective transport over the Tibetan Plateau. *Proceedings of the National Academy of Sciences*, *103*(15), 5664–5669.

Gao, P., Xu, X., & Zhang, X. (2015). Characteristics of the Trends in the Global Tropopause Estimated From COSMIC Radio Occultation Data. *IEEE Transactions on Geoscience and Remote Sensing*, *53*(12), 6813–6822.

Ge, F., Sielmann, F., Zhu, X., Fraedrich, K., Zhi, X., Peng, T., & Wang, L. (2017). The link between Tibetan Plateau monsoon and Indian summer precipitation: a linear diagnostic perspective. *Climate dynamics*, *49*(11-12), 4201–4215.

Guo, J., Li, Y., Cohen, J. B., Li, J., Chen, D., Xu, H., ... Zhai, P. (2019). Shift in the temporal trend of boundary layer height in China using long-term (1979–2016) radiosonde data. *Geophysical Research Letters*, *46*(11), 6080–6089.

Guo, J., Miao, Y., Zhang, Y., Liu, H., Li, Z., Zhang, W., ... Bian, L. (2016). The climatology of planetary boundary layer height in China derived from radiosonde and reanalysis data. *Atmospheric Chemistry and Physics*, *16*(20), 13309.

Guo, X., Wang, L., Tian, L., & Li, X. (2017). Elevation-dependent reductions in wind speed over and around the Tibetan Plateau. *International Journal of Climatology*, *37*(2), 1117–1126.

Ha, K.-J., Seo, Y.-W., Lee, J.-Y., Kripalani, R., & Yun, K.-S. (2018). Linkages between the South and East Asian summer monsoons: a review and revisit. *Climate dynamics*, *51*(11-12), 4207–4227.

Hamilton, M. (1987). Monsoons – an introduction. *Weather*, *42*(6), 186–193.

Hennermann, K., & Berrisford, P. (2019). *ERA5 data documentation.* `https://confluence.ecmwf.int/display/CKB/ERA5+data+documentation#ERA5datadocumentation`. (Accessed: 2019-09-05)

Hersbach, H. (2018). *Operational global reanalysis: Progress, future directions and synergies with NWP.* European Centre for Medium Range Weather Forecasts.

Highwood, E., & Hoskins, B. (1998). The tropical tropopause. *Quarterly Journal of the Royal Meteorological Society*, *124*(549), 1579–1604.

Hoinka, K. P. (1998). Statistics of the global tropopause pressure. *Monthly Weather Review*, *126*(12), 3303–3325.

Hurrell, J. W., Kushnir, Y., Ottersen, G., & Visbeck, M. (2003). An overview of the North Atlantic oscillation. *Geophysical Monograph-American Geophysical Union*, *134*, 1–36.

Immerzeel, W. W., Van Beek, L. P., & Bierkens, M. F. (2010). Climate change will affect the Asian water towers. *Science*, *328*(5984), 1382–1385.

IPCC. (2013). *Climate Change 2013: The Physical Science Basis. Contribution of Working Group I to the Fifth Assessment Report of the Intergovernmental Panel on Climate Change* (T. F. Stocker et al., Eds.). Cambridge, United Kingdom and New York, NY, US: Cambridge University Press.

Jiang, X., Wang, D., Xu, J., Zhang, Y., & Chiu, L. S. (2017). Characteristics of observed tropopause height derived from L-band sounder over the Tibetan Plateau and surrounding areas. *Asia-Pacific Journal of Atmospheric Sciences*, *53*(1), 1–10.

Jiang, X., Zhang, T., Tam, C.-Y., Chen, J., Lau, N.-C., Yang, S., & Wang, Z. (2019). Impacts of ENSO and IOD on Snow Depth Over the Tibetan Plateau: Roles of Convections Over the Western North Pacific and Indian Ocean. *Journal of Geophysical Research: Atmospheres*, *124*(22), 11961–11975.

Jianping, L., & Qingcun, Z. (2003). A new monsoon index and the geographical distribution of the global monsoons. *Advances in Atmospheric Sciences*, *20*(2), 299–302.

Jianping, L., & Wang, J. X. (2003). A new North Atlantic Oscillation index and its variability. *Advances in Atmospheric Sciences*, *20*(5), 661–676.

Johnson, W. B., & Viezee, W. (1981). Stratospheric ozone in the lower troposphere —I. Presentation and interpretation of aircraft measurements. *Atmospheric Environment (1967)*, *15*(7), 1309–1323.

Khan, A., & Jin, S. (2016). Tropopause variations in Tibet from COSMIC GPS Radio Occultation observations. In *2016 IEEE International Geoscience and Remote Sensing Symposium (IGARSS)* (pp. 3978–3981).

Kochanski, A. (1955). Cross sections of the mean zonal flow and temperature along 80°W. *Journal of Meteorology*, *12*(2), 95–106.

Koteswaram, P. (1958). The easterly jet stream in the tropics. *Tellus*, *10*(1), 43–57.

Kukulies, J., Chen, D., & Wang, M. (2019). Temporal and spatial variations of convection and precipitation over the Tibetan Plateau based on recent satellite observations. Part I: Cloud climatology derived from CloudSat and CALIPSO. *International Journal of Climatology*.

Kumar, K. K., Rajagopalan, B., Hoerling, M., Bates, G., & Cane, M. (2006). Unraveling the mystery of Indian monsoon failure during El Niño. *Science*, *314*(5796), 115–119.

Lei, Y., Zhu, Y., Wang, B., Yao, T., Yang, K., Zhang, X., ... Ma, N. (2019). Extreme lake level changes on the Tibetan Plateau associated with the 2015/2016 El Niño. *Geophysical Research Letters*, *46*(11), 5889–5898.

Li, J., & Zeng, Q. (2002). A unified monsoon index. *Geophysical Research Letters*, *29*(8), 115–1.

Li, X., Wang, L., Guo, X., & Chen, D. (2017). Does summer precipitation trend over and around the Tibetan Plateau depend on elevation? *International Journal of Climatology*, *37*, 1278–1284.

Linderholm, H. W., Ou, T., Jeong, J.-H., Folland, C. K., Gong, D., Liu, H., ... Chen, D. (2011). Interannual teleconnections between the summer North Atlantic Oscillation and the East Asian summer monsoon. *Journal of Geophysical Research: Atmospheres*, *116*(D13).

Liu, S., & Liang, X.-Z. (2010). Observed diurnal cycle climatology of planetary boundary layer height. *Journal of Climate*, *23*(21), 5790–5809.

Liu, X., & Chen, B. (2000). Climatic warming in the Tibetan Plateau during recent decades. *International Journal of Climatology: A Journal of the Royal Meteorological Society*, *20*(14), 1729–1742.

Liu, Y., Chen, H., Wang, H., & Qiu, Y. (2018). The impact of the NAO on the delayed break-up date of lake ice over the southern Tibetan Plateau. *Journal of Climate*, *31*(22), 9073–9086.

Maddox, E. M., & Mullendore, G. L. (2018). Determination of Best Tropopause Definition for Convective Transport Studies. *Journal of the Atmospheric Sciences*, *75*(10), 3433–3446.

Maher, N., Matei, D., Milinski, S., & Marotzke, J. (2018). ENSO change in climate projections: forced response or internal variability? *Geophysical Research Letters*, *45*(20), 11–390.

Martens, B., Schumacher, D., Wouters, H., Muñoz Sabater, J., Verhoest, N., & Miralles, D. (2020, 01). Evaluating the surface energy partitioning in ERA5. *Geoscientific Model Development*. doi: 10.5194/gmd-2019-315

McPhaden, M. J., Zebiak, S. E., & Glantz, M. H. (2006). ENSO as an integrating concept in earth science. *science*, *314*(5806), 1740–1745.

Mohanakumar, K. (2008). *Stratosphere troposphere interactions: an introduction*. Springer Science & Business Media.

Multivariate ENSO Index Version 2 (MEI.v2). (2020). `https://www.esrl.noaa.gov/psd/enso/mei/`. (Accessed: 2020-03-26)

Munchak, L. A., & Pan, L. L. (2014). Separation of the lapse rate and the cold point tropopauses in the tropics and the resulting impact on cloud top-tropopause relationships. *Journal of Geophysical Research: Atmospheres*, *119*(13), 7963–7978.

Oke, T. R. (2002). *Boundary layer climates*. Routledge.

Pan, L. L., Honomichl, S. B., Bui, T. V., Thornberry, T., Rollins, A., Hintsa, E., & Jensen, E. J. (2018). Lapse Rate or Cold Point: The Tropical Tropopause Identified by In Situ Trace Gas Measurements. *Geophysical Research Letters*, *45*(19), 10–756.

Patil, M., Patil, S., Waghmare, R., & Dharmaraj, T. (2013). Planetary Boundary Layer height over the Indian subcontinent during extreme monsoon years. *Journal of Atmospheric and Solar-Terrestrial Physics*, *92*, 94–99.

Randel, W. J., Seidel, D. J., & Pan, L. L. (2007). Observational characteristics of double tropopauses. *Journal of Geophysical Research: Atmospheres*, *112*(D7).

Rangwala, I., Miller, J. R., & Xu, M. (2009). Warming in the Tibetan Plateau: possible influences of the changes in surface water vapor. *Geophysical research letters*, *36*(6).

Reid, H., & Vaughan, G. (2004). Convective mixing in a tropopause fold. *Quarterly Journal of the Royal Meteorological Society*, *130*(599), 1195–1212.

Santer, B. D., Sausen, R., Wigley, T. M. L., Boyle, J. S., AchutaRao, K., Doutriaux, C., ... Taylor, K. E. (2003). Behavior of tropopause height and atmospheric temperature in models, reanalyses, and observations: Decadal changes. *J. Geophys. Res.*, *108*(D1), 4002. doi: 10.1029/2002JD002258

Sathyanadh, A., Prabhakaran, T., Patil, C., & Karipot, A. (2017). Planetary boundary layer height over the Indian subcontinent: Variability and controls with respect to monsoon. *Atmospheric research*, *195*, 44–61.

Sausen, R., & Santer, B. D. (2003). Use of changes in tropopause height to detect human influences on climate. *Meteorologische Zeitschrift*, *12*(3), 131-136. Retrieved from `http://dx.doi.org/10.1127/0941-2948/2003/0012-0131` doi: 10.1127/0941-2948/2003/0012-0131

Schmidt, T., Wickert, J., Beyerle, G., & Reigber, C. (2004). Tropical tropopause parameters derived from GPS radio occultation measurements with CHAMP. *Journal of Geophysical Research: Atmospheres*, *109*(D13).

Schulzweida, U. (2019, February). *CDO User Guide.* Retrieved from `https://doi.org/10.5281/zenodo.2558193` doi: 10.5281/zenodo.2558193

Seibert, P., Beyrich, F., Gryning, S.-E., Joffre, S., Rasmussen, A., & Tercier, P. (2000). Re-

view and intercomparison of operational methods for the determination of the mixing height. *Atmospheric environment*, *34*(7), 1001–1027.

Seidel, D. J., Ao, C. O., & Li, K. (2010). Estimating climatological planetary boundary layer heights from radiosonde observations: Comparison of methods and uncertainty analysis. *Journal of Geophysical Research: Atmospheres*, *115*(D16).

Seidel, D. J., Zhang, Y., Beljaars, A., Golaz, J.-C., Jacobson, A. R., & Medeiros, B. (2012). Climatology of the planetary boundary layer over the continental United States and Europe. *Journal of Geophysical Research: Atmospheres*, *117*(D17).

Shaman, J., & Tziperman, E. (2005). The effect of ENSO on Tibetan Plateau snow depth: A stationary wave teleconnection mechanism and implications for the South Asian monsoons. *Journal of Climate*, *18*(12), 2067–2079.

Škerlak, B., Pfahl, S., Sprenger, M., & Wernli, H. (2019). A numerical process study on the rapid transport of stratospheric air down to the surface over western North America and the Tibetan Plateau. *Atmospheric Chemistry and Physics*, *19*(9), 6535–6549.

Škerlak, B., Sprenger, M., & Wernli, H. (2014). A global climatology of stratosphere-troposphere exchange using the ERA-Interim data set from 1979 to 2011. *Atmospheric Chemistry and Physics*, *14*(2), 913–937.

Stocker, T., Clarke, G., Le Treut, H., Lindzen, R., Meleshko, V., Mugara, R., ... others (2001). Physical climate processes and feedbacks. In *IPCC, 2001: Climate Change 2001: The Scientific Basis. Contribution of Working Group I to the Third Assessment Report of the Intergovernmental Panel on Climate Change* (pp. 417–470). Cambridge University Press.

Stull, R. B. (2012). *An introduction to boundary layer meteorology* (Vol. 13). Springer Science & Business Media.

Sun, G., Zeyong, H., Ma, Y., Xie, Z., Yang, S., & Wang, J. (2020). Analysis of local land-atmosphere coupling in rainy season over a typical underlying surface in Tibetan Plateau based on field measurements and ERA5. *Atmospheric Research*, 105025.

Tao, S.-y., & Ding, Y.-h. (1981). Observational evidence of the influence of the Qinghai-Xizang (Tibet) Plateau on the occurrence of heavy rain and severe convective storms in China. *Bulletin of the American Meteorological Society*, *62*(1), 23–30.

The NCAR Command Language. (2017). *NCAR Command Language Version 6.4.0.* `http://dx.doi.org/10.5065/D6WD3XH5`. (Boulder, Colorado: UCAR/NCAR/CISL/VETS.)

The MathWorks, I. (2018-2019). *MATLAB r2018b, MATLAB r2019a.* (Natick, Massachusetts, United States.)

Trenberth, K. E., Fasullo, J. T., & Kiehl, J. (2009). Earth's global energy budget. *Bulletin of the American Meteorological Society*, *90*(3), 311–324.

Trenberth, K. E., Stepaniak, D. P., & Caron, J. M. (2000). The global monsoon as seen through the divergent atmospheric circulation. *Journal of Climate*, *13*(22), 3969–3993.

Vogelezang, D., & Holtslag, A. (1996). Evaluation and model impacts of alternative boundary-layer height formulations. *Boundary-Layer Meteorology*, *81*(3-4), 245–269.

Walker, G. T. and Bliss, E. W. (1932). *World Weather V* (Vol. 4; Royal Meteorological Society, Ed.). Great Britain: E. Stenford.

Wang, B. (2006). *The Asian monsoon*. Springer Science & Business Media.

Wang, B., Bao, Q., Hoskins, B., Wu, G., & Liu, Y. (2008). Tibetan Plateau warming and precipitation changes in East Asia. *Geophysical Research Letters*, *35*(14).

Wang, B., Ding, Q., & Liu, J. (2011). Concept of global monsoon. In C.-P. Chang, Y. Ding, N.-C. Lau, R. H. Johnson, B. Wang, & T. Yasunari (Eds.), *World Scientific Series on Asia-Pacific Weather and Climate - Vol. 5 The global monsoon system: research and forecast (2nd Edition)* (p. 3-14). Singapore: World Scientific Publishing Co. Pte. Ltd.

Wang, B., & Ho, L. (2002). Rainy season of the Asian–Pacific summer monsoon. *Journal of Climate*, *15*(4), 386–398.

Wang, B., Wu, R., & Lau, K. (2001). Interannual variability of the Asian summer monsoon: Contrasts between the Indian and the western North Pacific–East Asian monsoons. *Journal of climate*, *14*(20), 4073–4090.

Wang, M., Wang, J., Chen, D., Duan, A., Liu, Y., Zhou, S., ... Ju, W. (2019). Recent recovery of the boreal spring sensible heating over the Tibetan Plateau will continue in CMIP6 future projections. *Environmental Research Letters*, *14*(12), 124066.

Wang, Z., Duan, A., Yang, S., & Ullah, K. (2017). Atmospheric moisture budget and its regulation on the variability of summer precipitation over the Tibetan Plateau. *Journal of Geophysical Research: Atmospheres*, *122*(2), 614–630.

Webster, P., Magana, V., Palmer, T., Shukla, J., Thomas, R., Yanai, M., & Yasunari, T. (1998, 06). Monsoons: Processes, predictability, and the prospects for prediction. *Journal of Geophysical Research*, *1031*, 14451-14510. doi: 10.1029/97JC02719

Wolter, K., & Timlin, M. S. (1993). Monitoring ENSO in COADS with a Seasonally Adjusted Principal. In *Proc. of the 17th Climate Diagnostics Workshop, Norman, OK, NOAA/NMC/CAC, NSSL, Oklahoma Clim. Survey, CIMMS and the School of Meteor., Univ. of Oklahoma, 52* (Vol. 57).

World Meteorological Organization. (1957). Meteorology: A three-dimensional science, Second session of the commission for aerology. *WMO Bull.*, *6*(4), 134-138.

Wu, G., Duan, A., Liu, Y., Mao, J., Ren, R., Bao, Q., ... Hu, W. (2014). Tibetan Plateau climate dynamics: recent research progress and outlook. *National Science Review*, *2*(1), 100–116.

Wu, G., He, B., Duan, A., Liu, Y., & Yu, W. (2017). Formation and variation of the atmospheric heat source over the Tibetan Plateau and its climate effects. *Advances in Atmospheric Sciences*, *34*(10), 1169–1184.

Wu, G., Liu, Y., He, B., Bao, Q., Duan, A., & Jin, F.-F. (2012). Thermal controls on the Asian summer monsoon. *Scientific reports*, *2*, 404.

Wu, G., Liu, Y., Zhang, Q., Duan, A., Wang, T., Wan, R., ... Liang, X. (2007). The influence of mechanical and thermal forcing by the Tibetan Plateau on Asian climate. *Journal of Hydrometeorology*, *8*(4), 770–789.

Yanai, M., & Li, C. (1994). Mechanism of heating and the boundary layer over the Tibetan Plateau. *Monthly Weather Review*, *122*(2), 305–323.

Yanai, M., Li, C., & Song, Z. (1992). Seasonal heating of the Tibetan Plateau and its effects on the evolution of the Asian summer monsoon. *Journal of the Meteorological Society of Japan. Ser. II*, *70*(1B), 319–351.

Yang, K., Guo, X., & Wu, B. (2011). Recent trends in surface sensible heat flux on the Tibetan Plateau. *Science China Earth Sciences*, *54*(1), 19–28.

Yang, K., Koike, T., Fujii, H., Tamura, T., Xu, X., Bian, L., & Zhou, M. (2004). The daytime evolution of the atmospheric boundary layer and convection over the Tibetan Plateau: observations and simulations. *Journal of the Meteorological Society of Japan. Ser. II*, *82*(6), 1777–1792.

Yang, Q., & Zheng, D. (2004). *Tibetan Geography*. China Intercontinental Press.

Yao, T., Masson-Delmotte, V., Gao, J., Yu, W., Yang, X., Risi, C., ... He, Y. (2013). A review of climatic controls on δ18O in precipitation over the Tibetan Plateau: Observations and simulations. *Reviews of Geophysics*, *51*(4), 525–548.

Yao, T., Thompson, L., Yang, W., Yu, W., Gao, Y., Guo, X., ... Xu, B. (2012). Different glacier status with atmospheric circulations in Tibetan Plateau and surroundings. *Nature climate change*, *2*(9), 663.

Yao, T., Thompson, L. G., Mosbrugger, V., Zhang, F., Ma, Y., Luo, T., ... Wang, W. (2012). Third pole environment (TPE). *Environmental Development*, *3*, 52–64.

Yao, T., Xue, Y., Chen, D., Chen, F., Thompson, L., Cui, P., ... others (2019). Recent Third Pole's Rapid Warming Accompanies Cryospheric Melt and Water Cycle Intensification and Interactions between Monsoon and Environment: Multidisciplinary Approach with Observations, Modeling, and Analysis. *Bulletin of the American Meteorological Society*, *100*(3), 423–444.

Ye, D.-Z., & Wu, G.-X. (1998). The role of the heat source of the Tibetan Plateau in the general circulation. *Meteorology and Atmospheric Physics*, *67*(1-4), 181–198.

You, Q., Kang, S., Ren, G., Fraedrich, K., Pepin, N., Yan, Y., & Ma, L. (2011). Observed changes in snow depth and number of snow days in the eastern and central Tibetan Plateau. *Climate Research*, *46*(2), 171–183.

Yuan, C., Tozuka, T., Miyasaka, T., & Yamagata, T. (2009). Respective influences of IOD and ENSO on the Tibetan snow cover in early winter. *Climate dynamics*, *33*(4), 509.

Zhang, Q., Zhang, J., Qiao, J., & Wang, S. (2011). Relationship of atmospheric boundary layer depth with thermodynamic processes at the land surface in arid regions of china. *Science China Earth Sciences*, *54*(10), 1586.

Zhang, R., Koike, T., Xu, X., Ma, Y., & Yang, K. (2012). A China-Japan cooperative JICA atmospheric observing network over the Tibetan Plateau (JICA/Tibet Project): An overviews. *Journal of the Meteorological Society of Japan. Ser. II*, *90*, 1–16.

Zhang, Y., & Li, S. (2019). Climatological characteristics of planetary boundary layer height over Japan. *International Journal of Climatology*, *39*(10), 4015–4028.

Zhang, Y., Seidel, D. J., & Zhang, S. (2013). Trends in planetary boundary layer height over Europe. *Journal of climate*, *26*(24), 10071–10076.

Zhou, T., Hsu, H.-H., & Matsumoto, J. (2011). Summer monsoons in East Asia, Indochina and the Western North Pacific. In C.-P. Chang, Y. Ding, N.-C. Lau, R. H. Johnson, B. Wang, & T. Yasunari (Eds.), *World Scientific Series on Asia-Pacific Weather and Climate - Vol. 5 The global monsoon system: research and forecast (2nd Edition)* (p. 43-72). Singapore: World Scientific Publishing Co. Pte. Ltd.

Zhu, X., Wei, Z., Dong, W., Wen, X., Zheng, Z., Chen, G., & Liu, Y. (2019). Projected temperature and precipitation changes on the Tibetan Plateau: results from dynamical downscaling and CCSM4. *Theoretical and Applied Climatology*, 1–15.

Appendices

A Evaluation of the Effect of Reduced Vertical Resolution on LRTL Calculations

For a sample of data, LRTL was calculated from temperature on the full available vertical resolution (37 pressure levels) and compared to LRTL calculated from temperature on 19 pressure levels. The sample data were selected to represent different atmospheric conditions and cover 48 timesteps: The first of each month, at 00:00 and 12:00 UTC, for the years 1979 and 2018. Scatter plots of tropopause values calculated from temperatures with full versus reduced resolution show that the values agree except at the lower limit of allowed LRTL, regardless of whether this is set to 85 hPa as in the original NCL function, (Figure I, A) or 55 hPa (Figure I, B). The translated function was also tested against the original, and was found to agree except for minor differences in the decimals (Figure I, C). Root mean squared error (RMSE) was calculated for each time step across all grid cells (Figure I, D) and for each grid cell across all time steps (Figure I, E). The RMSE are confined to 4 timesteps and 11 grid cells.

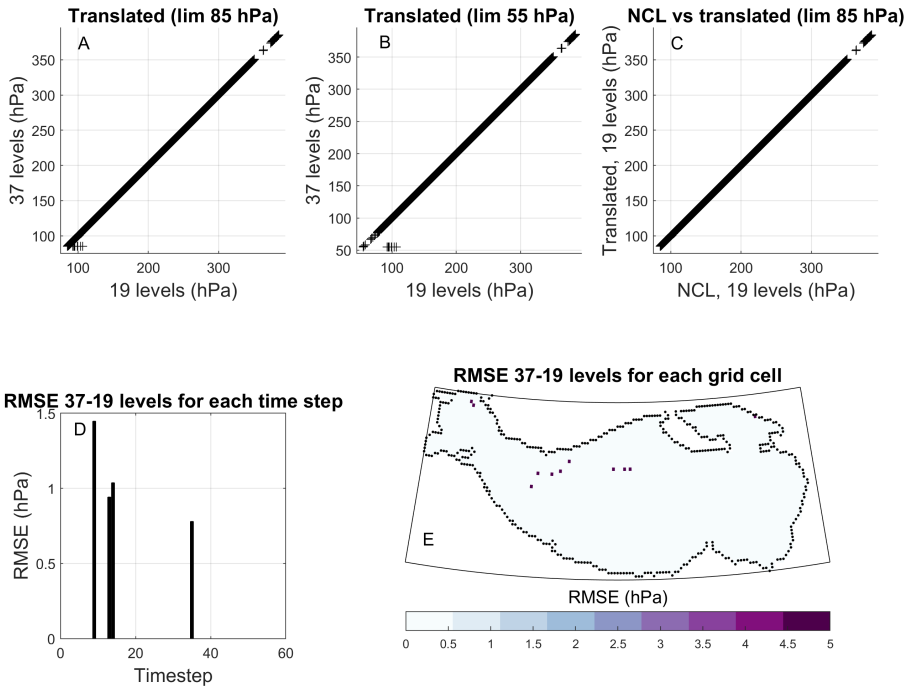

Figure I: Evaluation of the effect of reduced vertical resolution on Lapse Rate Tropopause Level (LRTL). A: Scatter plot of LRTL calculated with the translated NCL function from temperature on 19 (x axis) and 37 (y axis) vertical levels. The lower limit is 85 hPa. **B:** As A, but with the lower limit set to 55 hPa. **C:** LRTL calculated from temperatures with 19 level resolution and the lower limit at 85 hPa, for the original NCL function (x axis) and the translated function (y axis). **D:** Root mean square error (RMSE) between LRTL values from the full and reduced resolutions. **E:** Spatial distribution of RMSE between values from the full and reduced resolutions.

B Evaluation of the Effects of Cubic Spline Interpolation of Temperatures for Calculating CPTL

CPTL was calculated using a cubic spline interpolation. In order to increase computational speed, the number of levels was reduced to 7: the cold point level (as determined from the non-interpolated 19 levels) and the 3 levels lying directly above and below it. In cases were the first (highest) level in the data was less than 3 levels from the non-interpolated cold point, the levels included were those spanning from the first level to 3 levels below the non-interpolated cold point. The reasoning behind the usage of 7 input levels is explained below.

Figure II A shows a randomly selected temperature profile along with the interpolated profile for the 7 levels centred around the cold point. In Figure II B, a profile that yielded large differences in interpolated profiles depending on the selected number of input levels is shown, again with the interpolated profile for 7 levels around the cold point. Figure II C and D shows the same profiles but zooms in on the cold point and include interpolated

profiles using different numbers of input levels. For the relatively simple profile in II C, the interpolated profiles do not differ much. In II D in contrast, the profile that is interpolated using only 5 levels deviate from the others around the 110 hPa level. In addition, the cold point that is interpolated from 11 levels is found around 240 hPa (roughly 10.5 km height) while the cold point in the raw data is found at 70 hPa (roughly 18.5 km). It therefore seems that both too few and too many input levels can lead to erroneous CPTL. Hoping to reduce the risk of both types of errors, 7 input levels were used.

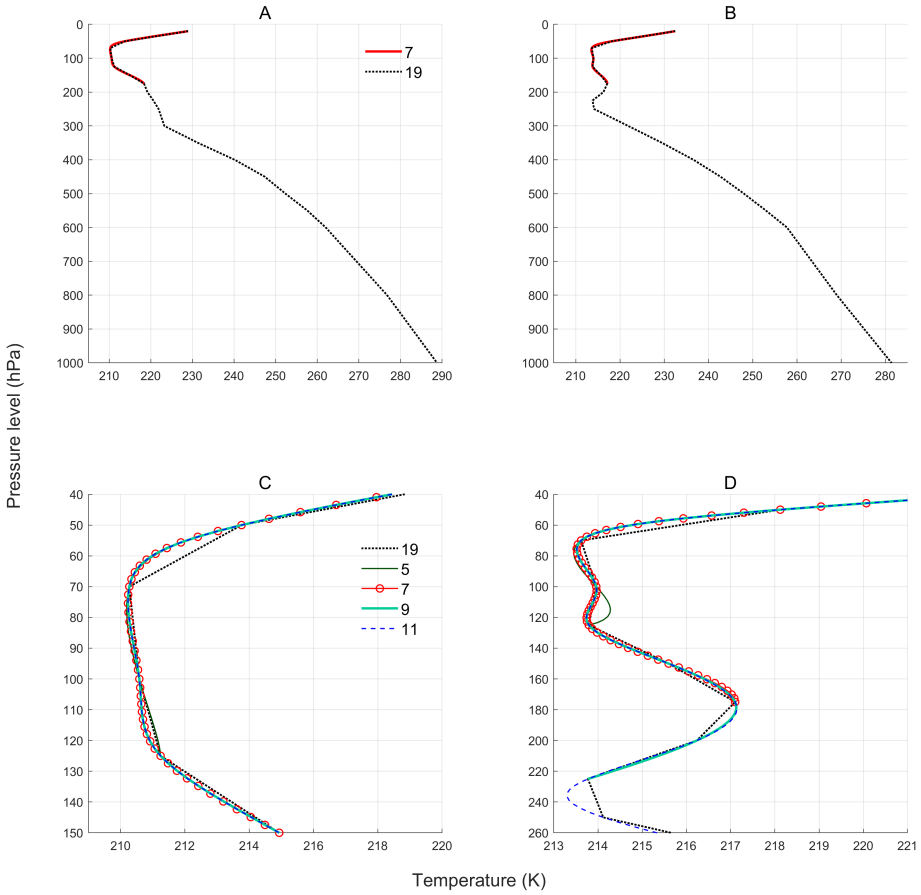

Figure II: Cubic spline interpolation of air temperature. Two vertical temperature profiles were interpolated with a cubic spline in the vicinity of the cold point. **A:** A non-interpolated randomly chosen temperature profile on 19 pressure levels (black dotted line) and interpolation of the same profile using 7 input levels (red line). **B:** As for A, but with a temperature profile selected because of the large difference among interpolations utilising different numbers of input levels. **C:** The same temperature profile as in A, but zoomed in around the cold point. In addition to the non-interpolated profile (black dotted line), interpolated profiles using different numbers of input levels are shown: 5 levels (dark-green solid line), 7 levels (red line with circle markers), 9 levels (turquoise, solid, fat line) and 11 levels (blue, dashed line). **D:** As C, but for the temperature profile displayed in B.

C Function for Cold Point Tropopause calculation

```
function [CptLevel] = CptSpline(PrLevs,Temps,nLev)

% --------------COLD POINT TROPOPAUSE (CPT)--------------------------------
%
% DESCRIPTION
%
% Find cold point (temperature minimum in a vertical column of atmospheric
% temperature) by "upsampling" the temperature and pressure levels to a
% higher resolution (interpolation with matlab function cubic spline).
%
% For computational effeciency, the cold point is first determined from the
% existing input levels.
% Secondly, the actual height of the cold point is sought with cubic spline,
% using only the level of the cold point and the nearest levels above and
% below it. The number of levels included are specified by the user.
%
% OUTPUT
% CptLevel: Pressure level of the cold point, as determined by cubic spline
% interpolation
%
% INPUT
% PrLevs: Vector of the pressure levels (hPa) on which the temperatures are given
% Temps: The temperatures (K)
% nLev: Number of levels to include when determining the CPT level. Must be
% an odd number. If e.g. "9" is given, the (uniterpolated) cold point along
% with the four nearest levels below it and the four nearest levels above it
% are used to find the CPT level. A larger nLev increases computation time.
%
% Written by Nils Slättberg and Johan Lund 2020


% % 1: Find CPT level among all the input levels
%
[~, CPTidx1] = min(Temps);
minus = CPTidx1 - ((nLev -1)/2);
plus  = CPTidx1 + ((nLev -1)/2);

if minus < 1
    minus = 1;
    plus = minus + nLev-1;
end

TFULLshort = Temps(minus:plus);
PFULLshort = PrLevs(minus:plus);

% % 2: Use cubic spline to interpolate CPT level between the input levels
% % close to the CPT level found above

x = 1:1:nLev;
resolution = 0.1;
xx = 1:resolution:nLev;

% Upsampling using cubic spline
TFULL_yy = spline(x,TFULLshort,xx);  % Temperatures
PFULL_yy = spline(x,PFULLshort,xx); % Pressure levels

% Index for cold point in the upsampled temperature
[~, CPTidx2] = min(TFULL_yy);  %("~" throws away min temps, we just need index
                                %of level of min temp)
```

```
% Using index of cold point to pick correct upsampled pressure level
CptLevel = PFULL_yy(CPTidx2);

end

% Description of matlab function cubic spline:
% s = spline(x,y,xq) returns a vector of interpolated
% values s corresponding to the query points in xq.
% The values of s are determined by cubic spline interpolation of x and y.
```